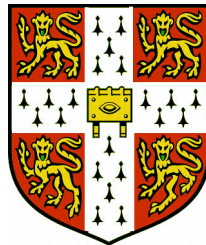# MAT-Test: A New Method for Thin-Film Materials Characterization

Submitted to the Board of Graduate Studies for the Degree of
Master of Philosophy by Research (MPhil)
in the Cambridge University Engineering Department

by Matthew A. Hopcroft

Supervisor: Dr. D. F. Moore

October 31, 2002

Abstract

Mechanical characterization of thin-film materials is a continuing challenge. Accurate material data is required for Micro-Electro-Mechanical Systems (MEMS) and Microsystems (MST) device design and manufacture. Previous investigators have reported methods for thin-film characterization, but in general, these methods are expensive, difficult, and often specific to a certain material. The research presented here describes a new test method for the mechanical characterization of thin films that is quick, inexpensive, and applicable to a wide range of materials. The test method is called MAT-Test.

MAT-Test is based on microbeam bending. Cantilever microbeams are fabricated in the material under test (MUT), and a surface profilometer is used to deflect the beams. Surface profilometers are inexpensive measurement devices that are found in every microfabrication laboratory. New theoretical analysis is presented that allows Young's modulus, breaking stress, and Poisson's ratio to be extracted from the surface profilometer data. Finite Element Method (FEM) simulations are used to support the theoretical analysis.

Experiments were performed to verify the analysis and demonstrate the test method. Samples of thin-film silicon carbide and silicon nitride deposited on silicon substrates were obtained and a micromachining laser was used to pattern cantilever microbeams in the thin films. The substrate was removed by etching in potassium hydroxide (KOH), and a second laser micromachining step was used to remove support structures. The cantilevers were measured with a surface profilometer and the data was analysed according to the theory presented here. The test method performed well, and the test results were in agreement with previously published work.

Acknowledgements

This thesis represents the summary of a complex project with many facets, and it would not have been possible without important contributions from a number of people; too many to list without forgetting someone, but I'll try:

At Cambridge, my supervisor, Dr. David Moore, created a positive research environment, where questioning is never criticised, and ideas are never in short supply. The other members of our research group: Billy Boyle, Harald Hoegh, and Johnny Han He, who were always ready for a discussion about beam bending no matter how many times we had been over it before, made every day possible. The students and staff in the Engineering Department, especially the Electronic Devices and Materials group, were uniformly helpful and positive, and I am proud to be associated with them. Many faculty were particularly supportive; Dr. Andrew Flewitt, Dr. John Williams, Prof. Mark Spearing (MIT), and Prof. Duane Boning (MIT) provided valuable feedback and encouragement. Many thanks also to Bernie Breton for assistance with SEM imaging.

The students and staff in the Optical and Semiconductor Devices research group at Imperial College, London, particularly Prof. Richard Syms, Dr. Munir Ahmad, and Michael Larsen, all went above and beyond the call of duty to help a research student who was not one of their own.

Of course, my family and friends who encouraged me, or simply tolerated my unpredictable schedule, made this work possible, and you should take your share of credit for this work. And of course Beth, who puts up with all of this for some reason, and I am eternally grateful that she does.

Table of Contents

Table of Contents (cont.)

The bending properties of a plate depend greatly on its thickness…

- S. Timoshenko in *Theory of Plates and Shells*

1. Introduction

This thesis describes a generally-applicable test method for measuring some key mechanical properties of thin films, including Young's modulus, breaking stress, and Poisson's ratio. The proposed test method is called MAT-Test. The MAT-Test project has developed from the design requirements of the Microclip project, the goal of which is to develop Micro-Electro-Mechanical Systems (MEMS) microclips and microclip fixturing and packaging systems for optoelectronic and MEMS devices.

Chapter 2 provides some background information for this work, beginning with a description of MEMS and MEMS microclips. There are three necessary precursors for effective design of microclips: materials characterization, microclip simulation, and prototype fabrication. These topics are introduced at the end of this chapter.

Chapter 3, Materials Characterization: MAT-Test, describes the MAT-Test test methodology, including theoretical foundation, simulation results, and design space.

Chapter 4, MAT-Test Experimental Procedure and Results, describes the results of experiments that demonstrate MAT-Test, including sample fabrication and testing.

Chapter 5 draws some conclusions about the project and discusses proposed applications for MAT-Test.

1.1 Notation Used in this Work

The study and analysis of beam bending problems is well established. Many of the standard reference texts on elastic beam behaviour were originally printed in the early 20th century, and some of the secondary references cited in this work date from the late 1800's. The notation used by various authors is often different and contradictory. With all due respect to those who have come before me, in this work, I have chosen to use the following notation, based on convenience and commonality of usage.

Notation used herein:

t thickness of a cantilever or of a thin film
w width of a cantilever
L length of a cantilever
E Young's modulus (elastic modulus)
ψ Young's modulus correction factor
σ stress
σ_b breaking stress (fracture stress)
ε strain
ν Poisson's ratio
P a load applied to a cantilever[1]
F a force applied to a cantilever
s intrinsic distance
θ, ϕ angles
x, y Cartesian coordinates

---

[1] For historical reasons, the force applied by a surface profilometer is specified in terms of an equivalent mass or load acting at one gravity, e.g., the profilometer applies a "10mg load" rather than a "981µN force".

2. Background

2.1 MEMS and Microclips

2.1.1 MEMS

Micro-Electro-Mechanical Systems (MEMS), or Microsystems (MST), are devices or mechanisms with dimensions that are measured in microns. That simple description, while accurate, fails to convey the power and potential that micro-scale devices possess when compared to their macro-scale counterparts. As well as being physically much smaller, micro-scale devices can be more efficient, more reliable, and cheaper to produce in volume than their macro-scale counterparts. In many cases, these properties enable completely new applications. For example, a single actuator that raises or lowers a flap with area less than 1mm^2 is not particularly useful by itself. However, if that actuator occupies little more area than the flap, and if thousands of these actuators can be manufactured for fractions of a penny, then an array of thousands of such actuators can be installed along an airplane wing to control the aircraft without using any other moving parts [1]. MEMS technology is derived from the technologies developed for integrated circuit (IC) manufacture, and there are many similarities between IC and MEMS fabrication techniques and challenges. MEMS devices have been designed for a wide variety of applications: sensors, displays, power generators, health-related applications, biological research, telecommunications, and so on [2-4]. In the 15 years since the first annual Institute of Electrical and Electronics Engineers (IEEE) conference on MEMS[2], MEMS devices have become a serious area of research and commercial activity. Annual sales of MEMS products by European companies reached £640 million in the year 2000, and growth rates of 10-15% are forecast for the through 2005 [5]. Forecasts for worldwide MEMS product sales at that time range from £6-£13 billion annually [6, 7].

2.1.2 Microclips

One of the current projects in the MEMS Research Group in the Cambridge University Engineering Department is an investigation of MEMS devices based on 'microclips'. Microclips are suspended or free-standing microbeams that are deformed in specific ways. A deformed clip exerts a mechanical force opposing the deformation, and this 'clip force' can perform useful functions. Figure 1 illustrates a single rectangular microclip. Microclip systems are composed of arrays of individual microclips. Microclips can be constructed with actuators, sensors, or electrical conductors and used in different ways. Figure 2 shows a proposed simple microclip system designed to hold a rectangular component perpendicular to a packaging substrate.
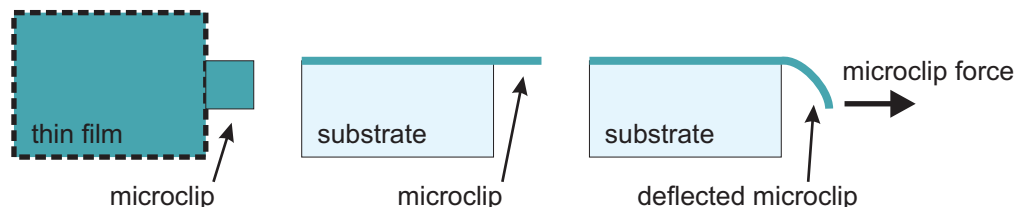
Figure 1 A single rectangular microclip

---

[2] The IEEE MEMS conference series began in 1987 as the Micro Robots and Teleoperators Workshop. It was subsequently renamed the IEEE Micro Electro Mechanical Systems Workshop, and since 1999 it has been known as the IEEE International Micro Electro Mechanical Systems Conference.
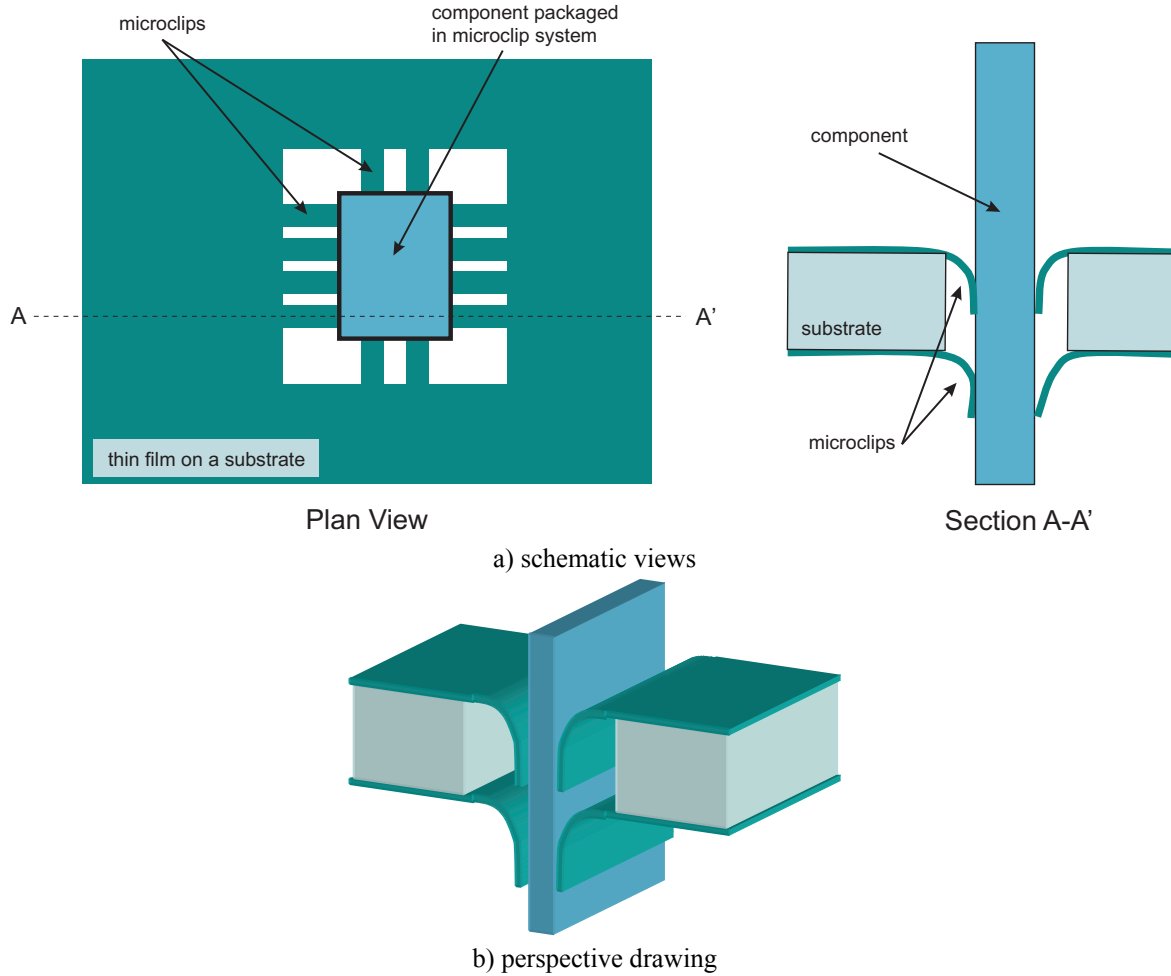
Figure 2 Proposed microclips for packaging

Previous work in this Department has demonstrated the use of silicon nitride microclips to hold optical fibres into V-grooves etched in silicon [8-11] (Figure 3). Other groups have demonstrated microclips fabricated in other materials, including silicon [12, 13] and aluminium [14]. The microclip designs that we are investigating now extend the microclip principles further and enable more applications than previous work.
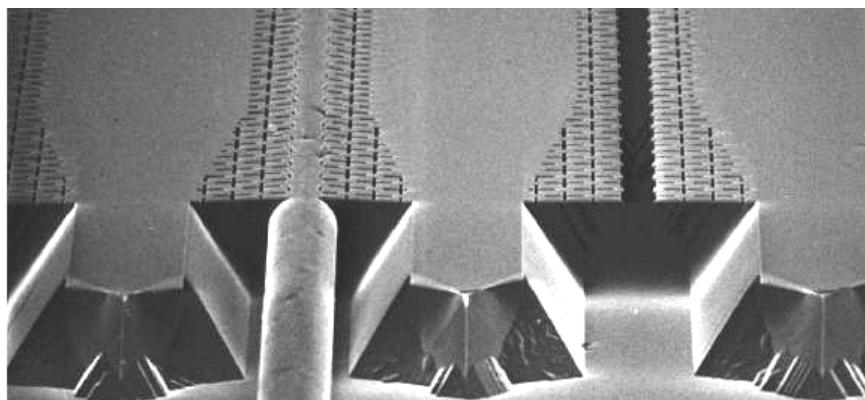
Figure 3 Microclips holding an optical fibre in a silicon V-groove [8]

3

2.2 Precursors for Designing Microclips

Microclips and microclip packaging systems present exciting possibilities for low-cost optoelectronic device packaging and other MEMS applications. However, there are three items that must be addressed before we are able to perform correct and accurate microclip design. These items are:

1) Characterization of the mechanical properties of the microclip material,
2) Simulation of microclips and microclip systems, and
3) Fabrication and testing of prototype devices.

With the insight gained from investigation of these areas, useful microclip systems can be designed and optimized. All three items are introduced in this section. Item 1, mechanical characterization of thin-film materials, is the topic of this thesis.

2.2.1 Materials Characterization

The design of a microclip system requires knowledge of the clip force that the microclips will produce due to their stiffness and the amount of bending they can withstand before breaking. Both the microclip stiffness and the amount of bending which the microclip can tolerate without breaking are related to fundamental mechanical properties of the microclip material, namely Young's modulus, E, and breaking stress, σ_b.

Microclips are typically constructed from thin films deposited on a substrate. Some suitable thin films are readily available; silicon nitride (SiN) and silicon dioxide (SiO_2), for example, are commonly used as passivation layers in IC manufacture processes. Other, more exotic, thin film materials such as diamond-like carbon (DLC) or titanium silicide may prove to be useful microclip materials. All of these materials have different values of E and σ_b. Clearly, some method of measuring the relevant mechanical properties of thin films and distinguishing between candidate materials is required. Traditional methods of mechanical testing are generally not applicable to thin films. Chapter 3 describes MAT-Test, which is a new method of thin film materials characterization.

2.2.2 Microclip Simulation

Microclip operation involves large-angle deflections of microbeams. This means that they are not amenable to analysis by the Euler simple beam equations, which are limited to structures with small-angle deflections. However, it has been shown [15] that large-angle deflections can be accurately simulated by using a lumped-mass analysis and considering the total energy state of the system. This allows us to predict the shape that each microclip will assume and the force that it will exert when bent.

The second simulation issue is modelling the performance of microclip packaging systems. Probabilistic models of systems composed of multiple microclips can be constructed using the results of the energy-based simulations of individual microclips. These models indicate what sort of performance we can expect from microclip systems and what areas of their design require further refinement.

The microclip simulation work is described in detail in recent publications from the MEMS group [16, 17].

2.2.3 Microclip Prototypes

Various forms of limited prototypes of microclips have been fabricated or have been designed. A photolithographic mask with a series of microclip system prototypes and test vehicles has been designed, submitted, and received in 2002. Microclip prototypes have also been fabricated using a semiconductor processing laser to pattern the films. The Engineering Department has a QuikLaze 50 micromachining laser from New-Wave Research [18], which we have used for patterning a variety of thin films for microclip experiments. Laser micromachining of thin films is discussed in section 4.1.

3. Materials Characterization: MAT-Test

The design and manufacture of MEMS microclips, as well as other MEMS devices based on elastic bending, requires knowledge of the mechanical properties of the materials that are used in the design. The majority of materials available to the MEMS designer are thin films (e.g. silicon nitride, polysilicon), single-crystal substrates (silicon, quartz), or amorphous substrates (glass, plastic). Many of these materials, because of their sample size and/or production methods, are difficult to characterize using traditional macro-scale testing methods. As a result, the reported values for mechanical properties of these materials vary widely and are not generally applicable [19].

MAT-Test is a testing method for measuring key mechanical properties of thin films. The test method is based on beam bending: MAT-Test uses a contact surface profilometer to apply a force to free-standing cantilever microbeam test structures constructed from the material under test (MUT). Young's modulus, E, fracture strength, σ_b, and Poisson's ratio, ν, of the MUT can then be determined from the force applied by the profilometer, the geometry of the test structure, and the resulting deflection of the test structure. A novel interpretation of the microbeam bending data allows the extracted parameters to be determined with high accuracy. MAT-Test is easy to perform and requires only standard microfabrication laboratory equipment, unlike other methods (e.g. tensile test, nanoindentation).

We have chosen to pursue a bending method over alternative methods such as resonant frequency measurement or pull-testing for several reasons. First, beam bending reflects our design requirements for microclips. Second, surface profilometers are an inexpensive, easy-to-use piece of laboratory equipment that is found in every IC and microtechnology laboratory. In addition, MAT-Test uses the profilometer capabilities in a novel manner that provides superior performance over previously published methods. The most popular beam bending methods that have been published previously (see section 3.6) rely on nanoindenters, which are expensive and rare. We believe that the combination of common equipment, ease of use, performance, and general applicability will allow the widespread adoption of MAT-Test both in Research, for investigations of new materials, and in Industry, for process quality control.

The name "MAT-Test" has two meanings: first, it is a shortening of the phrase "Materials Testing". Second, it is a reference to the "E-Test" used in the IC industry to characterize transistor production processes. It is also an acknowledgement of the "M-Test" test methodology published by Osterberg and Senturia [20], which was itself named after E-Test.

3.1 The MAT-Test Method

MAT-Test is based on controlled bending of test structures that are fabricated in the material under test (MUT). The test structures, cantilever microbeams, are first patterned in the MUT. After patterning, the substrate underneath the test structures is removed, leaving the cantilevers suspended. Figure 4 illustrates the test structure fabrication process for a generic MUT/substrate combination.

| 1) Substrate with Thin Film | 2) Pattern Test Structures | 3) Etch Substrate |
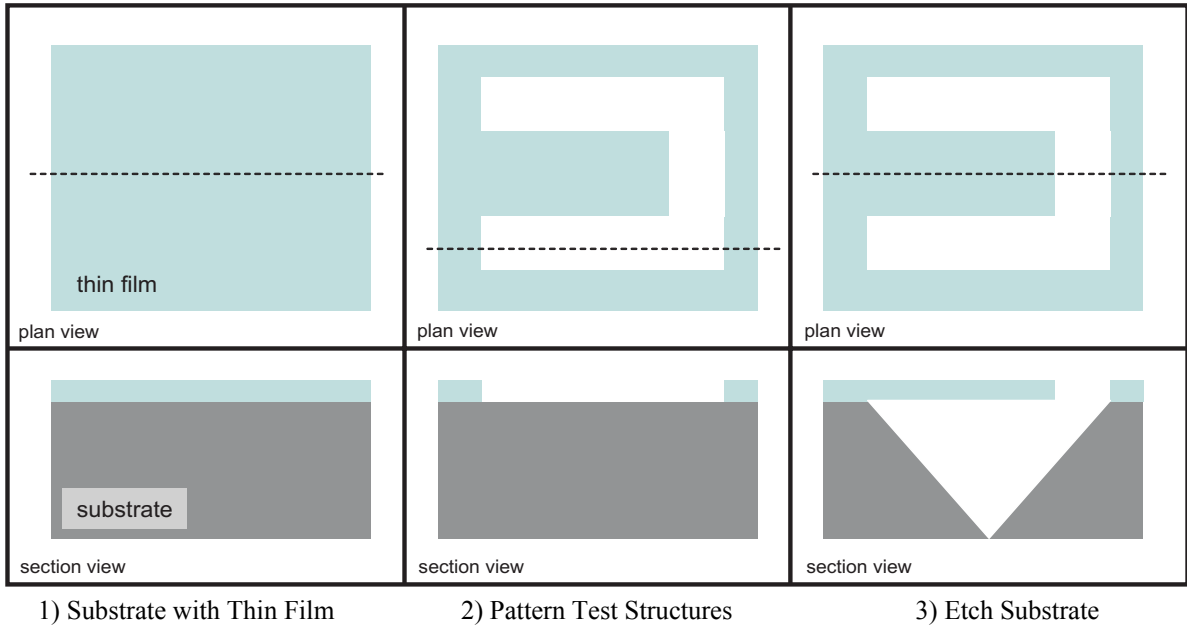
Figure 4 Fabrication of MAT-Test test structures.
An anisotropic substrate etch is shown in step 3, although other types of etches can be used.

A contact surface profilometer is then used to measure the suspended structures by scanning the profilometer stylus along the length of the beam (Figure 5). The force applied by the profilometer stylus deflects the test structures and the profilometer records the deflection. The applied force, deflection profile, and test structure geometry are then analysed to determine the mechanical properties of the MUT.
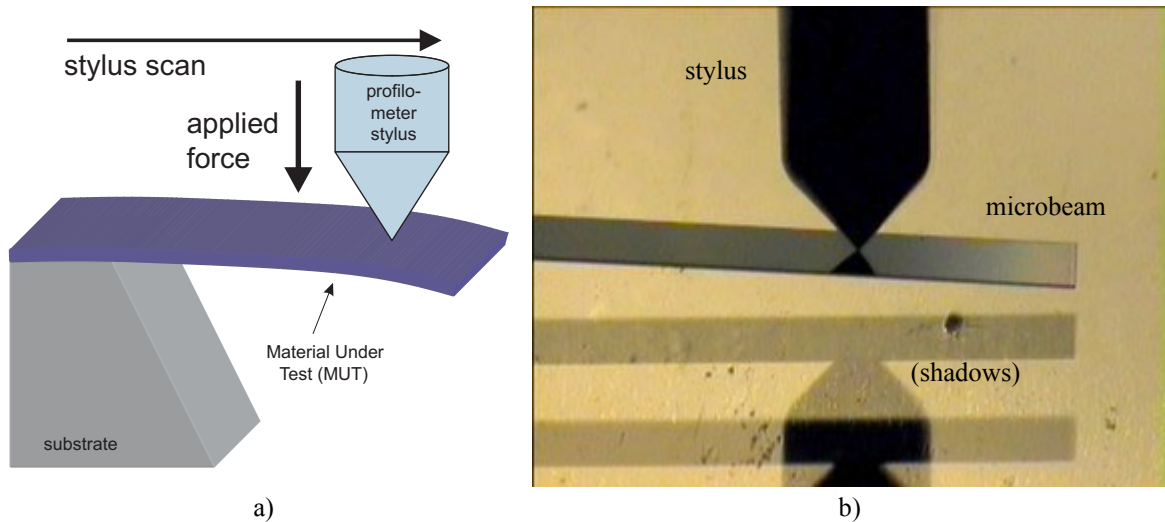
Figure 5 Using a surface profilometer to deflect microbeams.
a) schematic drawing. b) microphotograph of a surface profilometer stylus deflecting a microbeam. The microbeam is approximately 400µm wide. The stylus enters the picture from the top, and it casts a shadow at the bottom of the picture. A second shadow is seen at the bottom of the picture because the sample is mounted on a transparent glass slide.

The cantilever parameters for purposes of analysis are illustrated in Figure 6. The length of the cantilever is L, the vertical deflection is d, the applied force is F, Young's modulus is E, and the cantilever cross-section has thickness t and width w. The second moment of cross-sectional area, I (not shown), is a function of the cantilever cross-section.

For a rectangular cross-section, *I* has the value *wt³/12*. Note that all profilometer scans in this work proceed from the base of the cantilever towards the free end and all profilometer data plots are presented with the base of the cantilever on the left and the free end on the right, as shown in Figure 6.
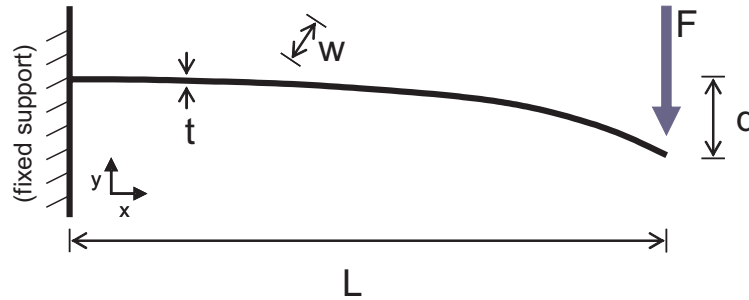
Figure 6 Parameters for simple cantilever deflection

3.1.1 Young's Modulus

Young's modulus, or elastic modulus, is a material property that relates elastic stress and strain. For a cantilever, the relationship between an applied force, the deflection of the cantilever, and the material properties of the MUT is given by the small deflection ("Euler") equation for a force applied at the free end, or tip, of the cantilever (see Appendix B for derivation):

$$d = \frac{FL^3}{3EI}$$

Equation 3-1

It is clear that Young's modulus, *E*, can be extracted from Equation 3-1 if the other quantities are known. The second moment of area, *I*, is known from the fabrication data, and can also be measured independently. Force, *F*, length, *L*, and deflection, *d*, are given by the surface profilometer.

3.1.2 Breaking Stress

Breaking stress, or fracture strength, is the stress at which a material will fail. The same measurement procedure can be used to measure the tensile breaking stress, σ_b, at which the MUT fractures. The stress developed in the cantilever due to the force applied to the end of the cantilever is given by the expression (see Appendix B for derivation):

$$\sigma = \frac{6F(L-x)}{wt^2}$$

Equation 3-2

The maximum stress occurs at the root of the cantilever ($x = 0$), and so we expect a loaded cantilever to fracture there, although it may fracture elsewhere due to defects or other micromechanical effects. If the force applied by the surface profilometer causes the beam to break during a scan, the position of the stylus when the break occurs (*L*) is known. The beam can then be inspected to determine the location of the break (*x*), and the resultant stress can be determined. Because the fracture mechanics of thin films are complex, many measurements should be taken to ensure statistical relevance of the breaking stress value, and the effect of stress concentrations due to the geometry of the beam must be considered (see section 3.4.2).

8

3.1.3 Poisson's ratio

Poisson's ratio, v, is a material property that relates perpendicular strain components in elastic deformation. The surface profilometer data can be used to determine the Poisson's ratio of the MUT if two samples of different thickness are available. This is because a beam subjected to bending by a point load experiences stiffening due to stresses related to the perpendicular strain components in the beam [21]. This stiffening causes the beam to bend with an effective Young's modulus, E_{eff}, rather than its true Young's modulus, E, and this effective modulus is measured during the beam bending test. The relationship between E and E_{eff} is expressed by ψ, which is a function of v.

$$E_{eff} = \psi E$$

<div align="right">Equation 3-3</div>

The stiffening effect is strongly dependent on the thickness of the film, as compared to the length and width. For thicker films, the effect is negligible ($\psi \approx 1$), but for thinner films, the stiffening is pronounced, so that the measured values of E on samples of different thicknesses will differ. A comparison of E measurements for a thick film and a thin film will yield a value of ψ, and hence v.

3.1.4 Applied Force

The force that deflects the cantilever test structure, F, is applied to the cantilever by the surface profilometer stylus. The accuracy of the applied force is not normally a figure of merit for surface profilometers; as long as the force applied by the stylus remains reasonably constant, it is not terribly important that it have a specific value. However, for MAT-Test, the accuracy of the applied force directly affects the accuracy of the MAT-Test results. Therefore, we need some way to measure the force applied by the profilometer. For this work, the applied force is measured using cantilever test structures fabricated from silicon. The Young's modulus of single-crystal silicon has been characterized by other methods [22-26] to within 2%, and so we can use Equation 3-1 to determine the force applied by the profilometer by measuring the deflection of silicon cantilevers.

3.2 Theoretical Basis

3.2.1 The Nature of the MAT-Test Data

The MAT-Test method uses a surface profilometer to deflect a cantilever microbeam, as shown in Figure 5. As the profilometer stylus moves along the length of the beam, it applies a force normal to the beam surface which causes the beam to be deflected downward and allows the stylus to descend. The profilometer simultaneously records the vertical and horizontal position of the stylus, producing a data plot of vertical deflection, d, versus horizontal position, x. The vertical deflection that is measured at each horizontal position x can be thought of as the deflection of a cantilever with length $L = x$ that is deflected by a force applied at its tip. Essentially, a profilometer data plot containing n data points represents the deflection of n individual cantilevers, each with length x, deflected by a force applied at their tip[3]. This idea is illustrated in Figure 7, which compares several calculated cross-sections of a cantilever microbeam that is deflected by a force applied at different points along its length. Also shown on the plot is a calculated set of points representing the data plot produced by a profilometer as it scans along the length of the

---

[3] This qualitative analysis neglects the mass of the cantilever, which is discussed in section 3.3.11.

same cantilever. The total length of the microbeam is referred to as L_L, while the "virtual length" of the cantilever as it is deflected by the stylus at each individual data point is L. If we consider the profilometer data in this way, we can then say that we expect the data plot to follow the relationship for tip deflection given in Equation 3-1, and we can analyze the data using this straightforward expression. A surface profilometer is the only instrument that collects this type of data, and it allows us to consider the bending of the cantilever test structure in a new way.
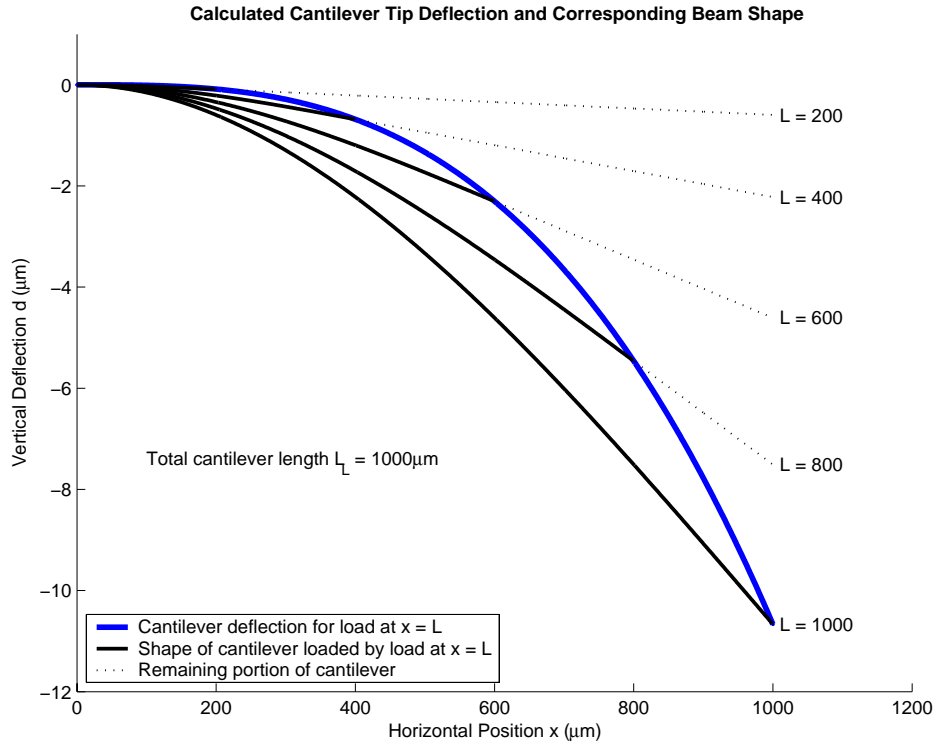
Figure 7 Calculated cantilever beam deflection by a profilometer stylus.
The solid blue line represents the tip deflection of a cantilever of length *x*, with the profilometer stylus applying a force at *x*. Corresponding microbeam cross-sections for selected horizontal positions are shown.

3.2.2 Extracting Young's modulus

The relationship given by Equation 3-1 describes the deflection of the tip of the cantilever due to a force applied at the tip. This force causes the beam to deflect as a function of L^3. This relationship is predicated on several assumptions; basically that the beam is homogenous, straight, and fixed at the root. Naturally, in practice, we find that the measured deflection of the beam is often quite different from the predicted amount. This is due to various additional bending effects and invalid assumptions. We shall refer to these additional bending effects and assumptions collectively as "error effects". The error effects are analysed in section 3.3.

The governing equation for small-deflection beam bending, from which Equation 3-1 is derived (see Appendix B.1), is a second-order linear differential equation. The general solution to the equation (for *x = L*) has the form:

$$d = YL^3 + UL^2 + SL + T$$

Equation 3-4

In the simplest case of bending, with no error effects, the coefficients U, S, and T are equal to zero, and the solution is Equation 3-1, with $Y=F/3EI$. It is shown in section 3.3 that the relevant error effects are not functions of L^3. By superposition, we can say that the deflection caused by the error effects is represented by the other coefficients. Therefore, if we perform a polynomial curve fit to the data from the surface profilometer, we get an expression of the form of Equation 3-4 which describes our deflection data, and we can extract Young's modulus from the Y coefficient (Equation 3-5), *without regard to the absolute deflection of the cantilever*.

$$E = \frac{F}{3YI}$$
<div align="right">Equation 3-5</div>

In general, the absolute deflection, d, measured on any given test structure is quite difficult to predict, as the various error effects are difficult to quantify. However, Equation 3-4 and the subsequent analysis allow us to ignore the absolute measured deflection and concentrate instead on the shape of the deflection data. The polynomial curve fitting is a form of regression analysis on a data set with a large number of values, and so the curve fitting will have very high precision. The appropriate order of the polynomial is determined by our knowledge of the physical nature of the system (i.e., small deflections of a cantilever beam).

This insight represents a significant advance in the analysis of beam bending test methods. As is described in section 3.6, previous beam-bending investigations have relied on measurement of absolute deflection, which is subject to numerous types of errors. Many investigators have gone to extreme lengths in attempts to quantify and reduce individual error effects. By concentrating on the shape of the data, rather than the specific values, we are able to avoid these difficulties. The contact surface profilometer, though not designed specifically for this type of experiment, is unique in that it records data that is appropriate for this analysis.

3.2.3 Determining Breaking Stress

The breaking stress is not a function of the amount of deflection of the cantilever (Equation 3-2), rather it is a function of the radius of curvature of the microbeam at the point of failure, which is due to the bending moment created by the applied force. The stress present at a point of failure is also influenced by the geometry of the test structure, as stress concentrations develop around geometric discontinuities, such as the corners where the cantilever joins the root. These stress concentrations can cause the actual stress to be greater than the simple stress due to curvature by a factor of two or more. Therefore, in order to know the stress which caused the beam to fail, we need to know the geometry of the beam at the location of the failure, I, the applied force, F, and the length, L, where the load was applied when the beam failed, and the location of the failure, and the magnitude of stress concentrations that are likely to be found at this location. The length L is apparent from the profilometer data, and the location of the failure can be determined simply by a second profilometer scan or by other inspection methods. The magnitude of the stress concentrations can be estimated from simulations (see section 3.4.2). Note that, as in the measurement of Young's modulus, we are not concerned with the absolute deflection of the cantilever.

The fracture mechanics of thin-films are complex, and open to investigation [27]. In general, they are very strong, due to their low volume, and low number of defects per

volume. However, individual samples may vary, and processing may introduce unexpected defects. The Weibull distribution is used to quantify the fracture strength of a material [28]:

$$\ln P_s(V) = -\frac{V}{V_0}\left(\frac{\sigma}{\sigma_0}\right)^m$$

Equation 3-6

where P_s is the probability of survival, m is the Weibull modulus, and V is the volume of the sample. The quantities V_0 and σ_0 represent baseline quantities for the distribution. By performing many MAT-Test breaking stress experiments, a distribution of failure stresses can be created and P_s determined. It has been proposed [29] that the various mechanisms of fracture observed in some thin films may be more accurately described by a combination of separate Weibull distributions.

3.2.4 Quantifying Poisson's ratio

Poisson's ratio, ν, is the ratio of longitudinal strain to lateral strain experienced by a body under uniaxial normal stress. This Poisson effect can be expressed for two dimensions as [30]:

$$\varepsilon_y = \nu \varepsilon_x$$

Equation 3-7

where ε is strain. For beam bending tests with a point load applied to the centre of the top surface of a beam, we encounter Poisson's ratio when we consider the effect of the width of the beam. As the beam is bent, an axial strain develops in the beam. A lateral strain is developed in the direction perpendicular to this axial strain, as given by Equation 3-7, and the "natural" reaction of the beam is to bend upward at the edges in an anticlastic manner (Figure 8).
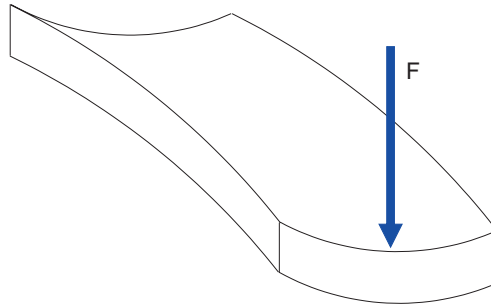
Figure 8 Anticlastic curvature of a beam deflected by force F (after [31])

As the beam is bent, however, a longitudinal stress is developed which serves to counteract the natural anticlastic curvature. The cross-section that results from the combination of these effects is complex [21]. For wide beams ($w \gg t$), the altered cross-section stiffens the beam significantly, causing it to deflect less than the amount predicted by simple beam theory. For wide beams, this stiffening effect is taken into account by using a modified Young's modulus, E_{plate}:

$$E_{plate} = \frac{E}{1-\nu^2}$$

Equation 3-8

This modified modulus is often called the *plate modulus*, and in simple beam-bending analysis, a choice is made between using E or E_{plate}, depending on the width of the beam. It has been shown that all bending beams experience some amount of stiffening, and that it is appropriate to use a continuous correction factor ψ (see Equation 3-3) with Young's modulus in the Euler beam equation to account for this stiffening:

$$d = \frac{FL^3}{3\psi EI}$$

Equation 3-9

The values of ψ range from 1 to $1/1\text{-}\nu^2$, the traditional value of E_{plate}. The complete expression for ψ is a complex function of ν, E, and the radius of curvature of the cantilever. This relationship can be understood in terms of the dimensionless parameter K, which determines the shape of various trigonometric functions in the analytical solution for ψ [21]. For cantilever beams, the expression for K is:

$$K = \frac{12FLw}{Et^4}$$

Equation 3-10

The value of ψ is proportional to the value of K, so in order to minimize ψ, we simply minimize K. We can see that the value of ψ, and therefore the accuracy of our measurement of E, is strongly dependent on the thickness of the film, compared to the length and width. For example, the value of ψ for a film with $t = 1\mu m$, $E = 400$ GPa, $w = 100\mu m$, $L = 1000\mu m$, $F = 981\mu N$, and $\nu = 1/3$ is nearly 1.12, giving a 12% error for the calculated value of E. For the same beam with $t = 5\mu m$, the error drops to well under 0.5%.

For a film with an unknown Poisson's ratio, MAT-Test is restricted to measuring relatively thick films, or measuring the effective modulus, E_{eff}, rather than E. However, we can measure E with confidence for sufficiently thick films. Furthermore, if we have both relatively thick and thin samples of the MUT available[4], a comparison of the E values extracted from both samples will yield a value of ψ, and hence of Poisson's ratio, ν.

Of course, if the value of Poisson's ratio for the MUT is known or assumed, we can measure the Young's modulus of films of any thickness. Thin films may also be measured if they are deposited on top of a thicker film and a bi-layer measurement is made (see Appendix B for the multi-layer beam equations).

3.3 The Error Effects

The various error effects that affect the deflection measured in cantilever microbeam bending experiments are analysed individually in this section. The analytical expressions are developed in a manner that expresses the relationship of the additional deflection caused by the error effect, d_{error}, to the length of the cantilever, L. The goal of the analyses is to show that the deflection contributed by the error effects is *not* a function of L^3, and so the MAT-Test method, described above, is immune to their influence. Unless stated otherwise, the results are specific to small deflections of the types of microbeams that are used in MAT-Test: microbeams that are homogenous, of rectangular cross-section with length and width much greater than thickness, and deflected by a point load. The results are summarized in a table at the end of this section.

---

[4] Assuming that the Young's modulus remains constant for different thicknesses of the deposited material.

3.3.1 Shear Stress

The Euler beam analysis assumes that the shear stresses acting in the beam are zero. This is usually true for microbeam bending, where the beams are very thin, and the effects of shear stresses can generally be neglected. However, an estimate of the additional deflection caused by shear stresses, d_τ, is given by [32]:

$$d_\tau = \frac{3FL(1+\nu)}{wtE} \qquad \qquad \text{Equation 3-11}$$

The additional deflection due to shear stresses, d_τ, is a linear function of L.

3.3.2 Torsional Deformation (twist)

Torsional deformation, or twist, is additional deflection caused by a point load that is applied away from the centreline of the beam (Figure 9).
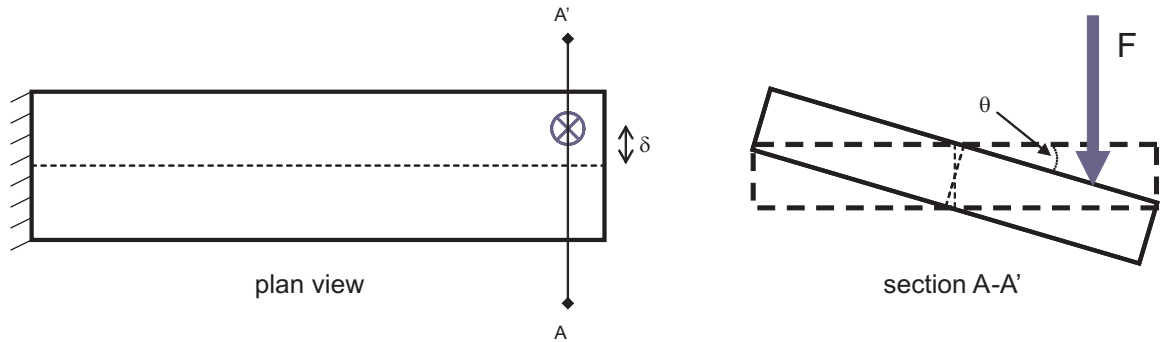
Figure 9 Deflection due to twisting of a beam with off-centre loading

An expression for deflection due to torsional deformation of a beam, d_t, can be derived from the expression for twist angle, θ, for a beam of rectangular cross-section, given in [33]. The additional deflection is simply:

$$d_t = \delta \sin \theta \qquad \qquad \text{Equation 3-12}$$

where δ is the distance from the centreline to the point of application of the load. The angles involved are quite small, and we can use the small angle approximation ($sin\theta \cong \theta$) to arrive at the expression:

$$d_t = \frac{\delta^2 FL(1+\nu)}{2EI\gamma} \qquad \qquad \text{Equation 3-13}$$

Following Menčik [34], the expression incorporates a cross-section shape factor, γ, which ranges from 1 for $w \gg t$, to 0.43 for $w = t$. This deflection is a function of L for deflection caused by a load located at a fixed point on the beam. However, in MAT-Test, the stylus travels along the length of the beam. It may travel off the centreline, either parallel to it or rotated by some angle ϕ (Figure 10). If ϕ is not zero, than the distance δ will be a function of L, and the deflection due to twist will be a function of L^3. Of course, the maximum value of δ is 0.5w, and so the magnitude of d_t is can be safely ignored. For example, for a cantilever test structure with width $w = 100\mu m$, length $L_L = 1000\mu m$,

thickness $t = 5\mu m$, and Poisson's ratio $v = 0.25$, the maximum possible additional deflection due to twisting at the tip of the cantilever is less than 0.5% of the deflection caused by the stylus. Simulations, discussed in section 3.4.1, indicate that this deflection does not have an appreciable impact on the MAT-Test data analysis.
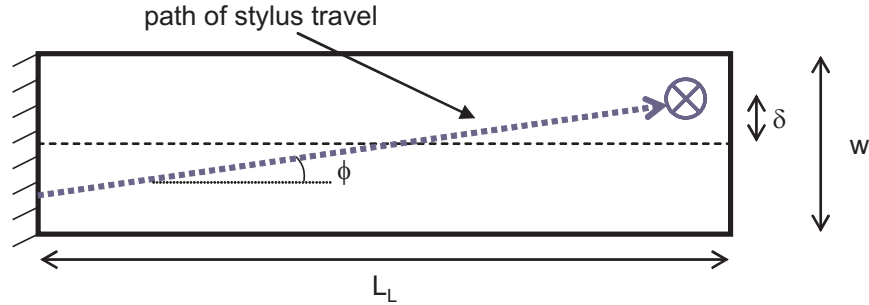
Figure 10 Stylus travel along a microbeam (plan view)

3.3.3 Indentation

Indentation refers to compression of the material underneath the stylus, resulting in a local area of reduced beam thickness. If the beam deflection is being measured by monitoring the position of the element that is applying the load, as in MAT-Test, then this indentation will result in an apparent additional deflection equal to the reduction in beam thickness. Deflection due to indentation, d_{indent}, can be analysed as a Hertzian contact between a rod with radius r (the stylus) and a body (the MUT sample):

$$d_{indent} = \left(\frac{9F^2}{16rE^{*2}} \right)^{\frac{1}{3}}$$

Equation 3-14

where E^* is an effective elastic modulus with the value:

$$E^* = \frac{1}{\dfrac{1-v_{stylus}^2}{E_{MUT}} + \dfrac{1-v_{MUT}^2}{E_{stylus}}}$$

Equation 3-15

Deflection due to indentation is a fixed value that is not a function of L.

3.3.4 Local Deflection

Local deflection is deflection of the beam in the area immediately surrounding the point load (Figure 11). This results in an additional "apparent" deflection, although the beam as a whole is not bent by this amount.

Figure 11 Local deflection of a beam

15

The magnitude of this deflection depends on the ratio of beam width to length, as wide beams have more area which is subject to local curvature. An approximate expression for the local deflection is given by Weihs, et al. [35]:

$$d_{ld} = \frac{6Fw^2\left(1 - \frac{2}{\pi}\right)\left(1 - v^2\right)}{Et^3\pi^3}$$

Equation 3-16

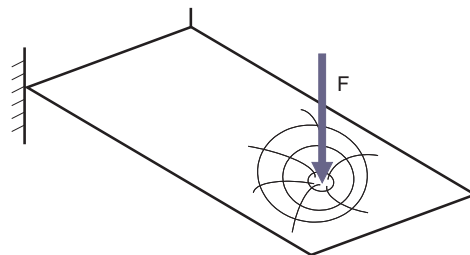This additional deflection is a fixed value that is not a function of *L*. d_{ld} is negligible for beams with a *w/L* ratio of less than 1/2.

3.3.5 Root Deflection and Rotation (undercut)

Root deflection and root rotation are the most significant sources of error in microbeam bending. These effects must be considered for deflection measurements where the microbeams are created by patterning a film deposited on a substrate and then etching the substrate. In general, the same process that removes the substrate underneath the cantilever will also remove some of the substrate from underneath the film at the root of the cantilever. This "over-etched" region of the film is called the undercut (Figure 12). This undercut region acts as an imperfect root support for the cantilever by deflecting substantially when the cantilever is loaded. In addition, the substrate itself may deform and contribute to the non-ideal behaviour of the root of the cantilever. This root deflection and rotation manifest as additional deflection when the microbeam deflection is measured.
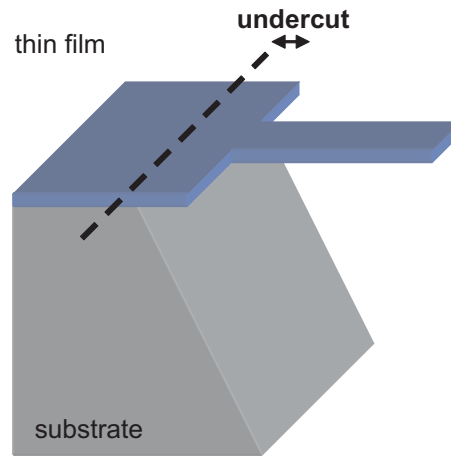
Figure 12 Undercut of cantilever root due to over-etching

It is difficult to derive an exact expression for the deflection of the undercut because its shape is not well defined, and will vary considerably for different processes and materials. A useful way to examine the problem is to consider the deflection of an undercut cantilever to be the deflection of a cantilever with two distinct parts: a wide section near the support (the undercut) and a thin section attached to it (the microbeam). We can then use energy methods to derive an expression for the deflection of a cantilever beam with a discontinuous cross-section. This situation is illustrated in Figure 13. The section attached to the support represents the undercut region of the film. It has length L_u and second moment of area I_u. The cross-section of the undercut region is based on an *effective width* [33] which creates a beam that has the same resisting moment as the undercut region. The second section of the cantilever, with length *L* and second moment of area *I*, represents the microbeam.
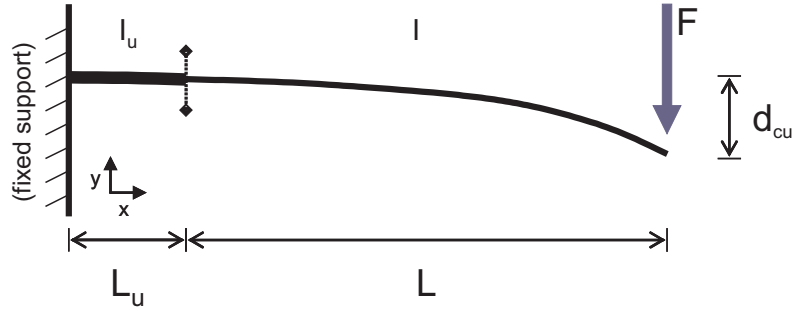
Figure 13 A beam with a discontinuous cross-section

We can solve for the deflection of this structure using Castigliano's Theorem, which describes deflections in terms of the energy equation for the system. The Castigliano's formulation for deflection, d, of a point-loaded cantilever is:

$$d = \int_0^L \frac{M\left(\dfrac{\partial M}{\partial F}\right)}{EI} dx$$

Equation 3-17

where M is the moment developed by the applied load. For the cantilever shown in Figure 13, $M = F(L + L_u - x)$. To solve the discontinuous cantilever system, we simply combine two integrals, one for each section of the cantilever, and use the appropriate I term for each integral. The resulting deflection of the composite beam, including the undercut, d_{cu}, is:

$$d_{cu} = \frac{F}{3E}\left[\frac{L^3}{I} + \frac{3L^2 L_u}{I_u} + \frac{3L L_u^2}{I_u} + \frac{L_u^3}{I_u}\right]$$

Equation 3-18

The leftmost term in the brackets of Equation 3-18 represents the deflection of the cantilever microbeam, and the remaining terms describe the additional deflection due to the undercut. We can see that the additional deflection is a function of both L^2 and L, but not of L^3, so a MAT-Test analysis will not be affected by the undercut.

This result is important because undercut is the most significant cause of additional deflection, and it deserves further investigation. A simple experiment was performed to verify this result. A cantilever was fabricated, scanned with a surface profilometer, and the data was analysed according to the theory described above. Then, using the micromachining laser, the cantilever was modified so that the undercut was removed (Figure 14). The analysis of the two data sets gives the same result, indicating that the presence or absence of the undercut does not affect the L^3 coefficient. Further discussion of experimental results is given in Chapter 4.
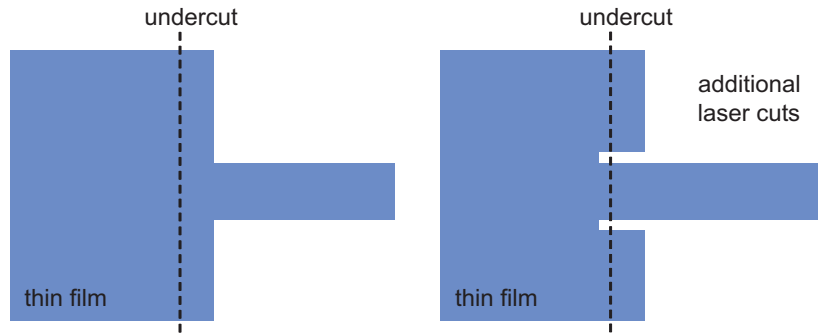
a) experiment schematic (plan view)
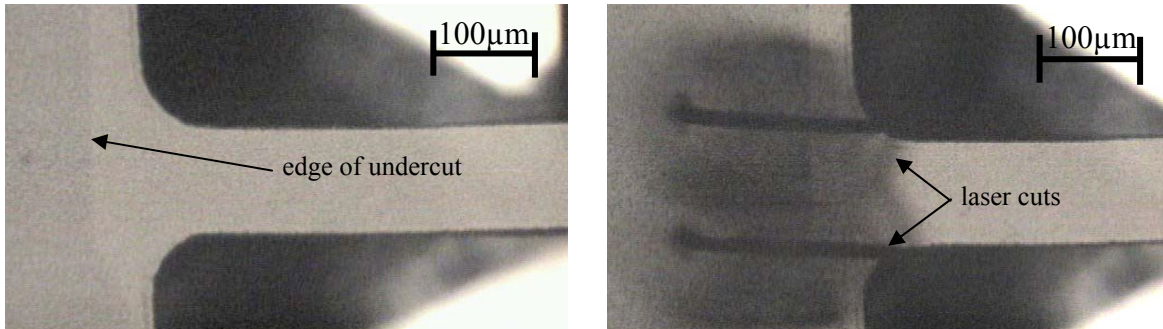
b) microphotographs of the sample: with undercut (l); with undercut removed (r)
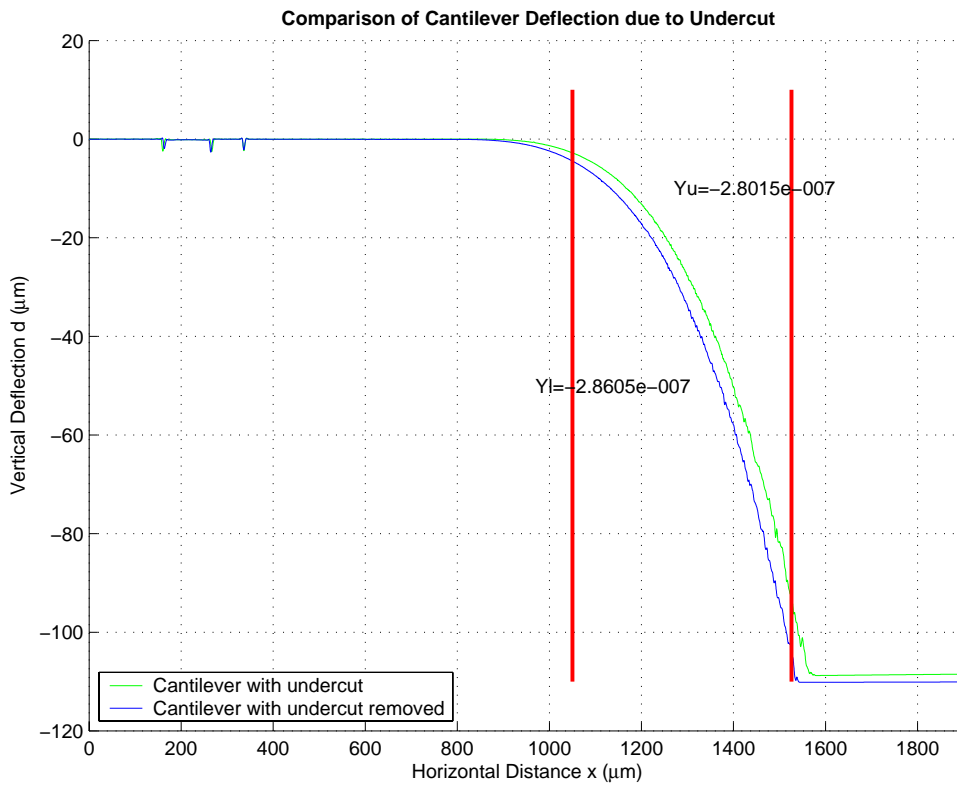
c) experiment data and results

Figure 14 The undercut experiment.
The effect of undercut on a microbeam can be removed by using a micromachining laser to extend the beam after the substrate has been removed. This is illustrated in a), and microphotographs of a sample are shown in b). The profilometer data from the same sample, with and without undercut, is compared in c). A curvefit is performed on each data set over the region between the vertical red lines, and the third-order coefficients, *Y*, from the curvefits are shown on the figure. The third-order coefficients are almost identical, indicating that the undercut does not contribute to deflection as a function of L^3.

Simulation and other data analysis results also support the conclusion that deflection due to undercut is a function of L^2 and L. Other investigators, including Menčik and Nix [34, 36], have reported similar results based on empirical analysis of their data. Zhang, et al. [37], report extensive modelling of imperfect root conditions based on Finite Element Method (FEM) simulations and coupled-spring models. They also conclude that the additional deflection due to imperfect root conditions can be described in terms of L^2 and L. FEM simulations performed for this work (see section 3.4.1) show that the undercut does not affect the L^3 coefficient.

Although the precise amount of additional deflection due to undercut remains difficult to predict for specific cases, we can safely conclude that it is not a function of L^3.

3.3.6 Substrate Deformation

Substrate deformation is compression or dislocation of the substrate at the root of the cantilever. Substrate deformation contributes to root rotation and deflection as functions of L^2 and L, as discussed above.

3.3.7 Beam Stiffening

Beam stiffening is the result of the combination of lateral and longitudinal stresses in the beam. These stresses cause the cross-section of the beam to deform in complex ways [21] and this causes the beam to become effectively stiffer than expected. This effect is described in relation to Poisson's ratio in section 3.2.4. The magnitude of stiffening can be expressed by the parameter K, which is (Equation 3-10 repeated):

$$K = \frac{12FLw}{Et^4}$$

<div style="text-align: right">Equation 3-19</div>

The magnitude of the stiffening effect depends on L. However, it manifests itself as a modification of the value of E, so it does not affect our interpretation of the MAT-Test bending data directly. Instead, it affects our interpretation of the value of E that we extract from the bending data. In order to maintain the accuracy of our measurement of E, we need to operate MAT-Test with low values of K (assuming that the value of Poisson's ratio for our material is not known). This condition effectively sets a lower limit on the film thickness that we can measure accurately. In practice, this limit is about $t = 3\mu m$ (see section 3.5.6). If we are measuring films above this limit, we can neglect the effects of beam stiffening.

3.3.8 Applied Force Direction

The direction of the applied force that loads the cantilever test structure (the profilometer stylus) is initially normal to the surface of the substrate, or close to it. As the stylus travels along the beam and deflects it, the rotation angle of the beam increases, so that a horizontal reaction force is developed (Figure 15). This reaction force contributes an additional moment. A similar moment will appear if the point load application does not slip smoothly along the beam as the rotation angle increases.
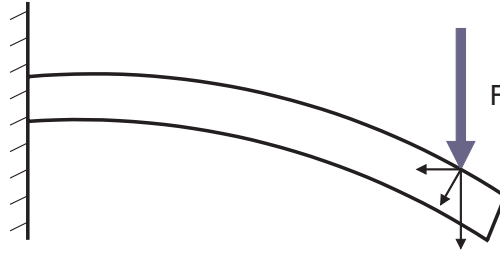
Figure 15 Additional force component due to large rotation

This additional moment does not contribute to deflection, but it does contribute to the stress developed in the beam, and so may affect the breaking stress measurements. A simple correction factor for stress can be used [38]:

$$\sigma_{corrected} = \sqrt{\frac{\tan\theta}{\theta}}\,\sigma_{measured}$$

Equation 3-20

where θ is the rotation angle of the tip of the beam. However, beams in MAT-Test are operated in the small-deflection regime, for which the rotation angle is small. The error in stress is fractions of a percent at most, so we can ignore the effects of applied force direction.

3.3.9 MUT Intrinsic Stress

Intrinsic Stress in deposited films is relatively common. An internal stress gradient in the MUT will cause the test structure to bend upward or downward with the internal moment caused by the stress. For a linear stress gradient, this internal moment, M_i, can be expressed as:

$$M_i = \frac{1}{6}wt^2\sigma_i$$

Equation 3-21

where σ_i is the maximum stress in the film, either at the top or the bottom surface. The magnitude and compressive or tensile nature of σ_i would determine the direction of the moment M_i. This moment manifests itself in deflection of the beam, d_σ:

$$d_\sigma = \frac{M_i L^2}{2EI}$$

Equation 3-22

The bending due to an internal stress gradient in the film is a function of L^2.

It should be noted that an internal stress gradient is different from a film stress due to interactions with the substrate (e.g., lattice or thermal expansion mismatch). Such a film stress in the cantilever is relieved when the substrate is removed from underneath it, and it has no effect on the deflection of the cantilever, except to contribute a small constant rotation at the root.

3.3.10 Friction and Stiction

Friction or stiction between the profilometer stylus and the MUT would manifest itself in two ways: as skewing or distortion in the profilometer data trace as the sample is

dragged or the scan distance is shortened by sliding friction between the stylus and the sample; or as dislocations in the data trace as the microbeam "stretches out" under the stylus and then releases suddenly when the accumulated elastic force overcomes stiction between the sample and the stylus. However, the profilometer stylus is typically made of diamond, which has a low coefficient of friction with standard materials, as well as a small contact area (12.5μm tip radius is typical) with the sample. The stylus travels relatively quickly (40-150μm/second is typical), so there is no opportunity for static stiction to develop, and the force applied by the stylus is not large enough to deform most samples appreciably. No such effects have been observed in any MAT-Test experiments, or reported in any related work, and they are considered to be negligible.

3.3.11 Beam Mass (self-weight)

The mass of the cantilever test structure will cause it to deflect under its own weight. This deflection is constant amount for a beam with total length L_L. The additional deflection measured by the surface profilometer is equal to the shape of the beam deflected under its own weight. For the MAT-Test data, this shape is given by:

$$d_{weight} = \frac{F_{weight}}{EI} \left[\frac{L_L L^3}{6} - \frac{L^4}{24} \right]$$

<div align="right">Equation 3-23</div>

where F_{weight} is the force applied per unit length along the beam by its own weight and L_T is the total length of the cantilever. This deflection *is* a function of L^3. However, the mass of the cantilever test structures, as with most MEMS components, is so small that the effects of gravity are easily negligible, and we can safely ignore it for our analysis. For example, assume that a MUT sample has the density of lead, 11340 kg/m^3. The additional deflection at the tip of a cantilever test structure with width w = 100μm, length L_L = 1000μm, and Young's modulus E = 300 GPa is approximately 0.02μm. The predicted tip deflection due to an applied load of 5mg, the smallest load used in this work, is more than 50μm.

3.3.12 Scan Path Misalignment

When the surface profilometer stylus is scanned along the length of the cantilever test structure, it is unlikely to be in perfect alignment with the centreline of the cantilever (Figure 10). This misalignment causes the surface profilometer to record a length, L_ϕ, that is slightly longer than the true length of the test structure. This can be expressed in terms of the misalignment angle, ϕ:

$$L_\phi = \frac{L}{\cos \phi}$$

<div align="right">Equation 3-24</div>

This error manifests as a constant scale factor in all values of L that are measured, so it should not present a problem for later analysis of the data. In any case, the maximum possible value for ϕ is $\tan^{-1}(w/L)$ of the cantilever, which is less than 4º for the MAT-Test test structure (see section 3.5 for a discussion of the design of the MAT-Test test structures). This corresponds to a 0.2% error in the length of L, in the most extreme case. Averaging several measured values of E can reduce this error even further. Therefore, we can safely disregard the effects of scan path misalignment.

3.3.13 Sample Horizontal Angle Misalignment (levelling)

Horizontal misalignment refers to a situation where the nominal zero level of the sample is not horizontal with respect to the scan path of the profilometer. This sort of misalignment is fairly common in surface profilometer measurements. It can be caused by a variety of things: a sample whose back side is not horizontal with respect to the front side, debris on the sample or on the sample stage, or stage misalignment.

This horizontal angle misalignment manifests itself as an additional deflection, d_{level}:

$$d_{level} = L \tan \vartheta \qquad \qquad \text{Equation 3-25}$$

Where ϑ is the angle of misalignment from the horizontal. d_{level} is a linear function of L. Surface profilometers generally include automatic routines for correcting the effects of ϑ. The use of these routines does not affect the use of the surface profilometer data for MAT-Test.

3.3.14 Data Horizontal Offset

When the data from the profilometer is analysed, the start of the data ($x = 0$) typically will not coincide with the root of the microbeam ($L = 0$). The test operator must select the region of the profilometer data that will be analysed, and there is an error involved in this process. This means that the profilometer data will effectively be analysed with an offset, x_0. However, this offset does not affect the value of the coefficient of the highest-order term in the polynomial:

$$Y \cdot \left(x - x_0\right)^3 + U \cdot \left(x - x_0\right)^2 + S \cdot \left(x - x_0\right) + T \qquad \qquad \text{Equation 3-26}$$

If we expand Equation 3-26 and collect terms, we find:

$$Y \cdot x^3 + \left(-3 \cdot Y \cdot x_0 + U\right) \cdot x^2 + \left(3 \cdot Y \cdot x_0^2 + S - 2 \cdot U \cdot x_0\right) \cdot x - Y \cdot x_0^3 + T - S \cdot x_0 + U \cdot x_0^2 \qquad \text{Equation 3-27}$$

We can see that the value of the third order coefficient (Y) is not affected by the x_0 offset, although the other coefficients are. Therefore, when the operator selects the portion of the profilometer data to analyse, the only criteria for the selection is that the data must not include areas that are not on the cantilever. For a left-to-right scan starting at the root, an arbitrary offset of the data origin to the right (x-x_o) has no effect on the MAT-Test analysis, but an offset of the origin to the left (x+x_0), will include data that does not represent the bending of the microbeam. As long as the profilometer data being analysed includes only data from bending of the microbeam, the position of the origin does not matter.

3.3.15 Test Equipment Errors

MAT-Test is designed to be used with a profilometer, and there are three possible sources of error that the surface profilometer can introduce.

The first task of the profilometer is the actual measurement of deflection. This is the primary measurement goal of a surface profilometer, and so in general their performance is very good, with typical quoted precision of +/- 0.1nm. In any case, the MAT-Test analysis does not depend on the measurement of absolute deflection, so we can assume that the deflection data is correct for our purposes.

The second task of the profilometer is to move the sample to a given position, or equivalently, to move the stylus tip a given amount. This is the second most important task of a profilometer, and again, their performance is quite good, with typical positioning accuracy of better than $0.1\mu m$. Tests on different profilometers have detected no measurable error in the stage or stylus horizontal movements. Because any offset in the MAT-Test position data is not relevant, the absolute position accuracy is not important, only the relative distances between data points are of concern. If the distances between data points were shown to be inaccurate by some scaling factor, the error could be removed from the data simply by multiplying the data by the scaling factor. So we can assume that the horizontal position data from the profilometer is correct for our purposes.

The third potential source of equipment error is the force applied by the surface profilometer. The accuracy of the force applied by the stylus does not affect the accuracy of the surface profilometer in normal use, and so we do not expect the profilometers to exhibit high performance in this area. Test structures were devised to measure the force actually applied by the surface profilometer (section 3.1.4), and this measured force is used in the MAT-Test analysis.

3.3.16 Summary of Error Effects

The error effects and their description as a coefficient in Equation 3-4 are summarized in below.

Error Effect	Coefficient of Bending Equation Term
1. Shear Stress [n]	L
2. Torsion (twisting) [n]	L^3, L
3. Indentation [n]	N/A
4. Local Deflection [n]	N/A
5. Root Deflection and Rotation (undercut)	L^2, L
6. Beam Stiffening	L
7. Applied Force Direction [n]	N/A
8. Internal Stress Gradient	L^2
9. Substrate Deformation	L^2, L
10. Friction/Stiction [n]	N/A
11. Beam Mass [n]	L^4, L^3
12. Scan Path Misalignment [n]	N/A
13. Vertical Angle Misalignment (levelling)	L
14. Horizontal Data Offset	N/A
15. Test Equipment Errors	N/A

[n] indicates a negligible effect for MAT-Test test structures

In the table above, all of the relevant error effects have been identified, along with their contribution to the coefficients of Equation 3-4. There are only two error effects which contribute to the cubic coefficient *Y*, from which we extract Young's modulus. Fortunately, they are both negligibly small effects: cantilever beam mass is miniscule, and careful design allows us to keep the torsion/scan path misalignment errors small. The most serious effects, those of root deflection and rotation due to undercut, manifest themselves in lower-order terms, so they do not affect the results of a MAT-Test analysis.

This list of errors applies to all beam-bending methods, but the list does not indicate their magnitude or potential for causing error in absolute deflection measurements. We can see that quantifying the precise value of all of the individual error effects in a given experiment would be a daunting task. Exactly this issue has limited the accuracy and applicability of previous work in this area.

3.4 Simulation

3.4.1 Deflection

Many of the deflection error effects discussed in section 3.3 are difficult or impossible to quantify for the MAT-Test test structures. Finite Element Method (FEM) simulations were used to attempt to simulate the bending of MAT-Test cantilevers in order to verify the theoretical analysis. The FEM simulations were performed using a FEM software package called FEMLAB [40]. FEMLAB is a plug-in software package for MATLAB [41], the popular data-manipulation software.

The simulations were performed using the Structure Mechanics Engineering module of FEMLAB. The mesh element used was the "Kirchhoff Plate", which is a two-dimensional element that permits loads in the z-direction and moments about the x and y axes. This element provides valid results if the thickness of the element is small compared to the other dimensions, which is true for the MAT-Test test structures.

From the discussion of error effects in section 3.3, we see that the most significant effect we need to investigate is the rotation and displacement at the root due to the undercut during the etch. We would also like to investigate the effect of torsional deformation (twist), because the theoretical analysis indicates that it can affect the third-order coefficient directly. FEMLAB codes were designed which simulated and compared three cases of undercut: no undercut, a rectangular undercut, and a semi-circular undercut. The simulation codes included the ability to simulate a stylus travelling away from the centreline of the beam.

Typical FEMLAB simulation results for beams with increasing undercut depth are shown in Figure 16. We can see that the deflection of the cantilever beam with an undercut is much greater than the corresponding ideal Euler beam, as expected. Figure 17 shows the results of a third-order polynomial curve fit to an individual simulated beam. The fit of the third-order polynomial is very good, with typical coefficient of determination (r^2) values of 0.9999 or better. The Young's modulus that was used in the simulation is extracted from the *Y* coefficient with less than 0.1% error for a variety or undercut shapes and sizes. The results serve to reinforce the contention, discussed in section 3.3.5, that the effect of undercut on the bending of the beam can be isolated from the simple bending of the beam. The results of simulations that included the stylus travelling away from the centreline show similarly negligible effects.
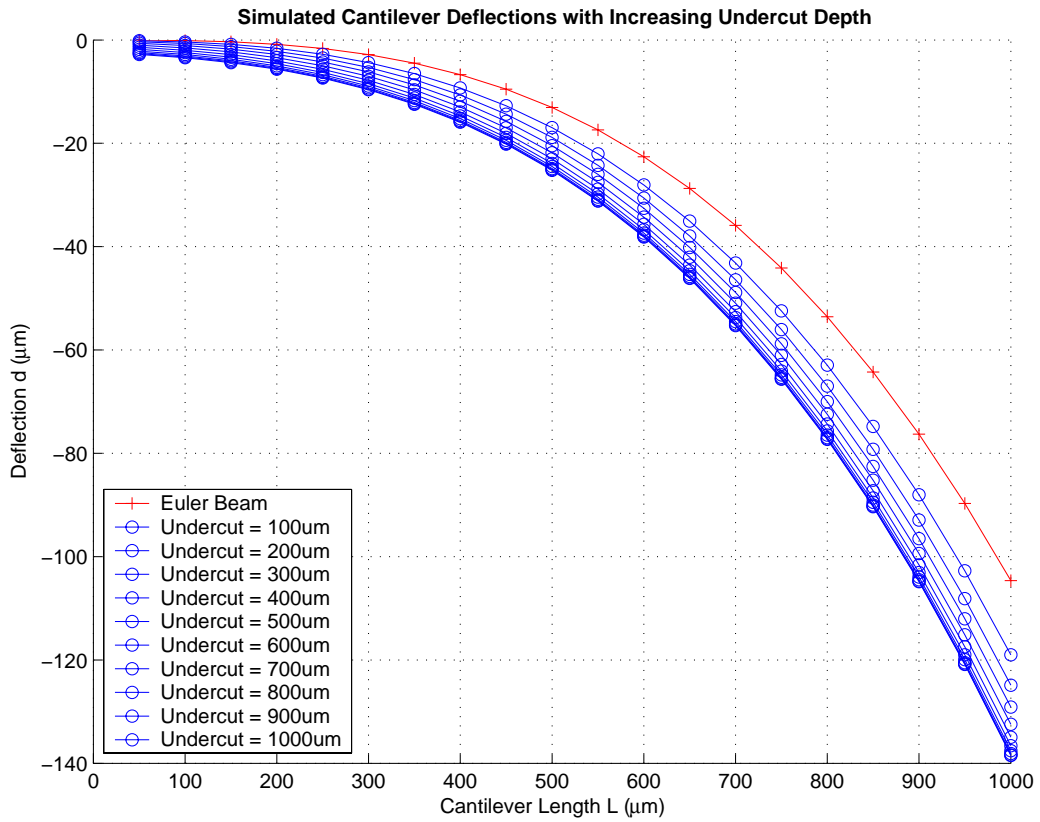
Figure 16 Simulated beam deflections (blue o) compared with ideal beam deflection (red +)
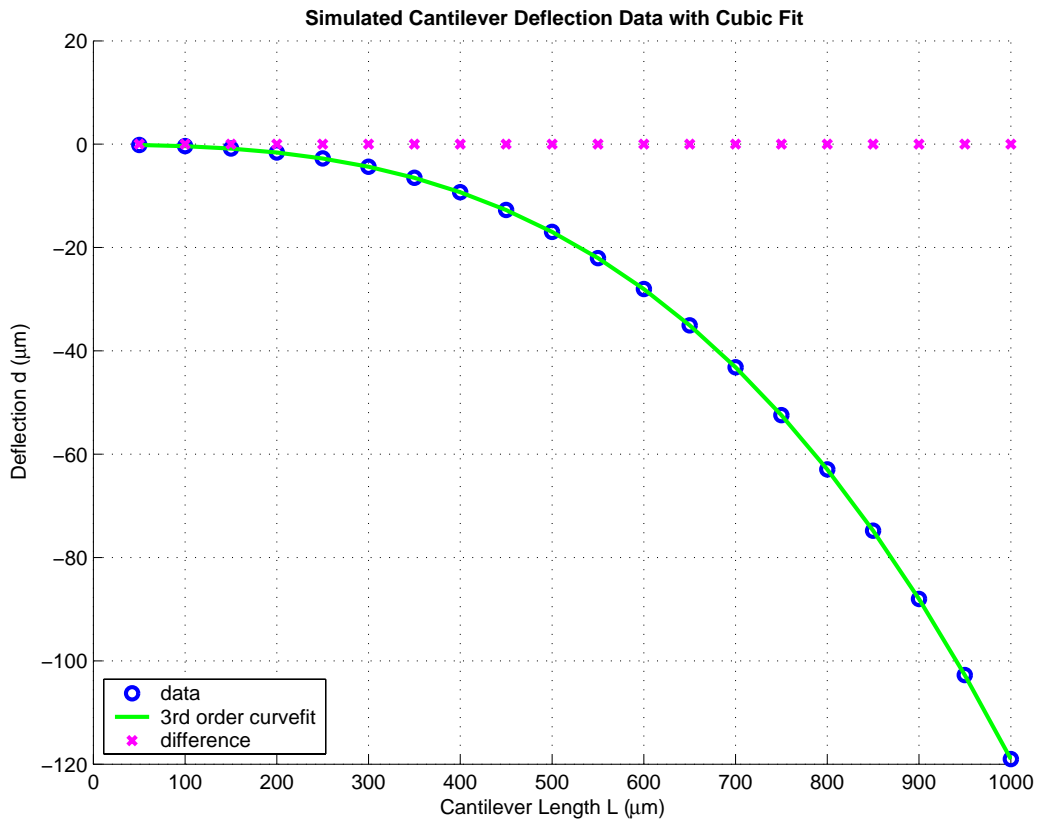

Figure 17 Simulated data (blue o) with curve fit (green line) and the difference between them (purple x)

3.4.2 Stress

FEMLAB simulations of the stress in the MAT-Test test structures were performed to investigate the effect of test structure geometry. Figure 18 shows a typical graphical output from FEMLAB, with stress magnitude plotted as colours on the surface. We expect stress concentrations to develop at discontinuities in the geometry of the test structures, particularly the corners where a rectangular cantilever joins the supporting base. These stress concentrations can cause the stress that occurs in the test structure to be significantly greater than the stress predicted by the moment equation given in Equation 3-2.

Stress concentrations can be quantified in terms of stress concentration factors (SCF), where the maximum stress developed at the location of a stress concentration is equal to the nominal stress multiplied by the SCF. In the case of the MAT-Test test structures, the SCF at the root of the cantilever can be related to the ratio of the radius of the corners to the width of the cantilever. A larger SCF is expected at a corner with a smaller radius of curvature or a larger cantilever width. Therefore, the breaking stress test structures were designed with large semi-circular cut-outs at the corners of the base of the beam. For a rectangular cantilever with a corner radius of 1μm and width of 100μm, standard references [42] give an SCF of between 4 and 4.5, and the FEMLAB simulations agree with this value. For a breaking stress test structure with semi-circular cut-outs at the corners (radius 37.5μm, width 25μm, see Figure 18 and also Figure 25 on page 33), simulations indicate that the stress will be only 3-5% greater than the stress predicted by the moment equation. The design of the breaking test structures is discussed further in section 3.5.4.
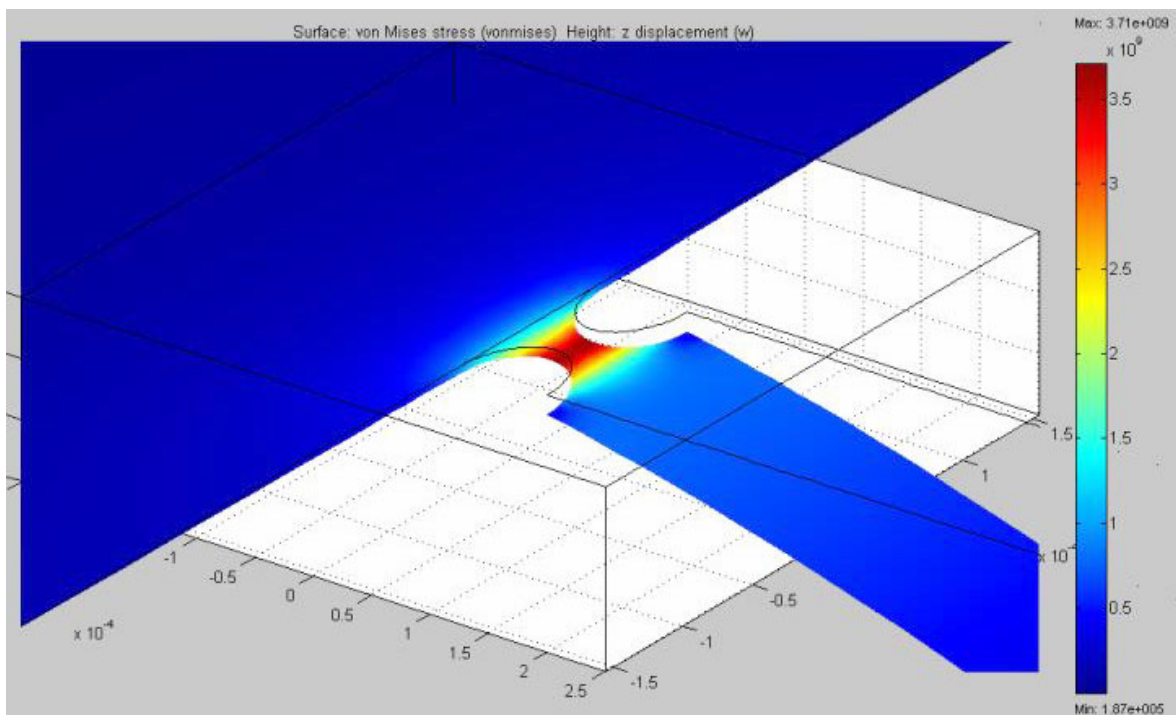

Figure 18 Graphical output from FEMLAB, showing a breaking stress test structure being deflected. Magnitude of stress (Tresca stress) is shown as colours on the surface.

Further discussion of the FEMLAB simulations and the FEMLAB codes written to perform the simulations is given in Appendix C.1.

3.5 MAT-Test Design

3.5.1 Measurement Design Goals

The desired measurement range of the quantities of interest are given below:

Mechanical Property	Desired Measurement Range
Young's modulus, E	10-1000 GPa
Breaking stress, σ_b	0.1-10 GPa
Poisson's ratio, ν	0.1-0.5

These values represent the expected values of thin films of interest, based on a survey of previously reported values for known films and desirable values for unidentified films.

3.5.2 Test Structure Form

The test structure chosen for MAT-Test is the rectangular cantilever microbeam, which achieves simplicity and isolation of the material properties of interest. Rectangular cantilevers are desirable because their width is constant along their length, so that the data from a single scan of a rectangular cantilever is equivalent to scanning many cantilevers of different lengths (see Figure 7 and section 3.2). Other microbeam shapes were considered, particularly triangular cantilevers, because they develop a uniform stress along their length when bent [43], as opposed to rectangular cantilevers which develop a maximum stress at the root. However, triangular cantilevers can not be analysed as described in section 3.2, because the effective shape changes as the point of application of the load moves along its length. Rectangular fixed-fixed beams were considered, and they offer advantages in terms of robustness during fabrication and reduced deflection requirements. However, cantilevers are free of the effects of film stress due to mismatch with the substrate, which can cause deformation and buckling of fixed-fixed beams.

3.5.3 Test Structure Design Constraints

There are two general constraints that inform the design space for the cantilever test structures: the constraints of the Euler approximation, and the capabilities of the equipment we intend to use.

The Euler Approximation

The Euler approximation relates the exact curvature of a bending beam in intrinsic coordinates s and θ to the position of the beam in Cartesian coordinates x and y [30]:

$$\frac{d\theta}{ds} \approx \frac{d^2 y}{dx^2}$$

<div align="right">Equation 3-28</div>

where deflection is in the y direction. This approximation forms the basis for the Euler small deflection equation (Equation 3-1). This equation is central to the MAT-Test analysis, so we must work within the limitations imposed by the Euler approximation.

The primary limitation imposed by the Euler approximation is that it is valid for only for small deflections, i.e., angles for which the slope dy/dx is small compared to one.

As the deflection increases, the error introduced by the Euler approximation increases. The analytical solution for the exact deflection of a beam is called the Elastica [44, 45]. The solution of the Elastica is difficult and inflexible, as it requires elliptic integrals, and so the Euler approximation is normally used for beam analysis. When the deflection is less than 10% of the length, the difference between the exact (Elastica) and approximate (Euler) deflections is approximately 1%. For deflection of 15% of length, the error is 2.3%. Figure 19 is a plot of Elastica deflection compared with Euler deflection, and Figure 20 is a plot of the percentage difference between the two. The results in Figures 19 and 20 show that we need to keep the deflection of the MAT-Test test structures to less than 15% of their length in order to keep the error introduced by the Euler approximation acceptably small.
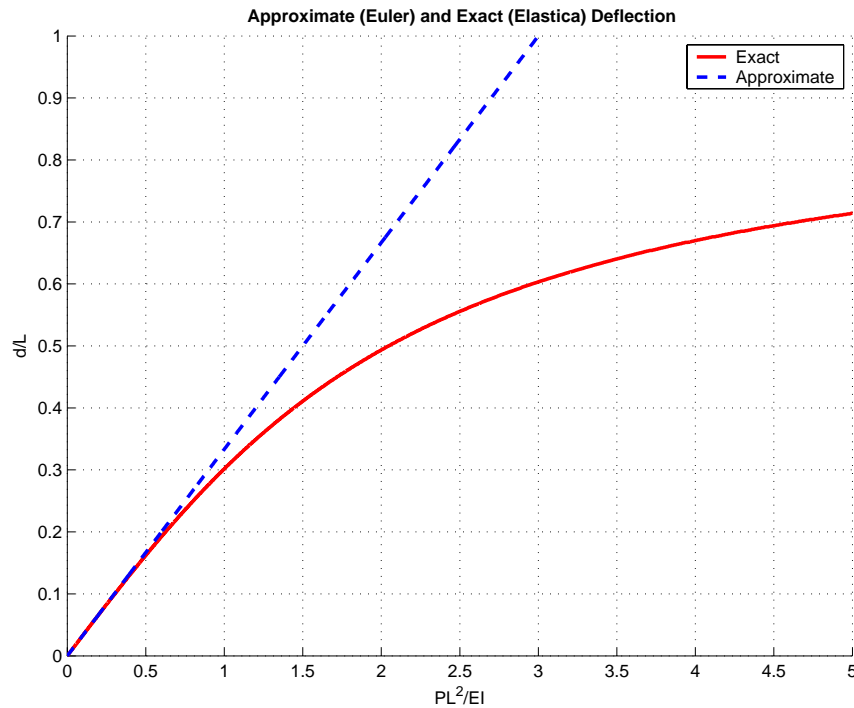
Figure 19 Elastica (exact) deflection and Euler (approximate) deflection of a cantilever beam

A second constraint of the Euler approximation is that the length to width ratio for the beam must be at least 5, so that we can safely describe the beam as a beam rather than a plate (see section 3.2.4 for a discussion of plate versus beam bending in MAT-Test).

The Euler approximation also imposes constraints on the film thickness, because the film thickness has a significant effect on the bending of the beam (for a given length and width). The flexural rigidity of the beam is a function both of I and E. I, the second moment of area, is a function of $1/t^3$ (Equation 3-1, Euler beam deflection), and E is a function of $1/t^4$ (Equation 3-10, Young's modulus correction factor). As the length and width of the cantilever are determined by equipment requirements (see below), this means that thicker is better for MAT-Test. In general, 1μm is the lower limit established by Euler beam deflection, and 3μm is the limit from the Young's modulus correction factor, although both are subject to other test parameters (see section 3.5.6).

28

Figure 20 Percentage error between Elastica deflection and Euler deflection

Surface Profilometer Capabilities
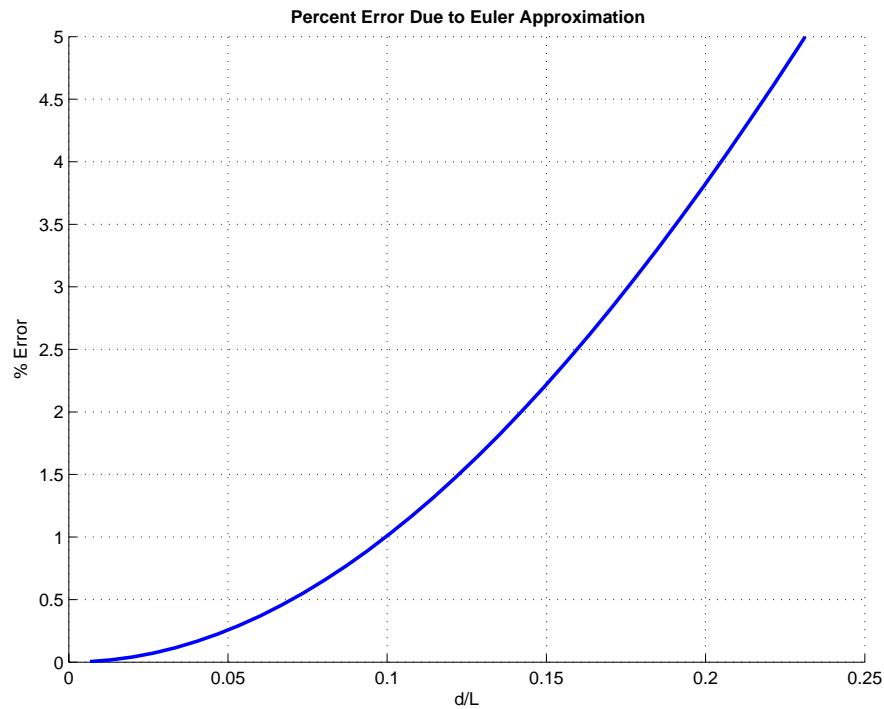
MAT-Test uses standard surface profilometers to deflect the test structures. Surface profilometers are typically used for measuring the thickness of deposited films, so they are not optimised for beam-bending tests. The relevant capabilities of contact surface profilometers are given below:

Capability	Typical Range
Applied load, P	1-50 mg
Microscope magnification	20-400 x
Scan Length	0.05-50 mm

These values are the largest range of values typical of surface profilometers used in microfabrication. Three surface profilometers were investigated during the course of this work: the Dektak IIA and the Dektak 3ST, both manufactured by Veeco, Inc. [46], and the AlphaStep 200, manufactured by Tencor Instruments, now called KLA-Tencor [47]. Specific machines, especially older models, may not have the capabilities listed above. This is a significant issue because surface profilometers tend to have a very long service life. The use of the profilometer is a low-stress operation that creates little wear and tear, and the few consumables can be easily replaced for much less than the cost of a new machine. Therefore, it is quite common to see 10-20 year old profilometers in active service, especially in research and development laboratories, and they have a high resale value.

3.5.4 Test Structure Design

Once the test goals, test structure format, analytical limitations, and equipment constraints have been identified, the MAT-Test test structures can be designed.

29

The first limiting constraint we must satisfy is the microscope magnification available on the surface profilometer. Basically, we have to be able to see the test structures. The operator of a surface profilometer must align the structure to be profiled with the profilometer stylus. The positioning microscope, often with a video camera attached, is focused on the stylus. The sample is placed on a stage and moved until it is in position, as verified by the view through the microscope (Figure 21).
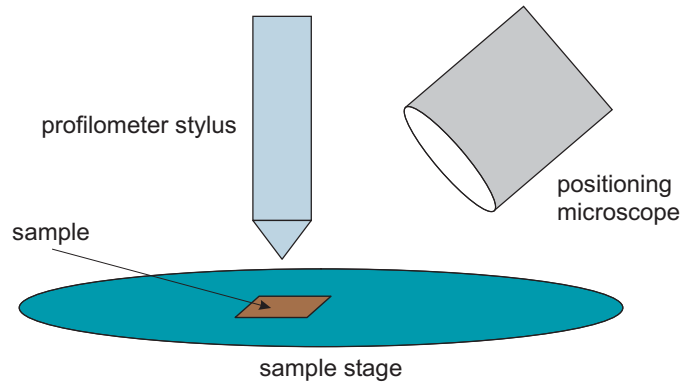

Figure 21 Surface profilometer schematic

From Figure 21, we can see that the microscope must be located away from the sample in order to allow the stylus to approach the sample. The positioning microscope is also mounted at a significant angle away from the normal, at least 30º, so that surface features can be seen in relief, to aid in positioning the stylus. The combination of long working distance and large viewing angle mean that the effective magnification of a surface profilometer positioning microscope is limited, often to less than 100x. The MAT-Test test structures must be large enough to allow the stylus to be aligned to the test structure over the whole of its length with confidence. Practical experience with different surface profilometers indicates that the test structures should be at least 100μm wide.

Now that the width, w, has been established, the total length, L_L, must be at least $5w$ to satisfy the Euler approximation. Because MAT-Test uses curve fitting, and curve fitting accuracy improves with the number of data points available, we would like to use longer beams. $L_L = 10w$, or $L_L = 1000$μm, is more than sufficient. The ideal MAT-Test test structure, then, is a rectangular cantilever 100μm wide and 1000μm long.

In practice, we find that we can use somewhat smaller cantilever test structures if necessary. A skilled operator using well-maintained equipment can work with cantilevers that are as small as 50μm wide, and useful data can be obtained from cantilevers as short as $L_L = 5w$, i.e., 50μm × 250μm. However, to ensure a robust test that can be used with accuracy with a variety MUT/surface profilometer combinations, cantilevers with dimensions $w = 100$μm and $L_L = 1000$μm are recommended.

3.5.5 Additional Design Issues

Additional features are desirable in the test structures to make them easier to use or to improve the quality of the data they produce.

Alignment marks are added to the basic cantilever design. The alignment marks consist of a pair of angled lines and a line perpendicular to the length of the cantilever (Figure 22). These marks provide a known reference point in the profilometer scan data, so

that distances can be easily measured for breaking stress measurements. The reference points created by the alignment marks can be seen near the left side of the profilometer data in Figure 40. The alignment marks also serve to reduce the maximum misalignment angle of the stylus to the cantilever by increasing the effective L_L. If the stylus passes over the alignment mark and across the end of the cantilever, than it must have travelled within the rectangle defined by the alignment mark and the cantilever. For a 100μm × 1000μm cantilever with the alignment mark 500μm away, the maximum misalignment angle is 3.8º (Figure 22). The additional angled alignment marks were designed to be used to align the scan path to the cantilever, although in practice this proved to be unnecessary.

The corners of the cantilever test structures where they join the remaining film (at the root) can cause stress concentrations which may cause unpredictable fracture effects. A corner fillet with a radius of 50μm was used to minimize these effects.
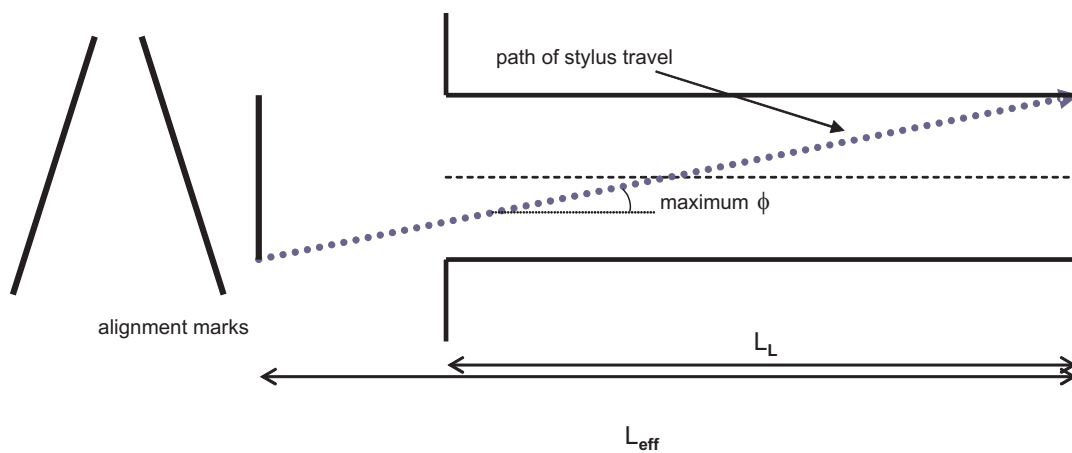

Figure 22 Maximum misalignment angle reduced by alignment marks

3.5.6 Measurement Space

Given the cantilever test structure design and the constraints of the small-deflection approximation and surface profilometer capabilities, we can now investigate the measurement space of MAT-Test. Note that the force specified by the profilometer is given in terms of an applied load (mass), P, in milligrams, rather than a force, F, in Newtons, because profilometers specify the force this way for historical reasons[5]. The applied force is, of course, $F = Pg$, where g is acceleration due to gravity (9.81 m/s).

Young's Modulus

Once the size of the cantilevers has been defined, the measurement space for Young's modulus is defined by the remaining variables in Equation 3-1, the Euler deflection equation: film thickness, the applied force, the deflection, and the Poisson's ratio of the material. In general, high values of E or large film thicknesses do not limit the possible measurements. Instead, achieving measurements of low values of E and working with thin films are the challenges. Essentially, we need to minimize the right hand term in Equation 3-5. This means that we want to work with the smallest test structures and lowest forces that we can use. Of course, the primary constraint for a given measurement depends

---

[5] Profilometers that were designed using Imperial units specified the applied load in pounds, which is the Imperial unit of *force*. When these designs were converted to SI units, pounds were converted to kilograms, which is standard practice for converting measures of weight. However, kilograms are the SI unit of *mass*.

on the specifics of the experiment. For example, a MUT sample may only be available in a certain thickness, or the available profilometer may have a limited force range.

The first parameter to consider is the error due to the Young's modulus correction factor, ψ. Figure 23 is a plot of the value of ψ as a function of film thickness and Poisson's ratio, for profilometer load of 5mg, an expected Young's modulus value of 300 GPa, and the ideal test structure size of 100 x 1000 μm. For films with a reasonable value of v (0.3), we can see that we would like to have at least a 3μm film in order to be reasonably confident of our measured value of E. If we assume the worst for v, then we would like to have a 4μm sample. Lower values of E increase the error, as the sample is more compliant.
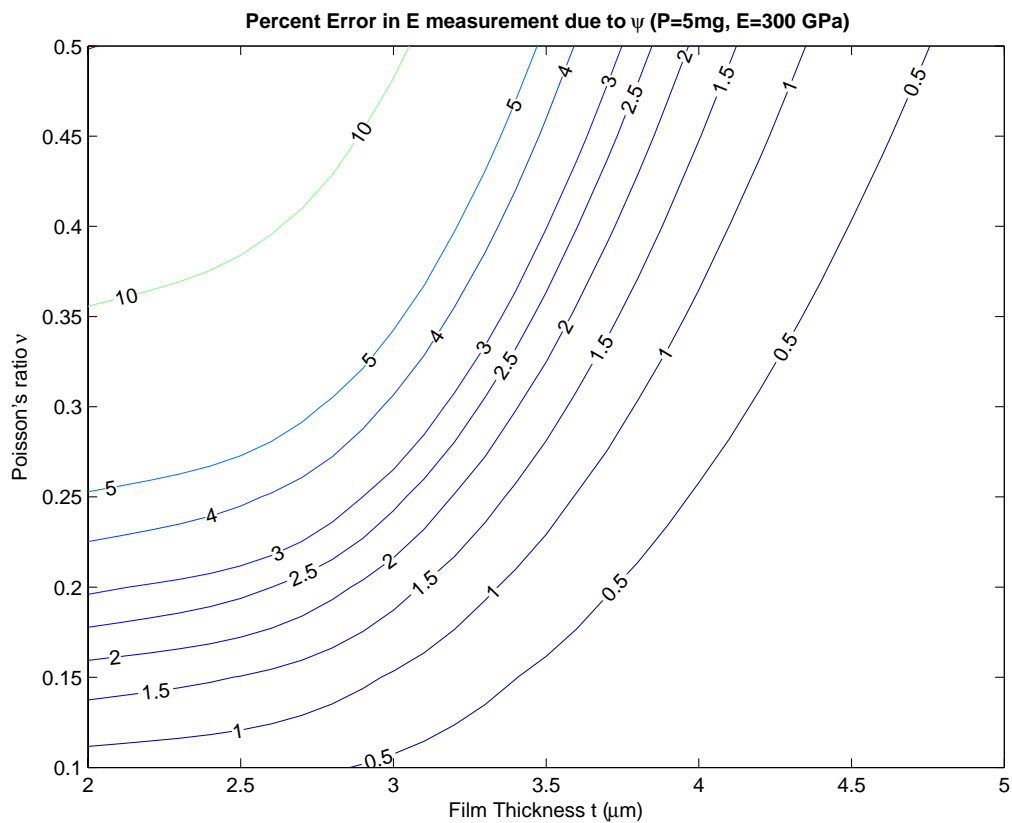
Figure 23 Percent Error in E due to ψ

The next consideration is the range of E values that can be measured for a given film thickness. Figure 24 is a plot of the percentage error in the measurement of E introduced by the Euler assumption for a range of film thicknesses, for the same values of cantilever dimensions and applied force. We can see that the effective measurement range is severely limited for thin and/or compliant films.

If we can adjust the other parameters of the test– lower the applied force, or reduce the size of the test structures– we can increase the range of film thicknesses that can be examined. The obvious route is to reduce the size of the test structures, but, as mentioned above, smaller test structures are difficult to work with using typical surface profilometers. However, we can expect all of the limits on the test to expand as the capabilities of surface profilometers are improved.
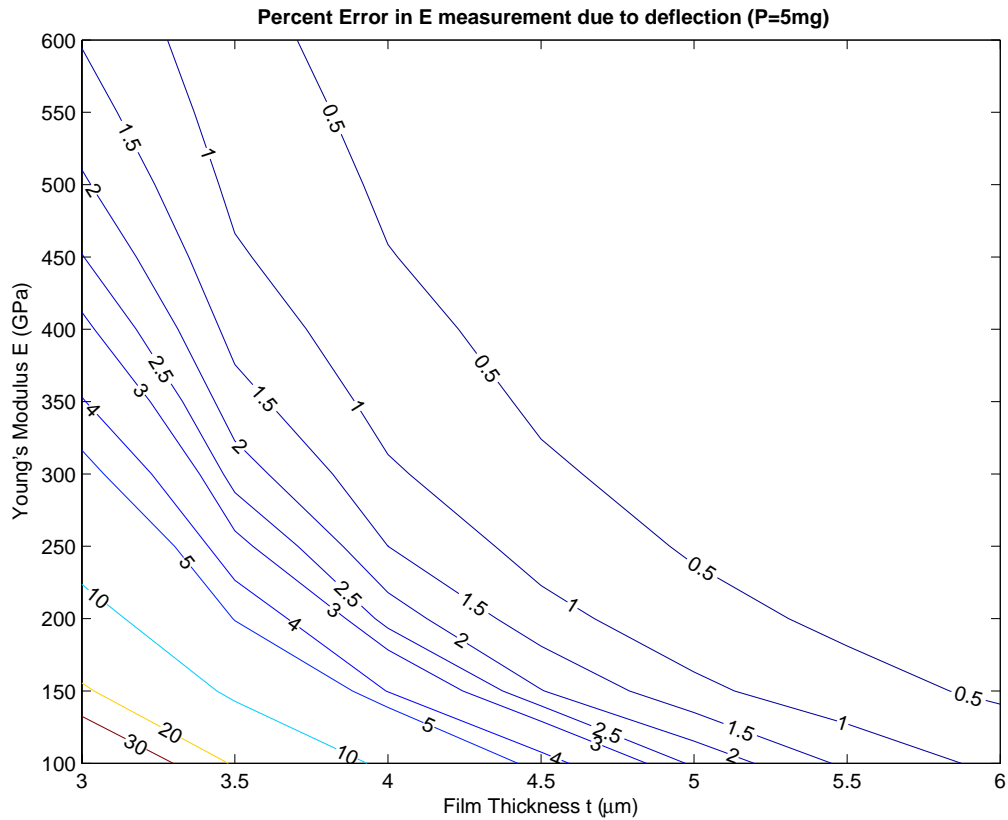
Figure 24 Percent Error in *E* due to *d/L*.
The error comes from the Euler small-deflection approximation, for which d/L must be kept small.

Breaking Stress

The maximum stress developed in a cantilever is given by Equation 3-2. In order to create stress in the beam equal to the breaking stress, σ_b, we need to maximize this expression, given that the maximum moment we can apply to the beam is determined by the length and the applied load. We can do this by reducing *w*. Of course, we need to keep the beam wide enough to work with, but because we can relate stress to the moment load at a location on the cantilever, we can simply reduce the width for a small portion of the beam, while keeping the remainder wide enough to work with. The reduced width portion of the beam has a semi-circular profile in order to reduce the effect of stress concentrations (section 3.4.2). Figure 25 shows the design of the breaking stress test structures.

Figure 25 Plan view of cantilever layout with reduced *w* for breaking stress measurements

Starting with a 100μm wide cantilever, we can reduce the width to 25μm without straining the patterning capabilities of a typical microfabrication facility. A plot of the

maximum stress we can create in the portion of reduced width is Figure 26. We see that we can cover the desired measurement range for most films and surface profilometers.
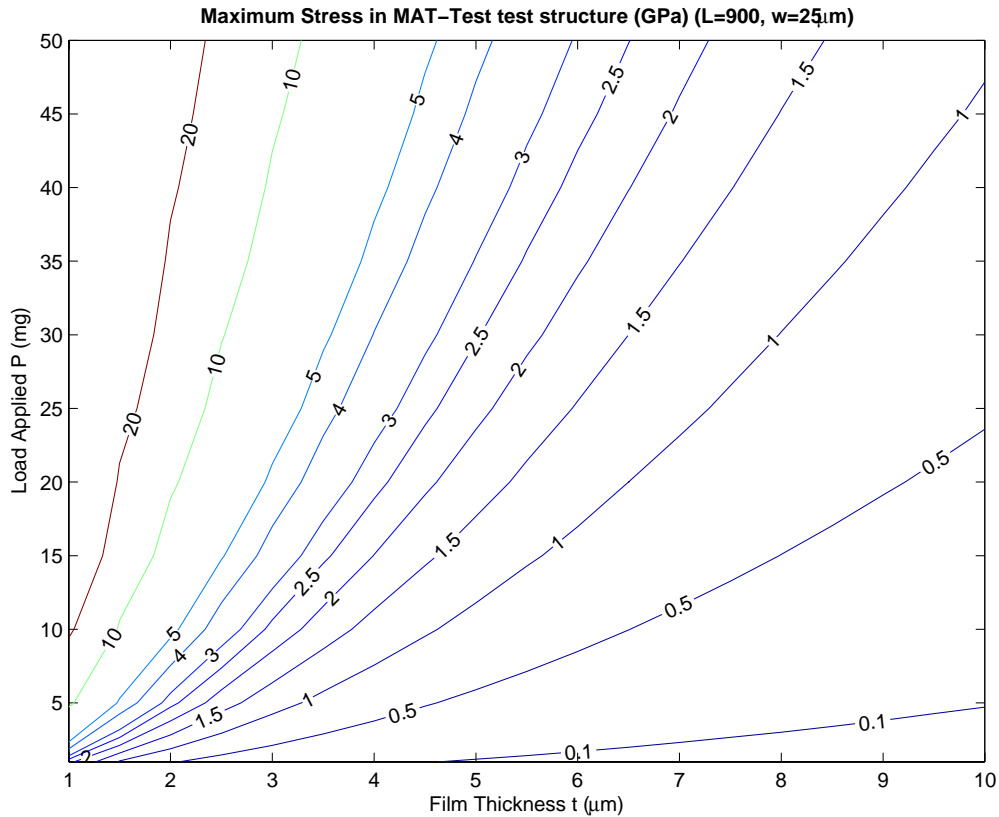
Figure 26 The measurement space for σ_b.

The contours are the maximum stress that we can develop in the reduced-width region of the cantilever.

Poisson's ratio

The Poisson' ratio measurements require having two thicknesses of the sample film available, and being able to measure the Young's modulus of the two samples. Therefore, the design considerations are the same as those for Young's modulus, except that we need to intentionally operate one of the samples in a range where the value of ψ is high, i.e., one of the films should be less than 3µm thick.

3.5.7 Expected Test Precision

The uncertainties in the MAT-Test outputs derive from the uncertainties in the inputs (test structure geometry, surface profilometer measurement) and from the data analysis procedures (the Euler approximations, regression analysis). For Young's modulus, the relevant quantities (assuming compliance with the constraints described above) are the applied force, F, the cantilever cross-section, t and w, and the measured deflection, d. The following uncertainties are typical:

Parameter	Uncertainty
E (Si)	± 2 GPa
F (measured)	2.5%
t	± 0.1µm
w	± 0.5µm

For these values, the uncertainty in the measurement of Young's modulus is 9.1%. It is important to characterize the cross-section of the MUT cantilevers well to minimize the uncertainty. The thickness characterization is especially important, as it enters into the calculation as a cubic term. The uncertainty in a single measurement of breaking stress is smaller, but the because the mechanics of fracture are complex, the breaking stress measurements must be treated statistically, and the final uncertainty depends on how many measurements are taken. The uncertainty in the Poisson's ratio measurements follow the calculations for Young's modulus.

3.6 Previous Work

The previous work on microbeam bending measurements can be grouped into three broad areas: measurement procedures and standards, development of mechanical methods including bending microbeams, and simulations of microbeam bending.

Although measurement of mechanical properties of thin films has been an issue of interest as long as thin films have been deposited, technological limitations have prevented systematic investigations into the topic until recently. The first systematic work on cantilever designs for MEMS material mechanical property measurements was published in 1979 [48]. However, micromachining was still in its infancy, and work proceeded slowly, generally focusing on membrane bulge testing (e.g. [49]), which is technologically less demanding. In the late 1980's, the Nix group at Stanford University [35, 50, 51] began investigating cantilever bending methods for thin film material properties measurement for microelectronic and microsystem applications. Additional work has been published on the topic throughout the intervening decade, primarily concerning improvements to the modelling of microbeams. Many of the recent studies make use of the greater computing power available today to perform extended simulation and computer modelling of microbeams in order to account for the deviations of actual beams from the ideal behaviour predicted by the small deflection equations.

The literature does include a few examples of using surface profilometers to deflect suspended structures and measure their deflection. However, no one has reported results using the profilometer in the manner that is described here: scanning the length of the suspended structure with a constant force. The reported work with surface profilometers uses them to measure absolute deflection as a function of a variable load for a fixed position.

3.6.1 Measurement Methodology and Standards

There have been relatively few attempts to document a standard test method for measuring mechanical properties of thin films, although this issue is gaining prominence as more MEMS/MST devices are designed for commercial, industrial, and defence applications where manufacturing standards and reliability are a concern.

The results of a thin film materials testing project, known as M-Test, were published in 1997 by Osterberg and Senturia at MIT [20]. The M-Test paper describes a general method for designing tests to measure the Young's modulus and intrinsic stress of thin films and presents an example of an implementation of that methodology for polysilicon films. The test method is based on electrostatic pull-in of suspended structures. The test structures consist of an electrode beneath a suspended beam or diaphragm. An increasing voltage is applied between the electrode and the beam, and the "pull-in

voltage", at which the suspended structure collapses, is recorded. The material properties are then extracted from the pull-in voltage, the test structure geometry, and fitting parameters. Repeated computer simulations are used to produce a "virtual database" of results from simulated test structures with deviations from the ideal geometry. The fitting parameters that account for the deviations of the test structures from the ideal model are determined from the simulation results. The polysilicon results described in M-Test are limited to conductive thin films and the test structures have complicated processing requirements.

There are not yet any published standards for measurement of thin film mechanical properties. The standards body ASTM International has assigned Task Group E08.05.03 to "develop standards for electronic and micromechanical applications", including mechanical properties [52]. In conjunction with the National Institute of Standards and Technology (NIST) in the United States, this Task Group publishes a test method for measuring the intrinsic stress in thin films using non-contact optical profilometry to measure the curvature of free-standing test structures. The committee has not yet published a test method for other material properties, such as Young's modulus, and it is not clear when they will do so. In 2000, the committee sponsored a symposium, *Symposium on Mechanical Properties of Structural Films,* which included many presentations on thin film testing methods. The material from the symposium has been published as ASTM Special Technical Publication 1413 [53].

ASTM STP 1413 includes a proposed wafer-scale test method [54] based on IMaP (Interferometry for Materials Property measurement) [55] test methods. IMaP is based on optical interferometry and electrostatic actuation. Interferometry is used to measure the profile of unconstrained microbeams and microbeams that are pulled in to the substrate electrostatically. Computer modelling is used to determine the effects of the test geometry. The test method presented in [54] uses custom-built optical microscopes to enable the interferometry measurements.

3.6.2 Beam-bending Methods

The bending of microbeams to study their material properties has been published by several groups. In all of these cases, a mechanism is used to vary the force applied to a microbeam and to measure the resulting absolute deflection.

The Nix group at Stanford University is perhaps the most well-known group working in this area. Nix and his collaborators used a MTS Nanoindenter [56] to deflect microbeams with dimensions on the order of 10's of microns [35, 36, 43, 50, 51, 57]. A nanoindenter is a machine which is designed to drive a micron-scale diamond tip into a material sample while recording the force used and the distance travelled. The material under the tip is compressed and displaced, and the mechanical properties of the sample on the atomic scale can be deduced from this action. The Nix group used this machine to deflect cantilevers composed of different materials and material combinations. Their most significant result for this work, besides demonstrating the effectiveness of the microbeam bending method, was the use of a fitting parameter to fit the experimental data to the analytical results [36]. A similar fitting parameter is also introduced by Menčik and Quandt, who published a discussion of similar beam bending tests using a nanoindenter in 1999 [34].

In both cases, the use of the fitting parameter (K_2 for Nix, l_c for Menčik) is an attempt to account for the observed dependence of the results of the beam bending tests on the length of the beam. This dependence is a result of root conditions that differ from the ideal cantilever root condition. This fitting parameter is derived by adding an additional length term to the beam bending equation:

$$d = \frac{F(L + L_{corr})^3}{3EI}$$

Equation 3-29

When this expression is expanded and the higher power terms of L_{corr} are set to zero, an assumption which is justified by the fact that $L \gg L_{corr}$, the expression becomes:

$$d = \frac{FL^3}{3EI} + CL^2$$

Equation 3-30

where C is the fitting parameter.[6]

J.-A. Schweitz and others at the Uppsala University have performed cantilever deflection measurements using a specially-designed micromanipulator [19, 38, 58, 59]. Because their experimental setup was designed to fit into their SEM chamber, they were able to capture what is perhaps the most famous microphotograph of a microbeam bending experiment (Figure 27). In addition to being able to directly observe their results, the Uppsala group can perform tests at high temperatures and other exotic conditions. Schweitz is the author of a useful survey of materials characterization methods [19].

100μm
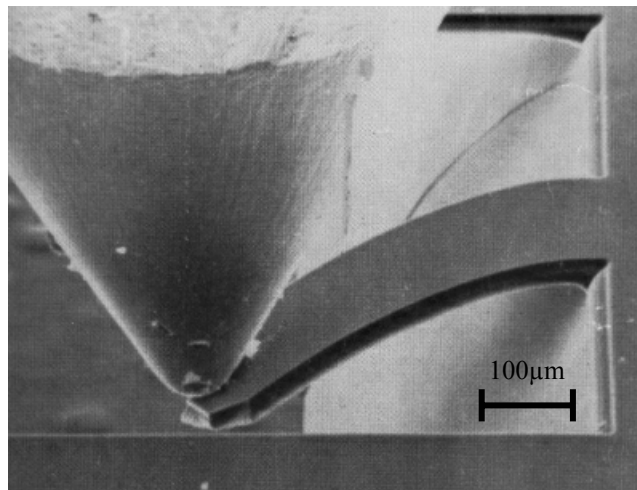
Figure 27 A SEM image of a micromanipulator deflecting a microbeam [19].

Wilson and collaborators, working at Hewlett-Packard Laboratories in the United States, did some interesting work with silicon microbeams [24, 60]. They assembled a combination of equipment (motorized stage, force transducer, microdisplacement gauges, etc) which they used to deflect silicon cantilever microbeams, both vertically and horizontally. They deflect their cantilevers at several different points along their length and

---

[6] It is interesting to note that the same fitting parameter can be arrived at using the Castigliano's theorem derivation described in section 3.3.5 if we assume that $L_p \ll L_c$, and set the higher power terms of L_p to zero (i.e., the two rightmost terms of Equation 3-18 are set to zero).

use an "effective length" to determine the Young's modulus of single-crystal silicon in the direction of the cantilevers.

Surface profilometers have been used previously to measure Young's modulus of thin films by deflection of suspended structures. Yu-Chong Tai and Richard Muller, working at the University of California Berkeley, published measurements of the Young's modulus of polysilicon that were made by deflecting fixed beams with a contact surface profilometer [61]. Their profilometer could vary the force applied to the sample, and they used the relationship between force and absolute deflection to determine the Young's modulus of their samples. They used relatively primitive computer simulations to account for the boundary conditions. Qin, et al., [62] also published similar work in which they attempt to eliminate the boundary condition error by using calibration structures with the same geometry as their test structures. More recently, a second group at Berkeley has used the same surface profilometer to deflect composite thin-film beams [63].

3.6.3 Other Micromechanical methods

Other authors have published results using deflection of various other structures, such as diaphragms or membranes [64-66], bilayer deformation [67-69], or other methods [49, 70]. However, all of these papers report results specific to certain films or test structures, using specialized equipment.

Prof. W. Sharpe has been performing variations of macro-scale tests on specimens of thin-film materials [71-74]. Because these results are based on traditional tests, such as pull-testing of machined specimens, results using other methods are often compared to this work. H. Ogawa has also published similar work [75]. However, testing thin-film materials with traditional methods requires specialized equipment and elaborate sample preparation, so it is not widely available.

3.6.4 Simulations of Microbeam Bending

Several authors [37, 61, 76, 77] have reported results based on computer simulations of deflecting microbeams. In general, simulations are used to attempt to quantify the various error effects which cause the measured deflection of a suspended structure to differ from the ideal deflection equations. Jensen, et al. [76] has reported simulations of cantilevers that were then measured optically. This comprehensive work uses a combination of profilometers, interferometers, electro-static actuation, and simulation to measure micro-cantilevers and extract material properties. Their work, however, used electrostatic actuation of polysilicon, and so its application is limited to conductive materials. Other authors [37, 69, 77] have published extensive discussions of microbeam root conditions. They conclude that deformation of the substrate is a significant cause of non-ideal behaviour of microbeams. A thorough analysis of root deformation effects for cantilever microbeams is given by Zhang, et al. [37]. They analysed the contribution of substrate deformation in terms of coupled springs, and determined the spring constants by Finite Element Method simulations. They concluded that the additional deflection can be described as a function of L^2 and L.

4. MAT-Test Experimental Procedure and Results

The procedure for performing a MAT-Test measurement consists of four steps:

1) Pattern the test structures in the MUT
2) Remove the substrate from underneath the test structures
3) Measure the test structures with a surface profilometer
4) Analyse the profilometer data to determine the material properties

Each of the steps are described here, with reference to actual experiments that were performed and alternative methods and optimisations.

4.1 Patterning Test Structures

Test structures in the MUT can be patterned using any convenient technology. Reactive ion etching (RIE), wet etching, selective deposition/shadowmasking, and laser micromachining are some technologies that can be used to pattern thin films. Laser micromachining was used in the examples presented here.

4.1.1 Design for Laser Micromachining

Laser micromachining for patterning thin films involves ablating selected portions of the film to expose the substrate and to separate regions of the film. Laser micromachining for the MAT-Test samples was performed using a New-Wave Research QuikLaze 50 Nd:YAG micromachining laser [18]. The laser is mounted on a microscope with a computer-controlled X-Y stage. The stage has a maximum travel range of 50mm in either direction, and a positioning precision of 1μm. The laser output can be tuned to two wavelengths of radiation: Green (532nm) or UV (355nm). It generates pulses that are approximately 3-4ns in duration, and pulses can be generated at up to 50Hz. The energy of each pulse can be varied up to a maximum of approximately 0.6mJ, but the spot size is controlled by a mechanical shutter that obscures the laser output, so that the flux density of each pulse is determined by both the spot size and the output energy. The laser impact spot is a rectangle which can be roughly 4 to 60 μm on a side. The computer laser control software can move the stage through a preset series of coordinates while controlling the laser output, so that complicated designs can be patterned on a sample automatically. Figure 28 is a schematic of the micromachining laser setup.
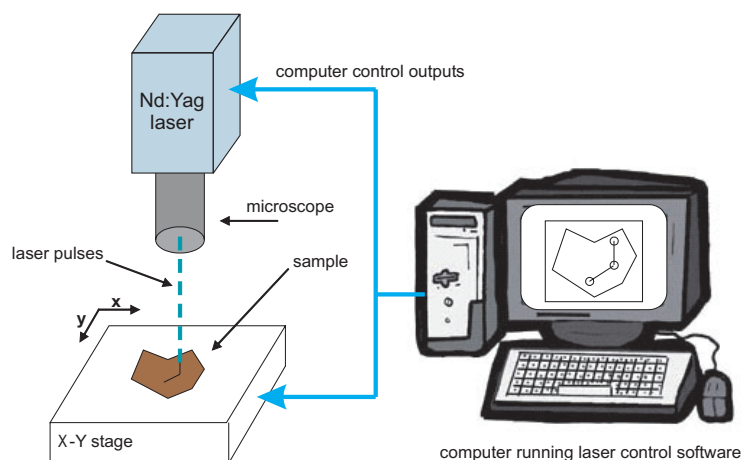

Figure 28 Micromachining laser setup.

A series of preset coordinates for the stage is called a "scan pattern". The New-Wave laser control software includes only limited capabilities for creating and modifying scan patterns, so additional software was written to allow us to create and manipulate scan patterns for the laser control software. The MAT-Test sample designs were created using this software. Discussion of the details of this software is given in Appendix C.2. Figure 29 is a screenshot from the laser design program, which is called lel [78].
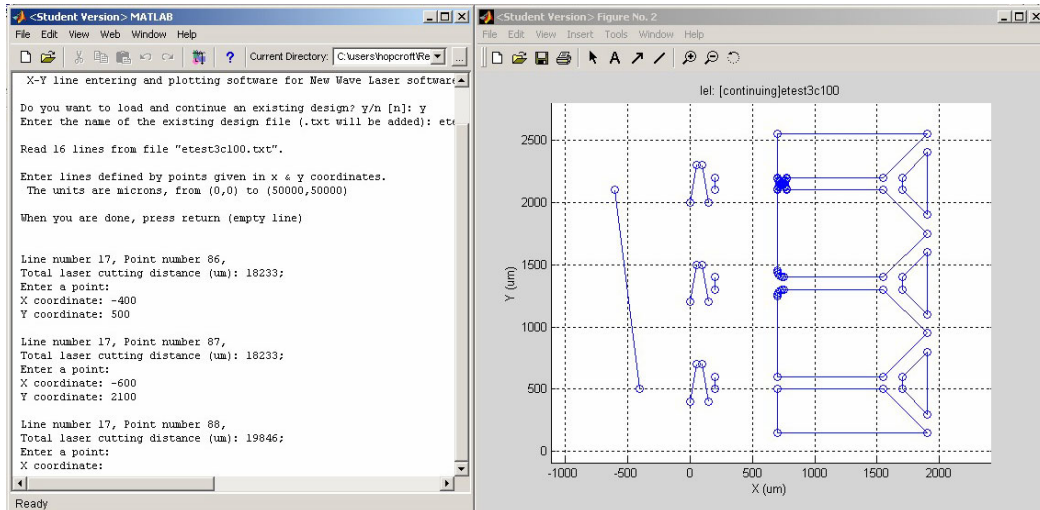

Figure 29 lel laser design software.
Coordinates are entered in the screen on the left. On the right, the laser design is displayed.

There are several variables which must be optimised for laser processing of any material. The first step is to determine which wavelength of laser radiation ablates the film most effectively. Different films absorb or reflect different amounts of energy from the different laser frequencies, with better or worse results for our purposes. Determining the optimum ablation conditions for a given film/substrate combination is largely an empirical process. Figures 30 - 32 show three samples which illustrate the results obtained with different laser frequencies. Figure 30 shows a sample of silicon carbide (SiC) film on silicon (Si), which has two open triangles patterned in it using the green laser wavelength with maximum power output. Figure 31 shows a silicon nitride (SiN) film on Si which was cut with the same settings as the sample in the previous figure. The cut in Figure 31 is very rough, and it is almost impossible to cut regular shapes. Figure 32 shows the same SiN material cut with the UV wavelength. The cut is much better, much like the smooth cut in Figure 30.
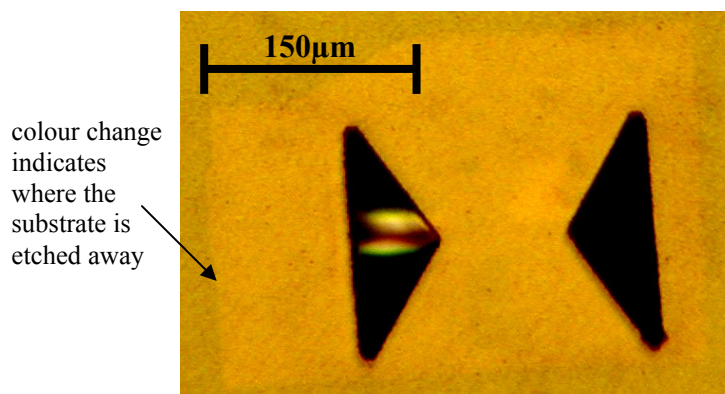

Figure 30 SiC, Green laser.
The laser cut shapes are clean. Note overetching of the substrate beyond the opening.

colour change
indicates
where the
substrate is
etched away

150μm
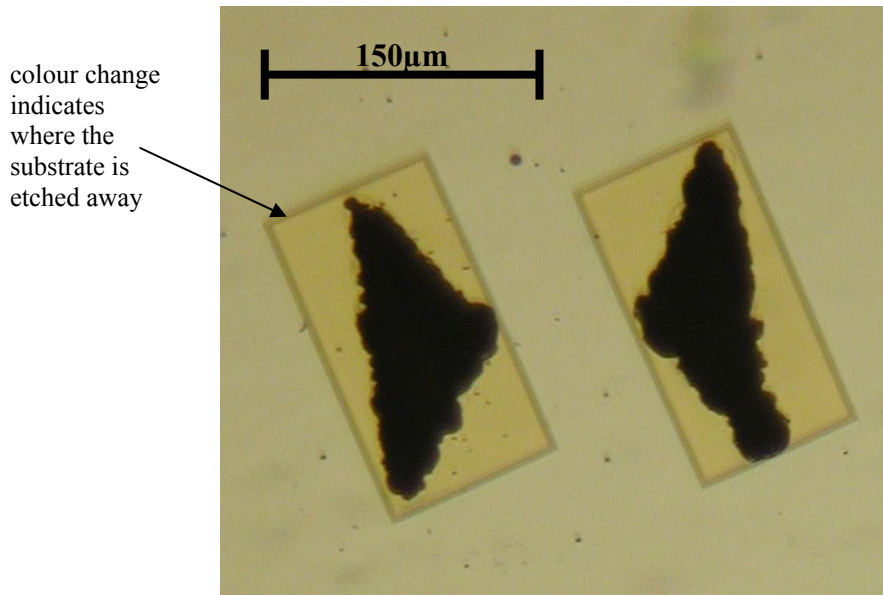
Figure 31 SiN, Green laser.
The laser cut shapes are irregular. Note how the substrate etch closely follows the opening.

colour change
indicates
where the
substrate is
etched away

100μm
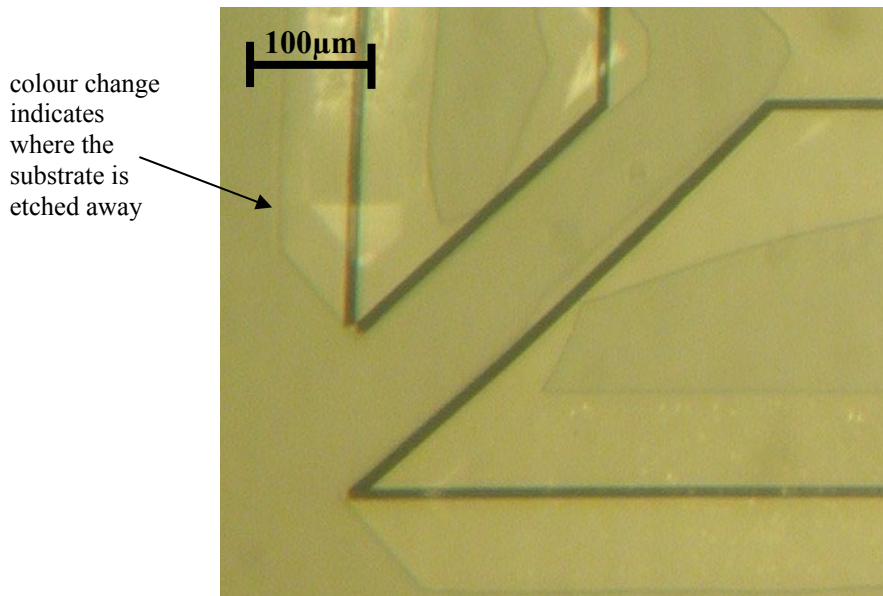
Figure 32 SiN, UV laser.
Laser cut is clean, with minimal overetch.

The next laser processing variable which must be considered is the power/laser aperture/stage travel speed combination. In general, these three variables are optimised to cut through the film with the minimum disruption of the film and substrate and the maximum horizontal travel speed. The goals for these variables depends on the design, however. For example, for MAT-Test, damaging the substrate is not an important concern, because the substrate will be etched in the next processing step. For large designs, maximizing the travel speed of the stage may be important to reduce the time required to process each design. The essential limit for these variables is the amount of laser exposure that is required to cut completely through the film. Laser ablation of a film is a complex phenomenon with several different modes of operation [79] and the optimum laser conditions for a given material system must be determined empirically.

4.1.2 Laser Micromachining Considerations

Laser micromachining has advantages for patterning thin films. It is flexible and easy to use. A design can be conceived, encoded in a computer file, and executed on a sample within an hour, where traditional lithography-based thin film patterning typically requires days or weeks and several processing steps. Laser processing is also applicable to a wide variety of films; every thin film is susceptible to some combination of laser frequency and dose.

However, there are limits and disadvantages to laser processing. The most significant of these are based on the energy from each laser pulse that must be dissipated. The micromachining laser used in this work has a laser pulse time of 3-4 ns, which is "long-pulse" operation. Long-pulse laser micromachining is characterized by laser pulse times which are longer than the heat diffusion time in the sample. The energy of the laser pulse is transferred to the sample as heat. If laser pulse is longer than the heat diffusion time, the heat from the laser pulse will spread to the area around the laser pulse impact site during the time that the laser is vaporizing the sample at the point of impact. The area around the laser impact site where heat effects are observed is called the Heat Affected Zone (HAZ) [80]. The material in the HAZ, surrounding the laser cut, is subject to a variety of undesirable effects, including redeposition, cracking, and film delamination [79, 80]. The exact effects are complex and specific to each film/substrate combination. The various negative heat-related effects of long-pulse lasers are depicted in Figure 33.
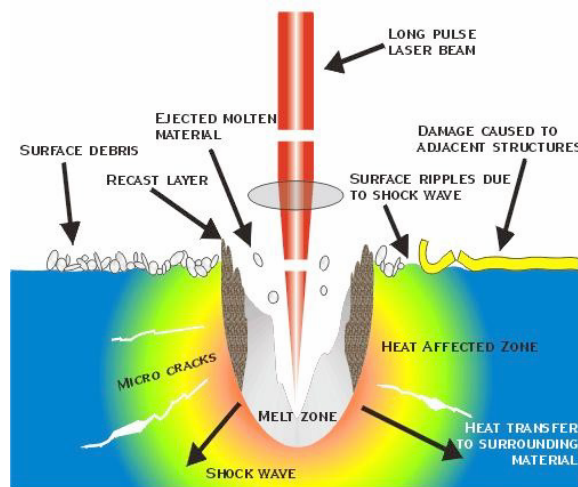
Figure 33 Laser micromachining heat effects (from [80])

Some of these heat effects are visible in the MAT-Test samples. A silicon carbide sample immediately after laser ablation is shown in Figure 34. Evidence of heat effects and surface debris can be seen in the area surrounding the laser cuts. Comparing Figure 30 and Figure 31, we can see that in Figure 31, the substrate etch is well confined to the mask opening, while in Figure 30, the etch has penetrated away from the laser cuts, creating a larger etch pit than we would expect. This suggests that in the SiN, more of the laser energy was dissipated kinetically in the film itself, causing a rougher laser cut and less film delamination, while in the SiC, more of the laser energy is dissipated in the HAZ, resulting in a smoother laser cut with more delamination of the film. Another example of heat effects observed in the MAT-Test samples is local cracking around the initiation and termination sites of laser cuts. Figure 35 shows a sample of silicon nitride that exhibits

cracking at the ends of laser cuts. The cracks appear to form in the corners of the cuts and curve toward the principal stress axes.
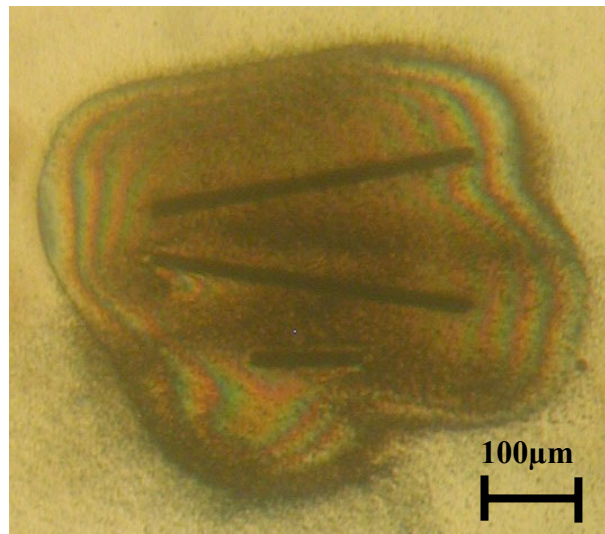
Figure 34 A silicon carbide sample immediately after ablation.
The HAZ region is clearly visible surrounding the laser impact areas.

Surface debris ejected from the laser cut was observed in all MAT-Test laser processing. Fortunately, the subsequent wet-etching in KOH served to clean up the debris. Figure 36 shows a comparison of the same sample immediately after laser etching, and then after KOH etching.
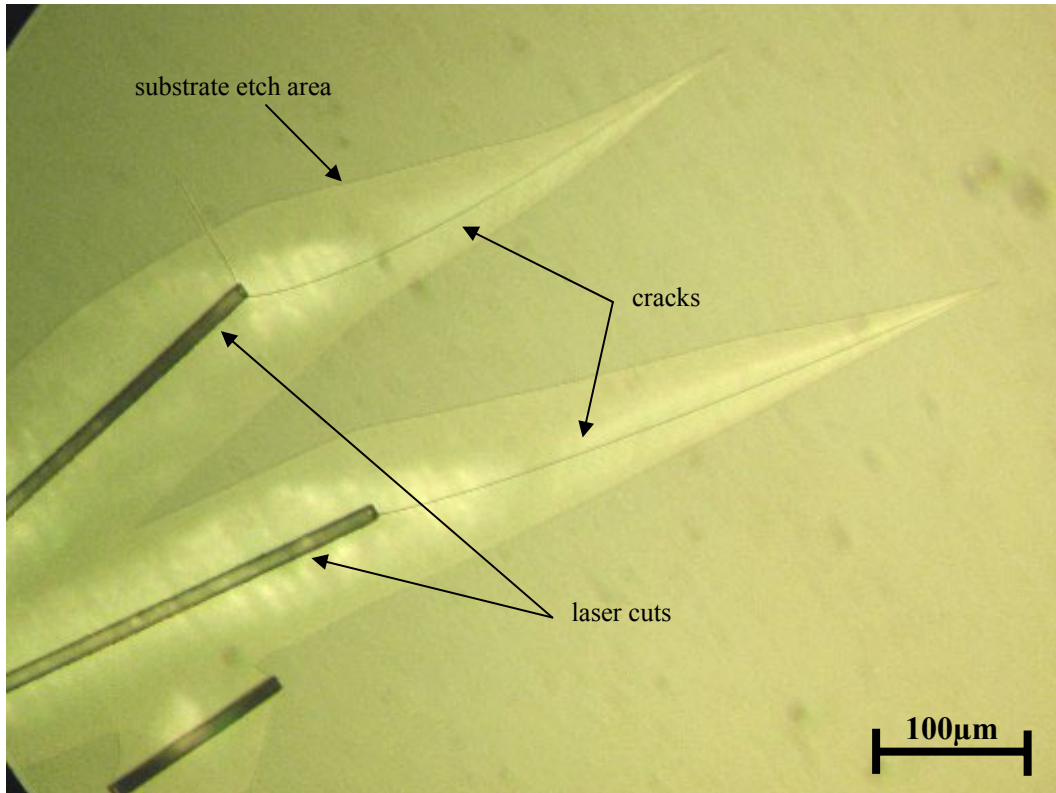
Figure 35 Cracking at laser cut initiation/termination sites.
The sample is 3μm thick LPCVD silicon nitride. The substrate has been etched in KOH, which serves to highlight the cracks.

| a) SiC, before KOH | b) SiC, after KOH |

Figure 36 Laser debris, before and after KOH etching.
The debris is completely removed by the etch. The laser cut line width is approximately 8μm.

4.2 Removing the Substrate

The substrate supporting the test structures can be removed using any convenient technology. Deep reactive ion etching (DRIE) and wet or dry chemical etching are some common technologies that are used to etch substrates. In general, selective chemical methods, such as wet etching, are preferred over mechanical methods such as DRIE because mechanical processes may leave a substrate residue on the test structures, affecting the measurements.

In the experiments presented here, the samples consisted of an MUT deposited on a silicon substrate. Wet etching with Potassium Hydroxide (KOH) was used to remove the substrate. The KOH etch recipe used for the MAT-Test samples was a 20% by weight KOH in water solution, heated to 70ºC in a constant-temperature bath. The patterned MUT served as the etch mask for the KOH etch.

4.2.1 Designing the Etch Mask

KOH is an anisotropic silicon etchant, which means that it etches some silicon crystal planes preferentially to others. KOH etches the {111} crystal faces much more slowly than the {100} and the {110} faces. This means that we can create specific shapes in the silicon substrate by exposing only certain areas of the substrate to the etchant. A thorough discussion of silicon micromachining with anisotropic etchants is given in [79, 81]. The MUT serves to mask the silicon for the etch; where it is removed in the patterning step, the silicon will be exposed to the etchant, and where the MUT remains, it will protect the silicon.

The shapes produced by anisotropic etching are produced according to relatively simple principles, but they may have unexpected ramifications for complex shapes. A software package from the University of Illinois called ACES [82] can be used to simulate the etch shape that an etch mask will produce. Figure 37 is a picture produced by ACES which shows the expected etch pit of a basic cantilever design. The simulated silicon wafer is cut so that the surface is oriented in the [100] direction. The primary axes for the silicon crystal in this orientation are the family of <100> directions, shown at left in Figure 37. The etch mask produced by laser ablation is shown in black outline. The etch mask in Figure 37 was aligned to the primary directions in the silicon crystal. The etch pit is well confined to the opening defined by the mask, but the silicon is still present underneath the cantilever, and the etch pit that has formed is rather shallow.
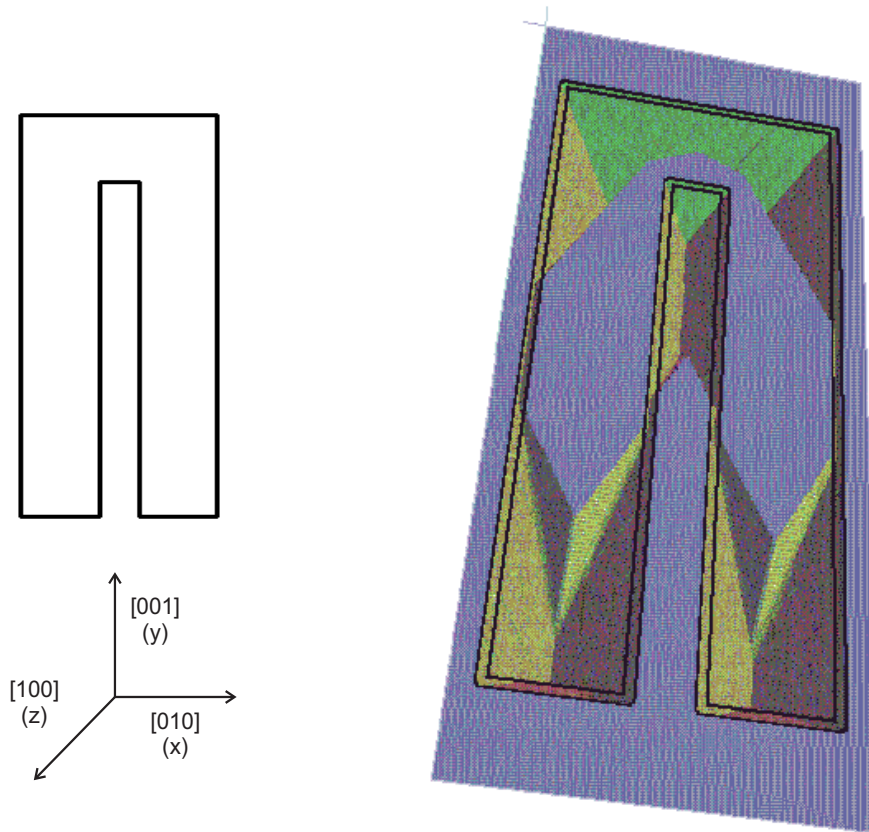
Figure 37 ACES simulation of etching a cantilever, with the mask aligned to the [100]/[010] directions. The mask created by the laser patterning of the MUT is shown at left, and the result of simulated KOH etching is at right. The outline of the etch mask is superimposed in black on the simulated etch results. The view angle is rotated slightly to display the etch pits.

Compare Figure 37 with Figure 38, which shows the same etch mask aligned at 30º from the main crystal axes. In this simulation, the etch time was only half of the etch time in the previous simulation. Even so, the cantilever is almost completely undercut, and the etch pit has already reached the same depth as in the previous simulation. Of course, the etch area has extended beyond the perimeter defined by the mask, and will continue to expand as the etch continues.

The etch mask that is produced by the laser patterning consists essentially of thin lines, and the desired shape is drawn in outline. If the etch mask consisted of large openings, as is typical in traditional photolithography patterning processes, the etch shown in Figure 37 and Figure 38 would proceed more quickly, because more of the substrate would be exposed. We can increase the amount of exposed substrate by additional laser ablation, for example by cutting wide zigzag lines across the etch pattern. Of course, this increases the time required for the laser patterning.
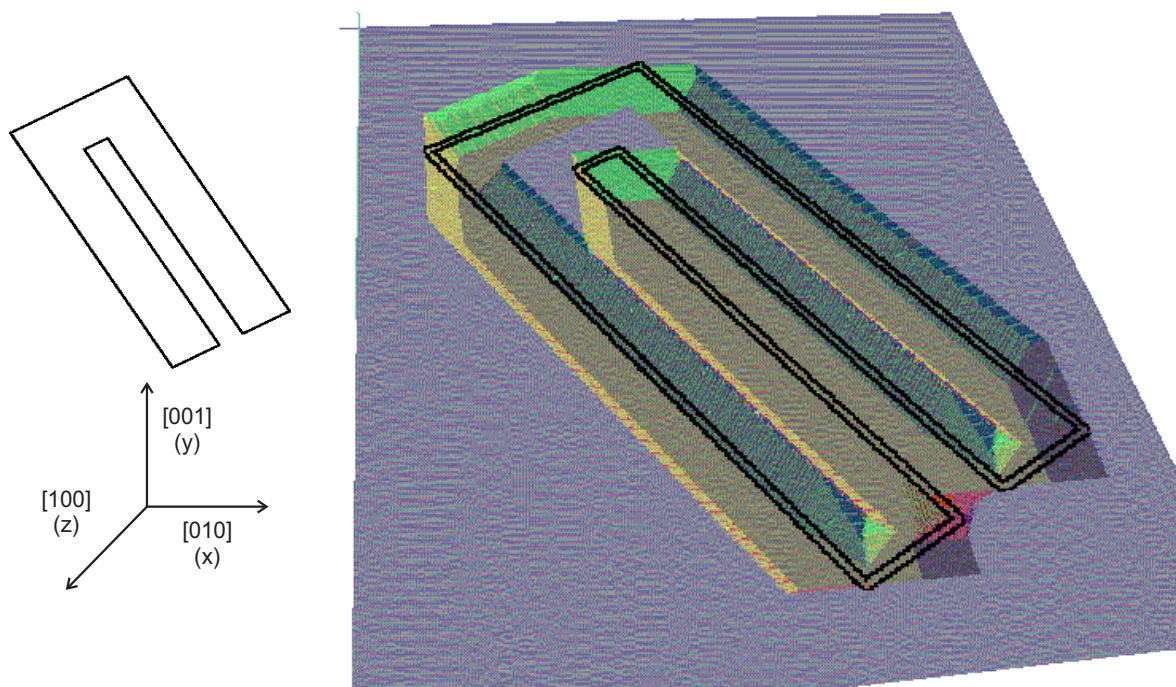
Figure 38 ACES simulation, with the mask aligned at 30º away from the primary crystal axes. The mask created by the laser patterning of the MUT is shown at left, and the result of simulated KOH etching is at right. The outline of the etch mask is superimposed in black on the simulated etch results. The view angle is rotated to display the etch pits.

The design of the MAT-Test test structures had two goals for the substrate removal: sufficient width and depth of the etch pit to allow the cantilevers to be deflected without touching the substrate, and minimum time required for etching. Reducing the time necessary for the KOH etching required additional laser ablation time to expose more areas of the substrate to the etchant, but the tradeoff was necessary because some of the films, SiN in particular, were not perfectly resistant to the KOH, and broke down after more than 2 hours of etching. The other method used to reduce the etching time was to align the test structures away from the <100> directions, so that the substrate underneath the cantilevers would etch faster, as in Figure 38. This has the effect of dramatically increasing the undercut, but we have shown that that is not a concern for MAT-Test.

4.2.2 Wet Etching Considerations

An important aspect of the KOH etch is that it is a wet etch, and the test structures are immersed in liquid. The liquid must be removed, typically by forced evaporation. During the drying process, the liquid between the cantilever and the bottom of the etch pit gradually evaporates, contracting into a smaller drop as it does so. This "meniscus effect" causes the cantilevers to be attracted to the bottom of the etch pit. If this issue is not addressed, many test structures, especially the breaking test structures, will not survive the wet etch. This sort of failure was directly observed in early MAT-Test designs.

There are two general approaches to this problem- reduce the meniscus effect, or support the structure so that it can resist the meniscus forces. The meniscus effect can be reduced by critical point drying (CPD) or by making the etch pit depth sufficiently large that the water drops cannot form between the bottom of the etch pit and the cantilever. However, for this work, it was possible to design a support structure for the free end of the cantilever which is removed by laser processing after the wet etch is complete. An example

of this support structure is shown in Figure 39. Two beams are used to allow the substrate etch to proceed under the beam.
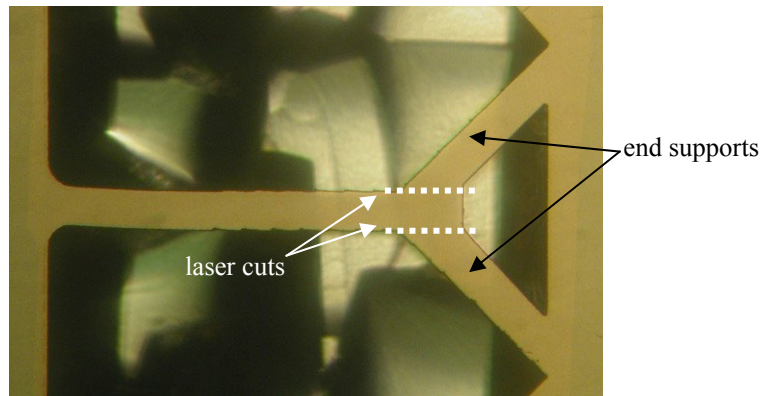
Figure 39 Typical MAT-Test test structure with end supports still attached.
The end supports prevent damage during drying. The supports are cut away using the micromachining laser after the etch is complete. The microbeam is approximately 100μm wide.

4.3 Measuring the Test Structures

The test structures were measured on different profilometers. Most of the measurements were taken using a Dektak 3ST, located in the Wolfson laboratory at Imperial College in London. The Dektak 3ST has an adjustable load range from 1-40mg. A typical data plot from the Dektak 3ST is shown in Figure 40. Data plots from other surface profilometers appear similar.
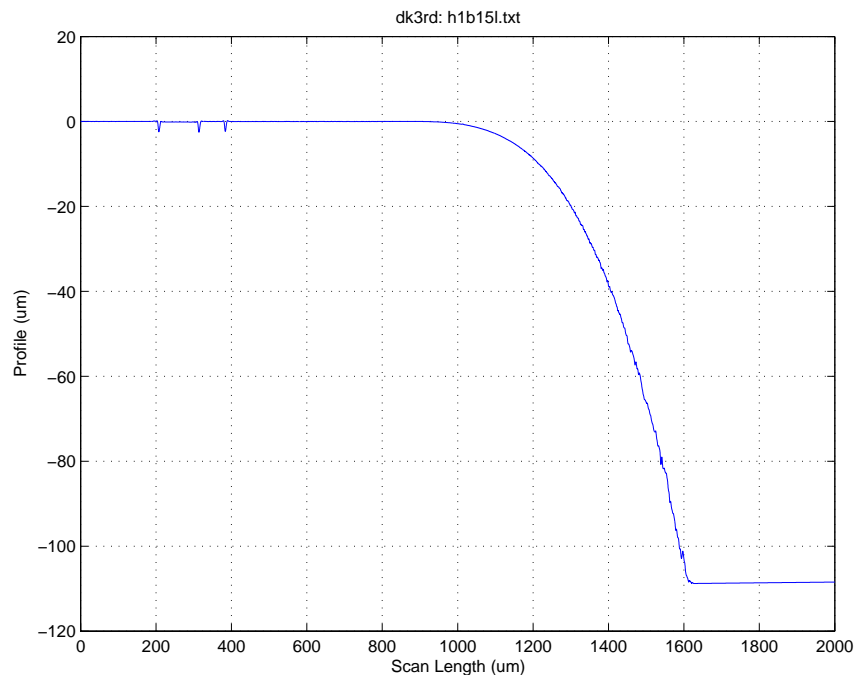
Figure 40 Typical MAT-Test surface profilometer data.
The sample is silicon carbide. The profilometer is a Dektak 3ST.

An important part of measuring the test structures is to calibrate the force applied by the surface profilometer. For these measurements, silicon cantilevers with well-controlled dimensions were used. The silicon cantilevers were scanned by the surface profilometers, and the Young's modulus of silicon was used to extract the force applied by

the surface profilometer. For the parameters given in section 3.5.7, the accuracy of each individual force measurement is about 2.5%. The silicon measurement cantilevers were originally fabricated for a different project, and the fabrication process is described in [83, 84]. Figure 41 is an SEM image of a typical silicon measurement cantilever.
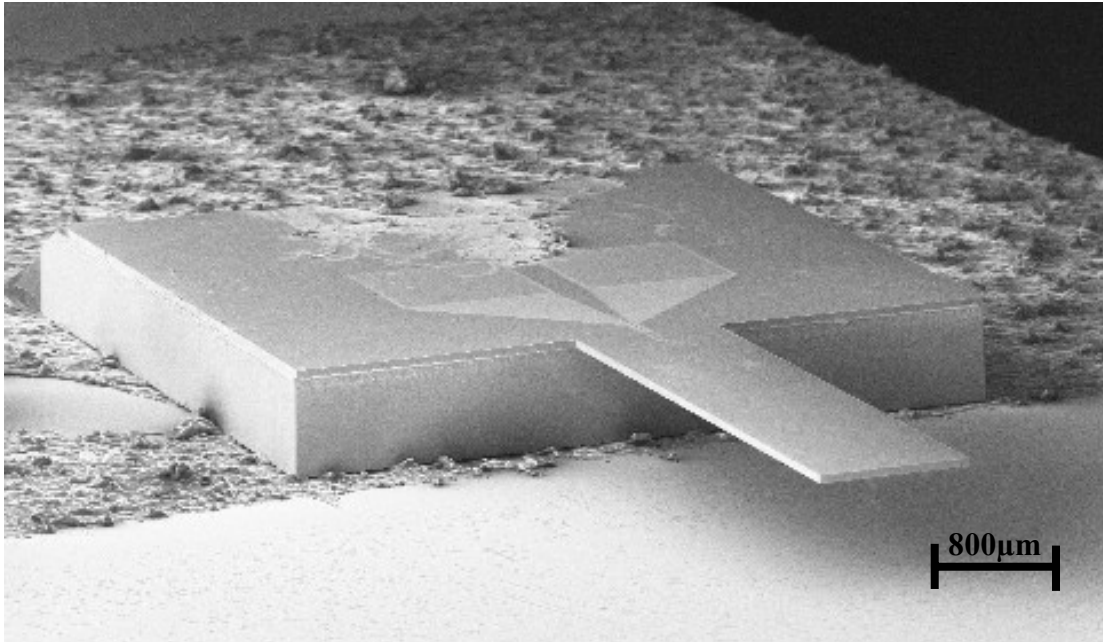
Figure 41 SEM image of a silicon measurement cantilever.
The regular patterns on the top of the base are locations of ion implants and silicide regions left by metal contacts which have been removed. The cantilever is mounted on a glass slide with adhesive.
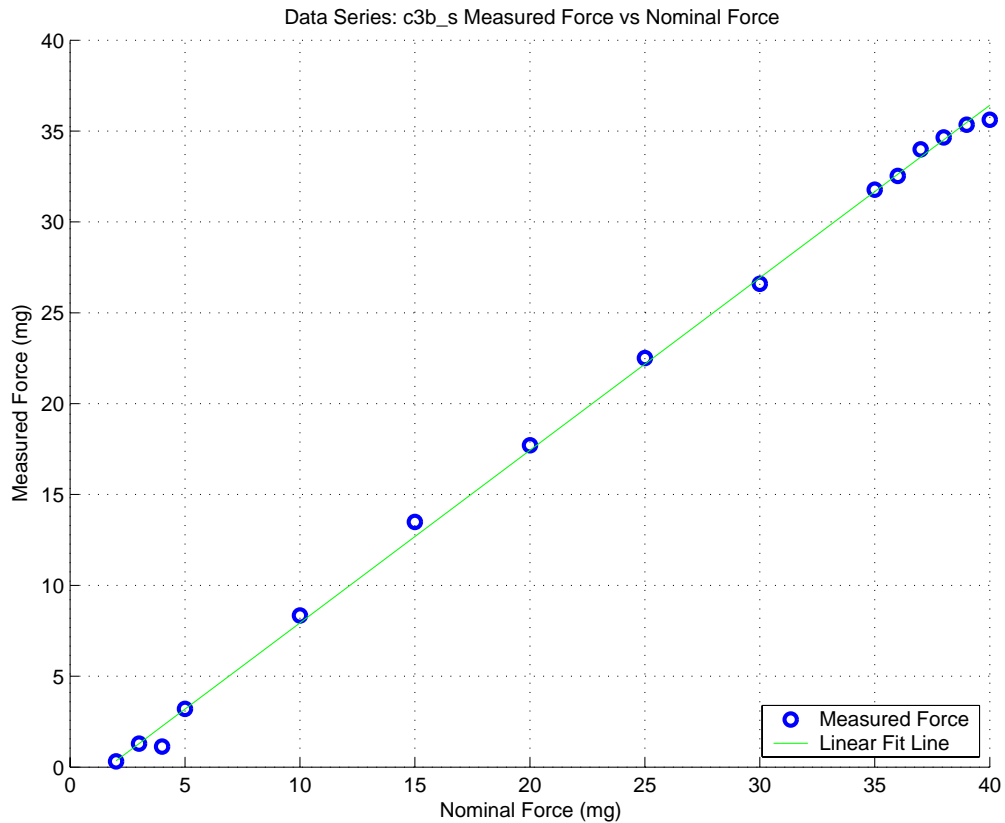
Figure 42 Force applied by the Dektak 3ST surface profilometer

We can see that the force actually applied by the surface profilometer differs from the force reported by the profilometer by up to 15%. This is not unexpected, as the accuracy of the applied force is not important for most surface profilometer measurements. Similar results for profilometer force characterization have been reported by other investigators [61].

4.4 Analysing the Data

The data is then analysed according to the theory described above. The first step is to measure the cross-section of the test structures. This can be done in several ways: from the fabrication data, optical inspection, profilometer, by calibrated SEM imaging, or by other means. For the results presented here, the cross-section was measured by comparing fabrication data and optical inspection. The thickness was determined by comparing process data and SEM measurements.

MATLAB software was written to perform the data analysis automatically, given the surface profilometer data and the test structure cross-section data. There are three different programs, one for each of the three material parameters that we want to measure. Discussion of the details of the programs is given in Appendix C.3. The use of the programs is described here.

4.4.1 Young's modulus

The program for extracting Young's modulus from the measured data is called "y1". First, the user is asked to load the profilometer data file. The program accepts data from any of the different types of profilometers used in this work, and modules for reading data files from other types of profilometers can be written easily. The user is also asked to enter the relevant geometry data for the test structure (width and thickness) and the applied load. The data is plotted, and then the user is asked to identify the region of beam bending (Figure 43).
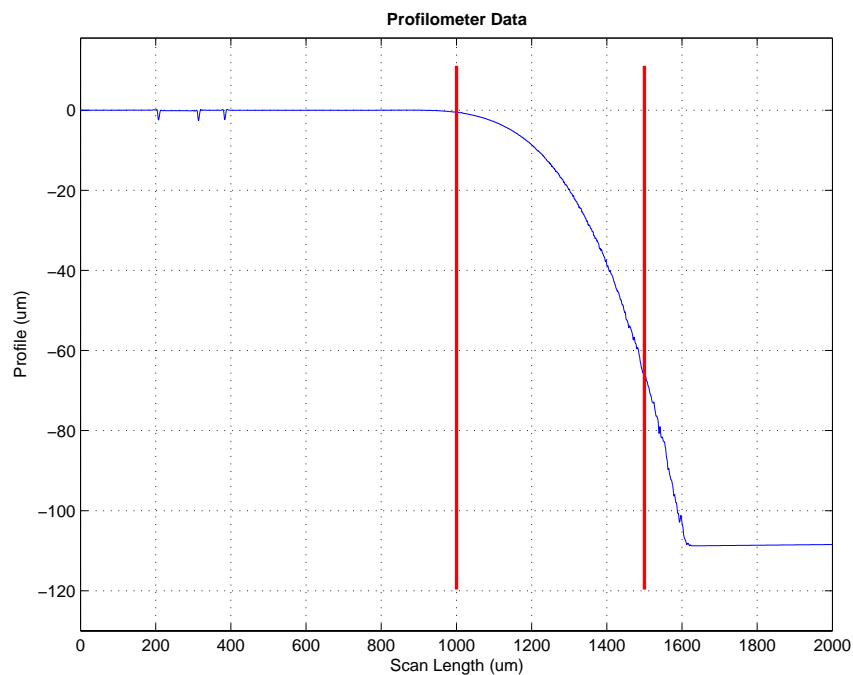
Figure 43 Screenshot of a MAT-Test program displaying profilometer data.
The user has identified the region between the vertical red lines as the region of beam bending.

The software then performs a polynomial curve fit to the selected data. The selected data is referred to as "Y-data" because it is used to determine the intermediate parameter *Y* and Young's modulus. The fit is performed using the least-squares method. The results of the fit are plotted along with the data for inspection (Figure 44). The value of the Y-parameter and Young's modulus are then displayed (Figure 45).
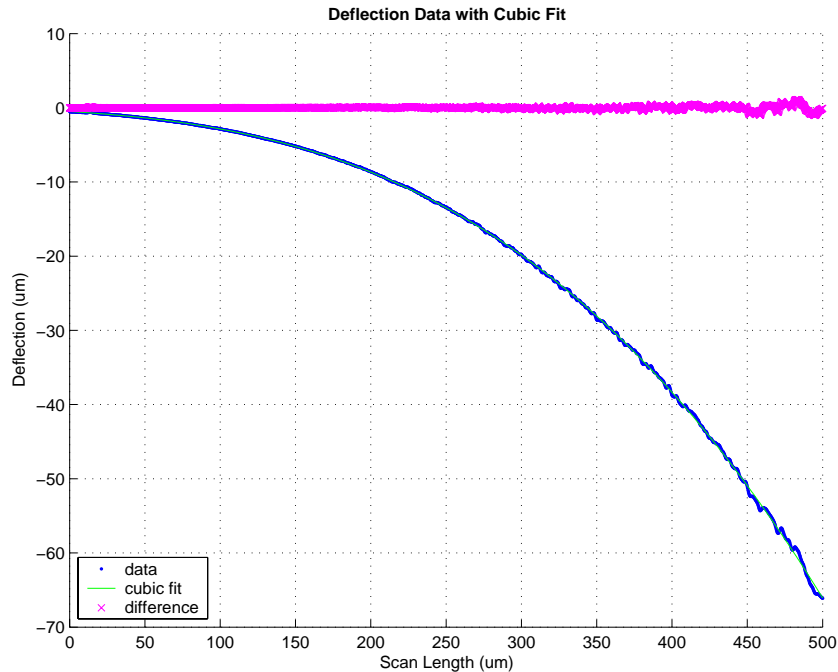
Figure 44 Screenshot of MAT-Test program y1 displaying the polynomial fit results:
the measured data (blue), the cubic fit to the data (green), and the difference between the two (purple).
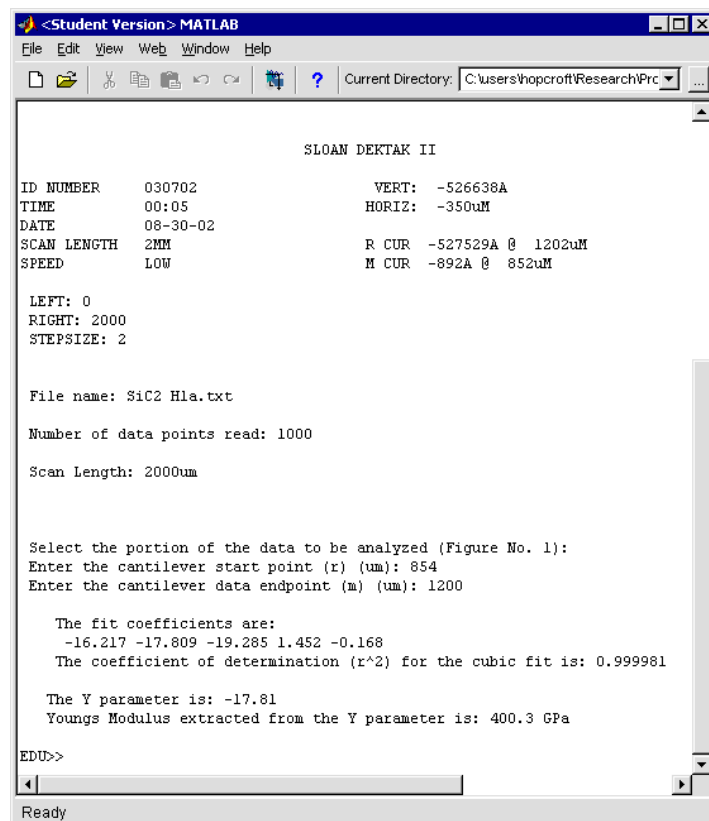
Figure 45 Typical output of program y1

4.4.2 Breaking Stress

The software that interprets breaking stress data is called "b1". It operates in a similar manner to y1. The user is asked to load a data file and enter the relevant geometry information, including the location of the fracture, in terms of distance from the root of the cantilever. Because the easiest way to determine the location of the point of failure is simply to run another surface profilometer scan with the same start point over the broken test structure, the user has the opportunity to view a second profilometer plot and to use it to determine the location of the failure. The distance, L_σ, between the point of failure and the location of the stylus at the time of failure is then calculated, and the resulting stress is displayed, along with the intermediate parameter L_σ. The procedure is repeated many times, and the results are stored for statistical analysis. A typical data plot from this program is shown in Figure 46.
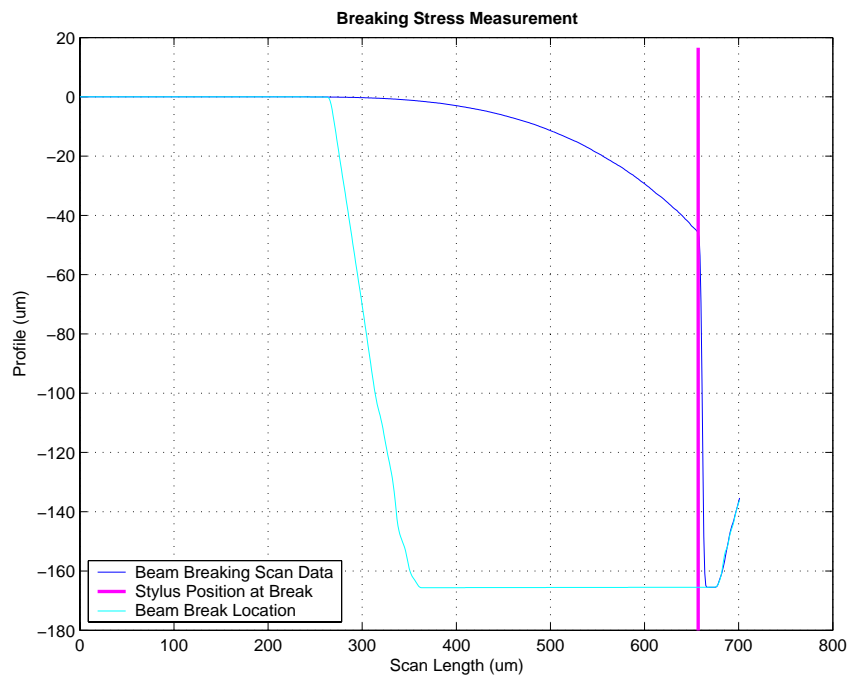
Figure 46 Typical data plot from program b1.
Two scans are plotted: the first causes the beam to break, and the second establishes the location of the break.

### *4.4.3 Poisson's ratio*

The software that interprets the Poisson's ratio data is called "p1". It operates in a similar manner to y1, except that it operates on two data files and compares the results: the user loads two data files, one from a thick sample and one from a thin sample. Following the procedure of y1, the value of Young's modulus is extracted from the two samples. The two values of E are compared (see section 3.2.4 for discussion of this analysis), and the values of ψ and ν are displayed.

4.5 Results

4.5.1 Materials Tested

Two different material samples were available for MAT-Test testing: silicon carbide and silicon nitride. Both materials were thin films deposited on silicon substrates by chemical vapour deposition (CVD). The silicon carbide samples were supplied by

Hyper-Therm, Inc. of Huntington Beach, California, USA. The silicon nitride samples were supplied by Twente Microproducts in Twente, Netherlands.

4.5.2 Variation in the Data

The experimental data collected to date exhibits more variation than the theoretical analysis predicts, due to noise in the data collected from the surface profilometers. This data is susceptible to two types of noise. The first is simple oscillation, where the cantilever is set into vibration, either by motion in the room, passing air currents, or the impact of the profilometer stylus. These oscillations are typically very small, and most pronounced away from the root of the cantilever. This sort of noise is not a problem for MAT-Test analysis, because a curve fit to regular oscillations produces values that are the mean of the magnitude of the oscillations, which is exactly what we want. Figure 47 is an example of this type of noise and the resulting curve fit.
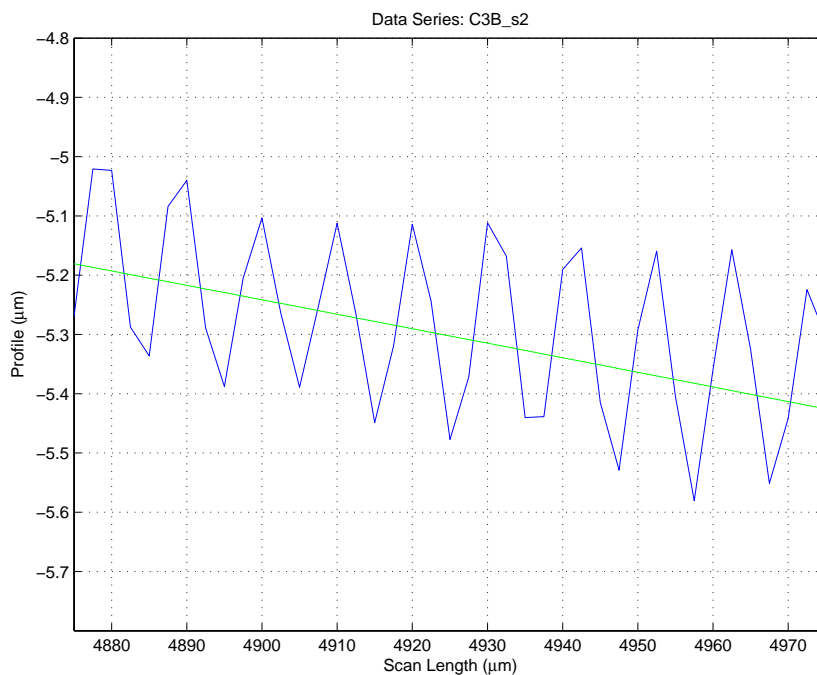
Figure 47 Typical oscillatory noise in profilometer data (blue), with curve fit (green)

The second type of noise found in the profilometer data is "bounce" or "hop" noise. This occurs when the profilometer stylus encounters an obstacle on the surface and bounces over it. This causes a positive bump in the data trace, and these bumps can significantly affect the result of a curve fit to the data. An example of this phenomenon is shown in Figure 48.
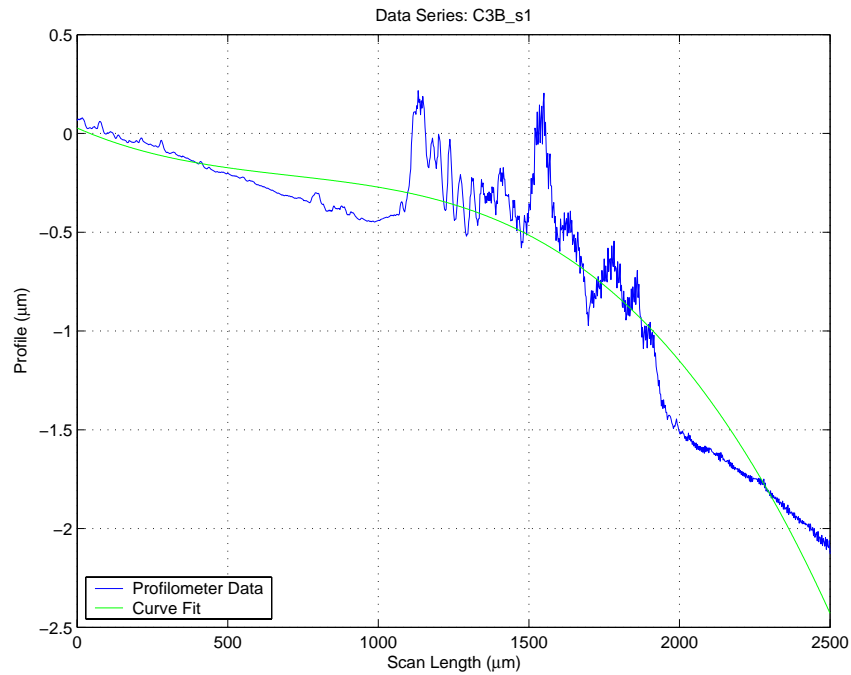
Figure 48 Example of hop noise in profilometer data (blue) and curve fit (green)

Hop noise is the primary cause of variation in the MAT-Test results. The magnitude of bounce events can be significantly reduced by reducing the horizontal scanning speed. Cleaning the samples can also help. Investigations of filtering and smoothing techniques to reduce the effects of hop noise after the data has been collected have not produced satisfactory results, so at this time, it is left to the judgement of the operator to determine which profilometer scans have produced the cleanest data, and which range of the data should be considered for analysis.

4.5.3 Experiments and Results

Pictures of some of the final MAT-Test test sites are shown in Figures 49 - 51. Each test site included three cantilevers: one simple rectangular cantilever, one cantilever with 50μm radius corner fillets, and one breaking stress test structure with a region of reduce beam width. The silicon carbide sample in Figure 49 appears to be in good condition after the test site fabrication process, while the silicon nitride (Figure 50), which is a thinner film with a greater stress mismatch with the substrate, has developed many severe cracks during fabrication. These cracks do not affect the MAT-Test Young's modulus results. However, it has proved impossible to fabricate a breaking test structure in the silicon nitride, as the stresses produced during the substrate etching process consistently destroyed the thinner cantilevers. Figure 51 shows microphotographs of the test samples being deflected by the profilometer stylus.
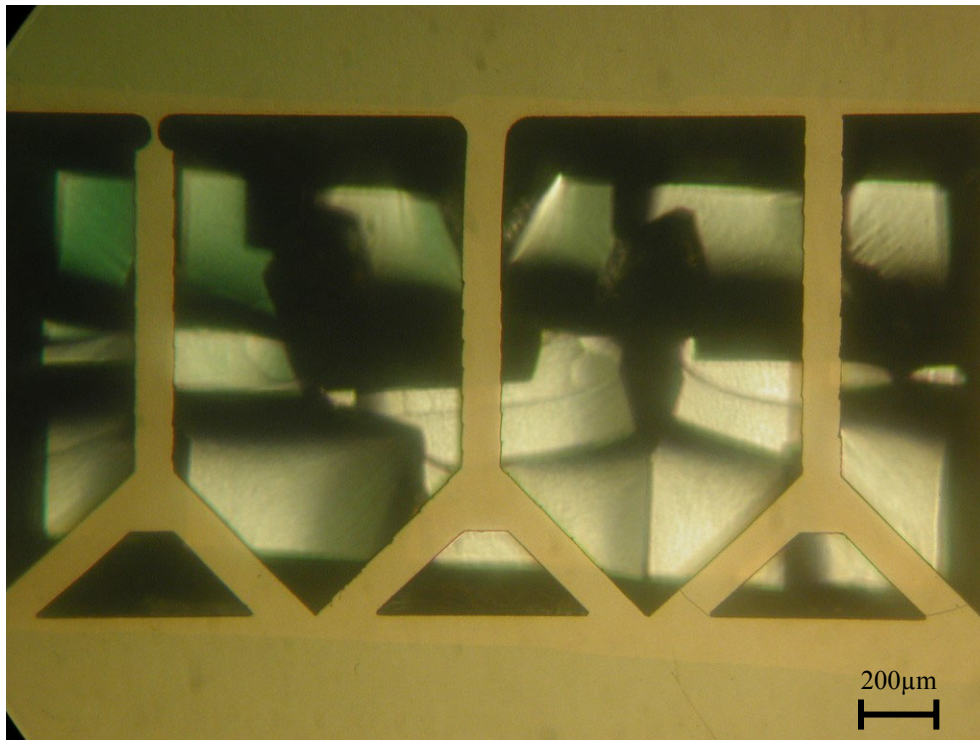
Figure 49 Silicon carbide test structures.
The end supports have not yet been removed from these cantilevers.
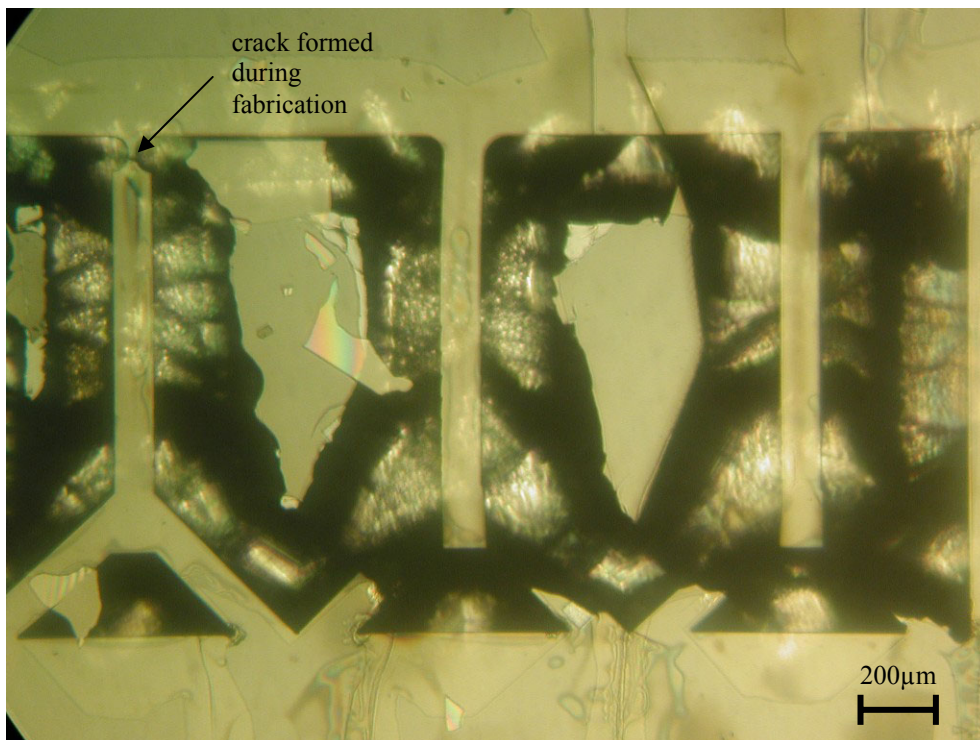
Figure 50 Silicon nitride test structures.
The end supports have been removed from the two rightmost cantilevers. Note that the breaking test structure (left) has cracked in the reduced-width region, making it useless.

<div align="center">a) silicon carbide   b) silicon nitride</div>
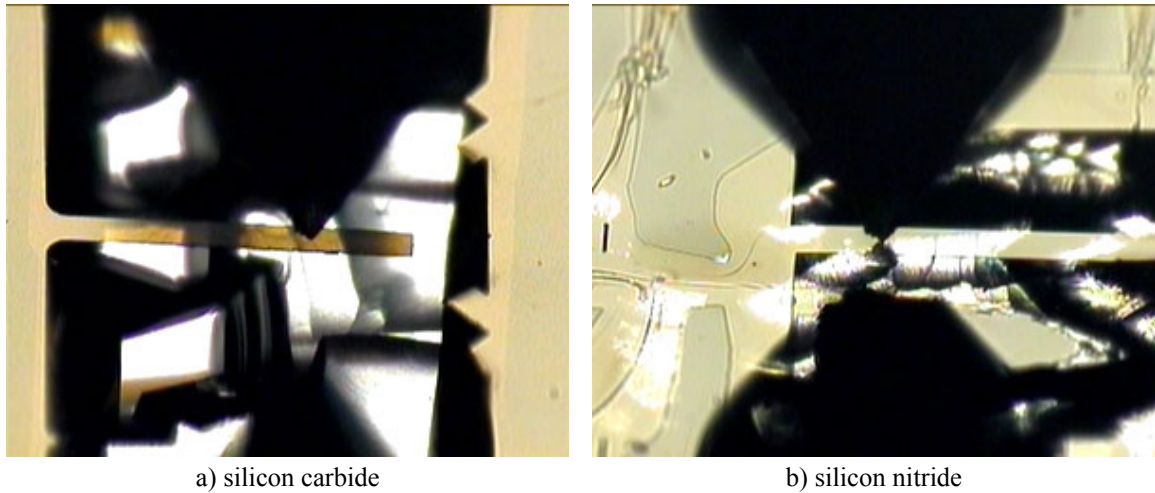
Figure 51 Test structures being deflected by the surface profilometer stylus.
The stylus is the large black triangle in the upper centre of each picture. The stylus casts a shadow at the bottom of each picture.

The results of MAT-Test measurements performed on the different material samples are summarized below. Different thicknesses of the samples were not available, so measurements of Poisson's ratio could not be made. On some samples, duplicate test sites were constructed at right angles to each other in order to investigate the anisotropy of the materials.

Material	Young's Modulus E (GPa)	Breaking Stress σ_b (GPa)[*]
Silicon Carbide, sample #1	437 ± 23	-
Silicon Carbide, sample #2	$228 \pm 7 / 272 \pm 16$	1.95
Silicon Nitride	$252 \pm 5 / 279 \pm 8$	-

Values separated by '/' indicate different orientations on the sample.
$\pm$ values indicate experimental reproducibility of the result over multiple measurements.
*insufficient samples were available to achieve statistical significance for the Breaking Stress measurements.

Some of these results are similar to previously published values, and some are not. CVD and other thin film deposition processes vary widely between foundry, and true comparisons of material parameter measurements can only be made between samples from the same process and fabrication run. However, the silicon carbide samples were prepared at the same foundry, using the same process, as silicon carbide used by other groups [29, 71], and their measurements agree with the results for sample #1, as well as being comparable with previous measurements [85]. However, the results for sample #2 are considerably lower than previously reported results. The only obvious difference between the two samples is that sample #2 experienced significantly longer KOH etching times than did sample #1; this may have altered the material, possibly through electrochemical reduction of the material, or simply etching of silicon-rich areas in the film, but this has not been confirmed. The silicon nitride results are also reasonable values. The reported values for similar nitride films vary from to 210 - 290 GPa [31, 86].

5. Conclusions and Future Work

5.1 MAT-Test

MAT-Test evolved from our requirements for thin film materials characterization in order to design microclips. It has emerged as a stand-alone project that is a significant achievement in itself: a general, easy-to-use method for measuring some key mechanical properties of thin films. It is applicable to quality control in manufacturing processes as well as experimental measurements of new materials. MAT-Test uses existing equipment in new ways and interprets the data in a novel manner to achieve these capabilities.

This thesis presents the work which has lead to the development of the first version of MAT-Test. Further developments of MAT-Test are possible, and it is hoped that work will continue, and that MAT-Test will be expanded to include additional capabilities. Of course, the measurement range of MAT-Test is strongly dependent on the capabilities of the surface profilometers being used, and these capabilities are being improved constantly. For example, the state-of-the-art profilometer currently offered by Veeco, Inc., can apply forces 100 times smaller than the lowest force applied by the profilometers examined in this work. This would allow MAT-Test to be used on much more compliant materials and thinner samples.

It is also interesting to note that the MAT-Test data analysis method can be applied to data gathered in other ways. For example, a nanoindenter could be fitted with a computer-controlled stage for moving the sample a known distance in x, and be used to produce a plot of d versus L. The SEM rig used by Schweitz, et al. [38], or the equipment used by Wilson, et al. [24] could be modified in a similar manner and data gathered from this equipment could be analysed using the MAT-Test method.

5.2 Proposed Applications

There are two main areas of proposed application for MAT-Test: Research and Design, and Process Quality Control.

Research and Design of MEMS components can benefit from an easy method for characterizing thin films. Researchers can characterize various types of films deposited with different processes, as well as composite stacks of films (see Appendix B.3). Designers and Engineers can use MAT-Test to choose between materials and different suppliers based on MAT-Test data. MAT-Test data can be used to create material selection charts [87] and design diagrams for MEMS materials. An example of a materials selection chart is shown in Figure 52.
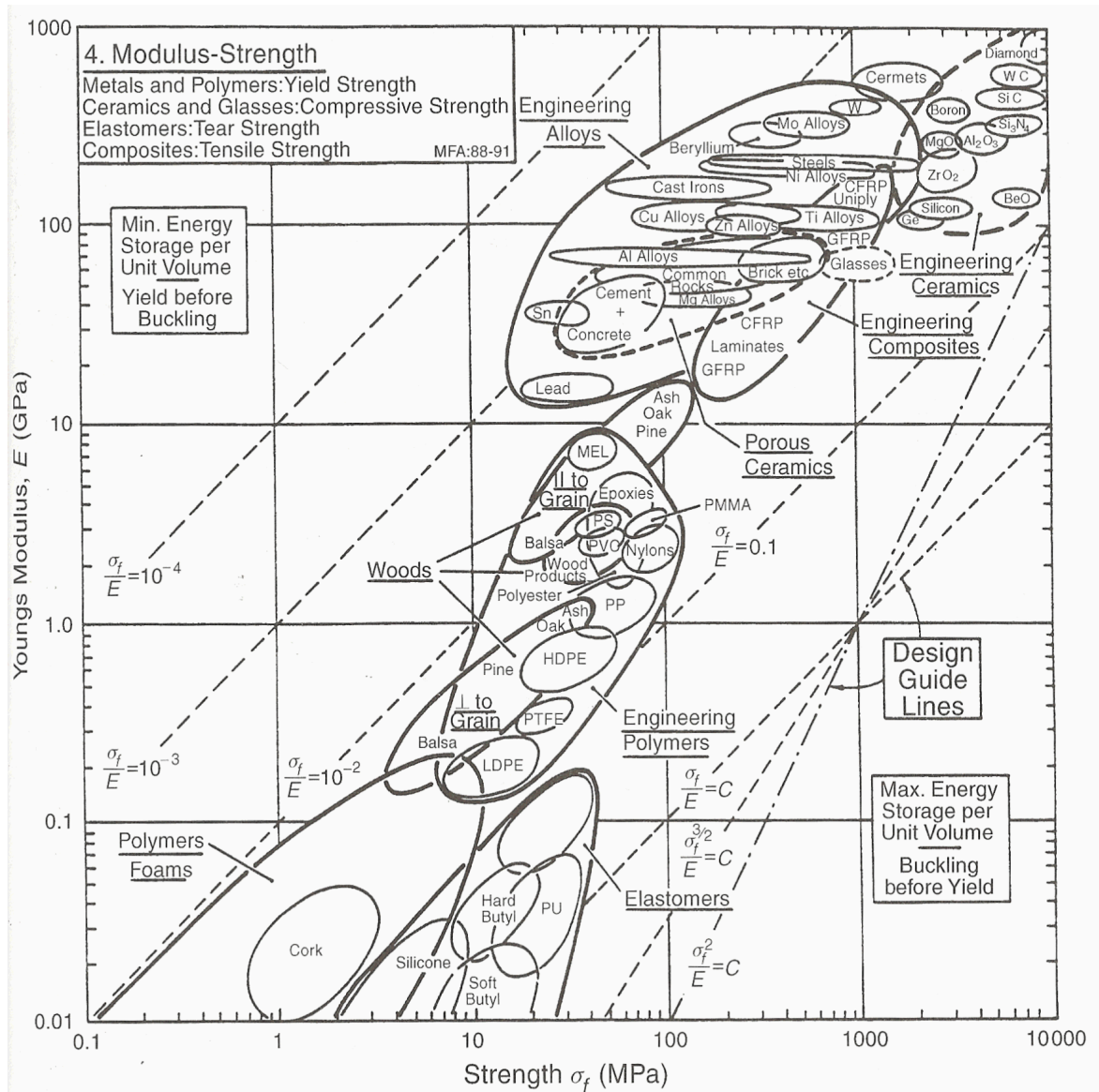
Figure 52 A Young's modulus-Strength materials selection chart for macro-scale engineering materials [87]

Deposition processes for commercial device production require some form of quality control and testing to enable delivery of a reliable product. Thin film deposition methods are currently foundry-specific: a deposited thin film material from one foundry may have very different properties than the same material from another foundry. Continuous monitoring of the MAT-Test intermediate parameters, Y and L_σ, can provide a useful measure of the variability of a deposition process over time and allow comparison of films from different foundries.

5.3 Future Work

There is additional work that can be done to exploit the full potential of MAT-Test. The first priority is simply to gain more experience with MAT-Test: test more materials, with different substrates, new processing conditions, and so forth. We are very interested in comparing the results of a MAT-Test analysis and alternative test methods on the same sample. There is also more work to do in evaluating the nature of noise and irregularities in the profilometer scan data, quantifying the effects of noise on the values extracted for

MAT-Test, and methods of filtering or reducing noise. We will also investigate more robust algorithms for computing the curve fit to the MAT-Test data.

It is hoped that the MAT-Test data analysis method can be modified to provide a measure of the intrinsic stress in a film. The analysis of intrinsic stress as an error effect on beam deflection shows it to be purely a function of L^2. If the other error effects that contribute to the L^2 term can be quantified or eliminated, then the intrinsic stress can be extracted from the U coefficient (Equation 3-4). It may also be shown that different shapes of test structures produce data that can be analysed in a similar manner to isolate the effects of intrinsic stress.

For process quality control applications, further investigation of the correlation between changes in the MAT-Test intermediate parameters, Y and L_σ, and changes in the material properties of the MUT would improve the utility of MAT-Test as a quality control tool.

Finally, we would like to interact with the manufacturers of surface profilometers to learn more about the design and operation of modern profilometers and to encourage adoption of MAT-Test by their customers.

A. Appendix: The Summarized MAT-Test Procedure

MAT-Test procedure for testing an unknown Material Under Test (MUT):

1) Fabricate suspended cantilevers in the MUT. The cantilever width, *w*, should be as narrow as possible for the capabilities of the surface profilometer that will be used. The length should be as long as possible: *10w* is best, although *5w* can work. Recommended test structure dimensions: width $w = 100\mu m$, length $L_L = 1000\mu m$. Alignment marks behind the base of the cantilever are recommended so that the position data of subsequent scans can be compared. A typical alignment mark would be a straight line of length *w*, at least $10\mu m$ wide, lying perpendicular to the length of the cantilever, located a distance $L_L/2$ from the base of the cantilever.

2) Scan the cantilevers with the surface profilometer to acquire Y-data for the Young's modulus measurement. Choose the applied force based on the MUT thickness, starting with the lowest force that still gives a reasonably clean profilometer trace. If thick and thin samples are available, scan both to determine Poisson's ratio. Scan the breaking stress test structures with increasing applied force until samples break. When samples break, immediately rescan the test site to establish a record of the location of the fracture. Scan with as low a horizontal speed as possible to reduce stylus bounce. Monitor the instrument during the scan, and re-scan samples with excessive noise. Scan each sample several times, at several different applied force levels, for comparison. Include the alignment marks in each scan.

3) If required, determine the force applied by the profilometer by scanning silicon measurement cantilevers. Analyse the data according to the guidelines in Step 4.

4) Analyse the data using the MAT-Test Software. When choosing the portion of the profilometer data to analyse for Young's modulus or Poisson's ratio, there are several considerations which need to be balanced. First, include as much data as possible, ideally enough that you are analysing a region that is at least 5 times as long as the beam is wide. Choose a portion of the beam that represents the cantilever, and be sure not to include data that represents the undercut area at the root of the cantilever. When in doubt, analyse only the area in which the deflection is apparent to the eye when viewing the plot of the profilometer data. Also, limit the amount of data that is analysed to avoid including areas of obvious noise. As these areas are often near the extremes of the cantilever (both beginning and end), having longer cantilevers will help ensure that you have sufficient data to analyse. When comparing different measurements on the same sample (e.g. as in Step 3), use the same horizontal range for analysing the all of the data sets. Comparison of multiple measurements at different forces is recommended.

B. Appendix: Derivations for Various Equations

This appendix contains the derivations of several equations that are important for the MAT-Test analysis. Figure 53 is a diagram of a cantilever with the relevant features labelled. Positive force is applied to the top surface of the beam, so positive deflection is "down".
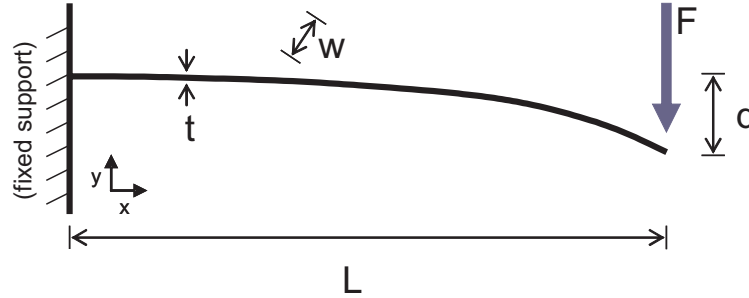
Figure 53 Cantilever deflection.
The positive y direction corresponds to deflection due to the load (i.e., "down").

B.1. Cantilever Tip Deflection

Small deflections of elastic beams can be predicted by using the Euler Approximation to relate the bending moment to the deflection of the beam.

$$M = F(L - x)$$
cantilever bending moment due to a point load

$$\frac{d\theta}{ds} = \frac{M}{EI} \cong \frac{d^2 y}{dx^2}$$
the Euler Approximation

$$\frac{d^2 y}{dx^2} = \frac{F(L-x)}{EI}$$
the second-order linear equation for small-deflection cantilever beam bending

$$EI\frac{dy}{dx} = FLx + \frac{Fx^2}{2} + C_1$$
at $x = 0$, $dy/dx = 0$, so $C_1 = 0$ (assuming perfect root conditions)

$$EIy = \frac{FLx^2}{2} + \frac{Fx^3}{6} + C_2$$
at $x = 0$, $y = 0$, so $C_2 = 0$ (assuming perfect root conditions)

$$d = \frac{FL^3}{3EI}$$
Deflection of the tip of the cantilever, d, at $x = L$. (Equation 3-1)

B.2. Tensile Stress in a Cantilever

The tensile stress developed in a bending cantilever can be related to the bending moment and the stiffness of the beam. This relationship can be used to determine the stress that was present at the point of failure of a deflected beam.

$$\frac{1}{\rho} \cong \frac{d^2 y}{dx^2} = \frac{M}{EI} = \frac{F(L-x)}{EI}$$

ρ is the radius of curvature of the beam

$$\varepsilon = \frac{h}{\rho} = \frac{F(L-x)h}{EI}$$

The stresses in the beam are a function of the radius of curvature of the beam and the distance, h, from the neutral axis.

$$\varepsilon = \frac{t}{2\rho} = \frac{tF(L-x)}{2EI}$$

The maximum tensile strain occurs at the top surface of the beam, at $t/2$.

$$\varepsilon = \frac{6F(L-x)}{wt^2 E}$$

Substitute for I.

$$\sigma = \frac{6F(L-x)}{wt^2}$$

$\sigma = \varepsilon E$

(Equation 3-2)

B.3. Composite Beam Bending

If an unknown material cannot be deposited in a layer of sufficient thickness for MAT-Test evaluation, it can be deposited on a second beam with a known value of E to create a composite beam of sufficient thickness (see section 3.2.4). In fact, the composite beam may have an arbitrary number of layers and unknown values of E, as long as multiple composite beams are used to eliminate the unknowns (as described in [63]). Each layer is assumed to have a rectangular cross-section with the same width as the whole beam. This composite beam can be evaluated in the same way as a single beam, with the appropriate modifications, shown below. The results of the MAT-Test data analysis are then solved for unknown E values.

$$d = \frac{FL^3}{3E_c I_c}$$

The composite beam can be treated a single beam with composite E_c and I_c.

$$I_i = \frac{wt_i^3}{12} + wt_i h_i^2$$

The equivalent second moment of area for each layer in the beam, I_i, can be evaluated in terms of the cross-section and the distance from the neutral axis, h.

$$E_c I_c = \sum_i E_i I_i$$

The composite $E_c I_c$ is the sum of the individual $E_i I_i$ terms.

$$E_c I_c = \frac{FL^3}{3Y}$$

The resulting equation (or system of equations for multiple layers and beams) is solved for the unknown E_i.

C. Appendix: Computer Code

Programs were written using the MATLAB programming language to perform three functions: execute FEM simulations of the bending beams (using FEMLAB), create design files for the micromachining laser, and to analyse the MAT-Test data.

Several thousand lines of computer code were written during the course of this project, and the complete source code listing for these programs is quite long. As few readers are expected to be interested in the details of the code, only representative parts of the source code for the various programs has been included. The complete source code for one of the FEM simulations is included here; the other simulation codes are similar. Full source codes for all of the simulations and programs written for MAT-Test are available from the author upon request.

C.1. FEM Simulation Codes

FEMLAB is a MATLAB application that implements finite element method (FEM) simulations. FEMLAB version 2.2 and above provides a module called the Structural Mechanics Engineering (SME) module, version 1.1. The scripts which perform the MAT-Test simulations were written in MATLAB, using the FEMLAB SME 1.1 module.

Three cases of microbeam bending were simulated: no undercut, a rectangular undercut fixed on three sides, and a semi-circular undercut fixed on the circular perimeter. The source code for the simulation of a rectangular undercut, called deflp4, is included here; the scripts for the other simulations are similar.

```
%deflp4
%
% Script for running a FEMLAB simulation of an undercut cantilever
% M.Hopcroft JUL2002
%
% deflp uses FEMLAB to simulate a cantilever connected to a rectangular plate
%
%       dp
%      ////
%    /|----|
%    /|    |            L
%    /|    |------------------------|
% wp /|    |   .   .   .   .   .|  w   <- load line (.)
%    /|    |------------------------|
%    /|    |
%    /|----|   (plate is an half-circle in 'cp' series)
%      ////
%
% The deflection data is saved in an unformatted text file.
%
% Parameters are entered in the script as constants.
% Parameters: L, w, t, the load line, P, E, nu, number of data points, saved data
file name
%
%
% Dependencies: FEMLAB, eulerd.m, fbdaX.m
%
%

clear;
close all;

%%%%
```

```
%set these constants
%%%%
E=300; %Young's modulus of the film
nu=0.3; %Poisson's Ratio
P=10; %the applied load in mg
t=5; %film thickness in microns

w=100; %cantilever width (um)
L=1000; %length of cantilever (um)

wp=1000*1e-6; %plate width (m)
dp=200*1e-6; %plate depth (m)

%set the loadline
%  The load will be applied to points on this line (see diagram)
%   coordinates in absolute units
%  Make sure that the start and end points are at the start and end of
%   the cantilever, i.e. xstart=0, xend=L . Modify the y-coord. to
%   simulate off-center stylus travel
%  The cantilever starts at x=0, and is symmetric about the x-axis
%  NOTE: do not cause points on the load line to coincide with points
%   in the geometry (i.e., corners)- this will cause smeexpand to fail.
xstart=0; ystart=0;
xend=L*1e-6; yend=0;

points=20; %number of data points to take, not including a data point at the root
stepsize=L/points; %distance between data points (um)

savefile='beamrp'; %the prefix for the name of the file where the data will be
saved
% filename will be: prefix_wp_w_L_P.txt

spoint=7; %spoint: which node is the first loadpoint? A function of the geometry
    %spoint=
    % 3 for rectangular cantilever
    % 7 for cantilever with rectangular plate
    % 6 for cantilever with curved plate
    %
    %NOTE: assuming no load point at root of cantilever

%%%%
%derivative constants, based on the user-specified constants above
%do not modify
force=-P*9.81; %the applied force (negative=down) in uNewtons
Ic=w*(t^3)/12; %second moment of area (um^4)
tc=t*1e-6; %film thickness (m)
wc=w*1e-6; %cantilever width (m)
Lc=L*1e-6; %length of cantilever (m)




%%%%%%%%%%%%%%%%%%%%%%%%%%%%%%%%%%%%%%%%%%%%%%%%%%%%%%%%%
%Simulation

%check time
tstamp=clock; tstamp=fix(tstamp);

fprintf(1,'\n %s\n  %s\n', 'deflp4: Parameteric simulation of cantilever tip
deflection with', 'rectangular undercut plate:');
fprintf(1,'  %s %02d%s%02d\n\n', date, tstamp(4), ':', tstamp(5));


fprintf(1,'\n %s  ', 'Setting up the problem geometry...');
```

63

```
%generate the FEMLAB model and solve it

% FEMLAB/SME Model M-file
% Generated 08-Aug-2002 16:43:30 by FEMLAB 2.3.0.145.

flclear sme

% FEMLAB Version
clear vrsn;
vrsn.name='FEMLAB 2.3';
vrsn.major=0;
vrsn.build=145;
vrsn.rcs='$Name:  $';
vrsn.date='$Date: 2002/06/10 19:39:20 $';
sme.version=vrsn;

% Application mode
clear appl
appl.mode=flsmeki('curr_linearity', 1, 'material', 1, 'temp', 1);
sme.appl=appl;

% Number of global variables
sme.nv=3;

% Rayleigh damping coefficients
sme.al=1;
sme.be=0.001;

% Damping for frequency response analys
modal.damp='modal';
modal.ratio=0.03;
sme.modal=modal;
clear s c p
%the basic cantilever
cantilever=rect2(0, Lc, -(wc/2), (wc/2), 0);
%the undercut plate
% just a rectangle
plate=rect2(-dp, 0, -wp, wp, 0);
% a half-circle
%plate1=rect2(0, dp, -wp, wp, 0);
%circ1=circ2(0,0,dp);
%plate=circ1-plate1;


objs={cantilever,plate};
names={'cantilever','plate'};
s.objs=objs;
s.name=names;

%there are no curve objects
objs={};
names={};
c.objs=objs;
c.name=names;


%the load is applied at points named loadpointX
%  The points lie on the line determined by the endpoints
%   (xstart,ystart), (xend,yend)

xinc=(xend-xstart)/points;
yinc=(yend-ystart)/points;

%create the points of the loadline (skip root)
for i=1:points
    pointlist=point2(xstart+(xinc*i),ystart+(yinc*i)); %point2 creates a point
    %fprintf(1,'\n%f %f',xstart+(xinc*i),ystart+(yinc*i)); %debugging
    objs(i)={pointlist}; %save as a cell in objs
```

```
    names(i)={strcat('loadpoint',num2str(i))}; %give the points different names
end

%save the points in p
p.objs=objs;
p.name=names;


%create the geometry
drawstruct=struct('s',s,'c',c,'p',p);
sme.draw=drawstruct;
sme.geom=geomcsg(sme);


%plot the geometry so we can check it looks right
geomplot(sme,'Edgelabels','on','Pointlabels','on');
title('Simulation Geometry');
xlabel('dimensions in meters (m)')
ylabel('dimensions in meters (m)')
axis equal;


fprintf(1,' %s\n\n', 'done.'); %finished setting up problem geometry


% Recorded command sequence

fprintf(1,'\n %s  ', 'Creating geometry mesh...');

% Initialize mesh
sme.mesh=gridinit(sme,...
        'el',     {{elkidkt(1) [1 2] } },...
        'jiggle', 'mean',...
        'Hgrad',  1.3,...
        'Hcurve', 0.33333333333333331);

% Refine mesh
sme.mesh=gridrefine(sme);


fprintf(1,' %s\n\n', 'done.'); %finished mesh

% Define variables
sme.variables={};


fprintf(1,'\n %s  ', 'Defining materials and loadcases...');

%define loads, constraints, and material properties
% Loadcases
% see SME manual page 5-9 for descriptions of sme.case data structure
%  loadcase is a temporary variable; further down, sme.case=loadcase
% Loadcases
clear loadcase

loadcase.load{1}{1}.dt=0; %the load is applied to a point
%loadcase.load{1}{1}.n=step; %index to what the load is applied to;
loadcase.load{1}{1}.L{1}=num2str(force*1e-6); %the load, first displacement
component, as a string (N)
loadcase.load{1}{1}.L{2}='0';
loadcase.load{1}{1}.L{3}='0';
loadcase.load{1}{1}.Q='0';

%constraints
% for the curved plate, there are two edges that need to be constrained
loadcase.constr{1}.dt=1;    %dt=  0-point, 1-edge, 2-subdomain
loadcase.constr{1}.n=1;    %index to point/edge/subdomain (1 for rect, 8&9 for
half-circle)
```

```
loadcase.constr{1}.i=0;
loadcase.constr{1}.H{1,1}='1';
loadcase.constr{1}.H{1,2}='0';
loadcase.constr{1}.H{1,3}='0';
loadcase.constr{1}.H{2,1}='0';
loadcase.constr{1}.H{2,2}='1';
loadcase.constr{1}.H{2,3}='0';
loadcase.constr{1}.H{3,1}='0';
loadcase.constr{1}.H{3,2}='0';
loadcase.constr{1}.H{3,3}='1';
loadcase.constr{1}.R{1,1}='0';
loadcase.constr{1}.R{2,1}='0';
loadcase.constr{1}.R{3,1}='0';
loadcase.constr{1}.coord='global';
% second edge ( constr{2} ) bottom edge of plate
loadcase.constr{2}.dt=1;
loadcase.constr{2}.n=2;
loadcase.constr{2}.i=0;
loadcase.constr{2}.H{1,1}='1';
loadcase.constr{2}.H{1,2}='0';
loadcase.constr{2}.H{1,3}='0';
loadcase.constr{2}.H{2,1}='0';
loadcase.constr{2}.H{2,2}='1';
loadcase.constr{2}.H{2,3}='0';
loadcase.constr{2}.H{3,1}='0';
loadcase.constr{2}.H{3,2}='0';
loadcase.constr{2}.H{3,3}='1';
loadcase.constr{2}.R{1,1}='0';
loadcase.constr{2}.R{2,1}='0';
loadcase.constr{2}.R{3,1}='0';
loadcase.constr{2}.coord='global';
%top edge of plate
loadcase.constr{3}.dt=1;
loadcase.constr{3}.n=3;
loadcase.constr{3}.i=0;
loadcase.constr{3}.H{1,1}='1';
loadcase.constr{3}.H{1,2}='0';
loadcase.constr{3}.H{1,3}='0';
loadcase.constr{3}.H{2,1}='0';
loadcase.constr{3}.H{2,2}='1';
loadcase.constr{3}.H{2,3}='0';
loadcase.constr{3}.H{3,1}='0';
loadcase.constr{3}.H{3,2}='0';
loadcase.constr{3}.H{3,3}='1';
loadcase.constr{3}.R{1,1}='0';
loadcase.constr{3}.R{2,1}='0';
loadcase.constr{3}.R{3,1}='0';
loadcase.constr{3}.coord='global';


%materials: mater1 is edges, mater2 is subdomains
%mater1 is the edges
loadcase.mater1{1}.t=num2str(tc); %material thickness, as a string
loadcase.mater1{1}.E=num2str(E*1e9); %youngs modulus, as a string
loadcase.mater1{1}.nu=num2str(nu); %Poisson's ratio, as a string
loadcase.mater1{1}.rho='7850';
loadcase.mater1{1}.H='10e9';
loadcase.mater1{1}.s0='500e6';
loadcase.mater1{1}.k='55';
loadcase.mater1{1}.al='12e-6';
loadcase.mater1{1}.h='0';
loadcase.mater1{1}.name='Silicon Carbide';
loadcase.mater1{1}.n=1:9;
%mater2 is the subdomains
loadcase.mater2{1}.t=num2str(tc); %material thickness, as a string
loadcase.mater2{1}.E=num2str(E*1e9); %youngs modulus, as a string
loadcase.mater2{1}.nu=num2str(nu); %Poisson's ratio, as a string
loadcase.mater2{1}.rho='7850';
```

```
loadcase.mater2{1}.H='10e9';
loadcase.mater2{1}.s0='500e6';
loadcase.mater2{1}.k='55';
loadcase.mater2{1}.al='12e-6';
loadcase.mater2{1}.h='0';
loadcase.mater2{1}.name='Silicon Carbide';
loadcase.mater2{1}.n=[1 2];
loadcase.prop{1}.A='2124*1E-6';
loadcase.prop{1}.I='3.492*1E-6';
loadcase.prop{1}.K='4.83e-006';
loadcase.prop{1}.Sf='1.2';
loadcase.prop{1}.z1='48*1E-3';
loadcase.prop{1}.z2='48*1E-3';
loadcase.prop{1}.name='HEA 100';
loadcase.prop{1}.n=1:9;
loadcase.init={};
%sme.case=loadcase;


fprintf(1,' %s\n\n', 'done.'); %finished loadcase setup

fprintf(1,'\n %s\n\n', 'Solving Individual Load Cases:');


%Iterations
%The model geometry has been defined, with points where the load will be applied.
%  The mesh creates nodes at the points.
%Now we iterate:
%  Apply the load to a point on the 'loadline'
%  Solve
%  Save the deflection at the point where the load is applied
%  Repeat

%keep time
tic;
steptime=toc;
toctime=toc;

ind=0; %index var

for step=[spoint:points+(spoint-1)-1 points+(spoint-1)+1] %start at root and skip
final node (point)
                %iterations: [r:points+(r-1)-1 points+(r-1)+1]

    steptime=toc-toctime;
    toctime=toc;
    ind=ind+1; %data array indexing

    fprintf(1,'\n  %s %d%s%d  %s %0.2f  %s %0.2f\n', 'Step No.:', ind, '/',
points, 'Step time (sec):', steptime, 'Elapsed time (sec):', toc);

%The load is applied above, except for the index to the node that gets the load
%  here, we apply the
loadcase.load{1}{1}.n=step; %index to what the load is applied to;

%save the new load
sme.case=loadcase;

% Current loadcase
sme.loadcase=1;

% Extend element grid
sme.mesh=gridextend(sme);

% Expand problem data
sme.expand=smeexpand(sme,...
      'loadstep',1,...
      'context','local');
```

```
% Assemble and Solve linear static problem
sme.sol=smeassem(sme,...
      'temp',    'off',...
      'method', 'eliminate',...
      'out',     {'sol'},...
      'expand', 'off',...
      'context','local');



%problem is now solved
%save tip deflection data
% The nodes are numbered in order. The geometry points (including individual
points and
%  shape boundaries) are the first nodes in the list, and they are numbered left-
to-right,
%  and bottom-to-top. For a geometry of two rectangles, the start point is node
7, and
%  the last node falls between the two corners of the end of the cantilever.
defl(ind,1)=sqrt(((xinc*ind)^2)+((yinc*ind)^2))+xstart; %calculate true distance
travelled
defl_data=smeeval(sme,'w','Nodedata','on'); %get the deflection solution at all
nodes
defl(ind,2)=defl_data(step); %save the deflection data from the node of interest

 %print status
    fprintf(1,'   %s %d   %s %f\n', 'Node:', step, 'Deflection at loadpoint
(um):', defl_data(step)*1e6);



%%%%%%%%%%%%%
end %end of the FEM iterations loop
%tip deflection is now stored in defl

fprintf(1,'\n %s\n\n', '... done.'); %finished solving

%save the data for analysis

%convert deflection data to microns
deflection=defl.*1e6;

%save the data to a file
%  save as a simple text file with two columns; we can use load later to load it
save([savefile '_' num2str(dp*1e6) '_' num2str(w) '_' num2str(L) '_' num2str(P),
'.txt'],'deflection','-ASCII');
%save all of the variables to a binary file that we can load later
save([savefile '_' num2str(dp*1e6) '_' num2str(w) '_' num2str(L) '_'
num2str(P)]);


fprintf(1,'\n  %s %s\n','The deflection data has been saved to the file:', ...
    [savefile '_' num2str(dp*1e6) '_' num2str(w) '_' num2str(L) '_' num2str(P)
'.txt']);
fprintf(1,'\n  %s %s\n','All data has been saved to the file:', ...
    [savefile '_' num2str(dp*1e6) '_' num2str(w) '_' num2str(L) '_' num2str(P)
'.mat']);

fprintf(1,'\n');

%%%%%%%%%%%%%%%%%%%%%%%%%%%%%%%%%%%%%%%%%%%%%%%%%%%%%%%%%%%%%%%%
%data analysis- call fbdaX
fbda4
```

C.2. Laser Design Software

The micromachining laser is controlled by a PC running the laser control software from New-Wave Research (NWR). This laser control software includes only primitive capabilities for creating designs. A group of MATLAB programs, called the "l Series", was written to provide a design environment for creating the MAT-Test designs. The source code for all of the l Series programs is quite long, so only the help file from the primary program, lel, is included here.

```
%lel - Enter Lines for New Wave laser lines file format
%Laser file format utility: enter lines for cutting, display the result, and save
as Laser lines file.
%M. Hopcroft, CUED MEMS JUL2002
%version 1.1
%
%  About New Wave Laser file formats
%  -------------------------------
% The New Wave QuikLaze software can store a series of cuts in various shapes for
automated cutting.
%  The series of line cuts can be saved as a text file with the format:
%
% LINE
% x1,y1,z1
% x2,y2,z2
% x3,y3,z3
% LINE
% ...
%
%  where the coordinate groups represent points in the line.
%   A 'line' is a series of connected points; we
%   could define a square with the statement:
%
% LINE
% 0,0,0
% 2,0,0
% 2,2,0
% 0,2,0
%
%  This format is referred to as a Laser lines file.
%   It is saved as a text file with the extension .txt .
%
% For matlab, it is easier to read a text file that has a line-wise regular
format.
%  For the laser data, a text file with the line-wise regular format
%
% x1,y1,z1
% x2,y2,z2
% x3,y3,z3
% ...
%
%  is referred to as a Laser points file. it is saved as a text file with the
extension _p.txt .
%
%
%  About lel
%  ---------
% lel allows the user to enter X-Y-Z data points for a New Wave Laser cutting
design,
%  and to view the design as it is entered.
%
% The user has the option to continue an existing design or start a new one.
% The X-Y coordinates are entered in um (microns), from (0,0) to (50000,50000).
% The Z coordinates are entered in um, for each line (not each point) as the
distance
%  below the initial focus point.
```

```
%  For example, if you enter "10", the microscope head will be lowered 10 um for
that line.
%  The default is zero, i.e., no change in Z.
%  Note that the Z-coordinate remains constant for each line, so you enter it
only once at
%   the beginning of each line.
% The lines are plotted for viewing as they are entered. Z-coordinates are not
shown on the plot.
% The user then has the option to save the points as a Laser line file.
%
% Usage:
% Start lel at the matlab prompt by typing "lel". lel asks the user if they wish
to continue a
%  previous design. If yes, the user is prompted to enter the name of a Laser
lines file.
%  The file is read in and displayed.
%
% The user is prompted to enter a series of points. The lines/line segments
between the points
%  are displayed on the plot as they are entered. Points are entered until the
user presses
%  return (empty line) at the end of each line. Then the user has the option to
enter more lines
%  or to quit and save the design as a Laser lines file.
%
%

%%%%%%%
```

C.3. MAT-Test Data Analysis

Programs were written to perform the MAT-Test analysis automatically, given the data from the surface profilometer and the test structure cross-section information. The programs, described in section 4.4, implement the analysis described in Chapter 3. The source code for the program y1 is given below; the other programs are similar. y1 calculates the value of Young's modulus from MAT-Test data.

```
%y1
%MAT-Test data analysis software Y
%  version 1.0
%
%y1 is a script for analyzing MAT-Test Y-data.
% The user will be asked to name the data file containing surface profilometer
data.
% They will then select the region of valid data by inspecting the plot of the
data, and enter the cross-section information.
% A polynomial fit will be performed, and the results will be plotted for
viewing.
% The Y-parameter and the Young's modulus will be displayed.
%
%Script Dependencies: dk2rd, as2rd, dk3rd, p10rd, dslice
%
%M. Hopcroft
%CUED MEMS Research Group
%August 2002
%

close all;
clear;
%clc;


fprintf(1, '\n\n %s\n', 'y1: MAT-Test Data Analysis for Y-Parameter and Young''s
modulus');
fprintf(1, '     %s\n\n', 'CUED MEMS Research Group / M. Hopcroft AUG2002');

%check time
tstamp=clock; tstamp=fix(tstamp);
fprintf(1,'\n  %s %02d%s%02d\n\n', date, tstamp(4), ':', tstamp(5));

%%0
%get filename
filename=input(' Enter the name of the profilometer data file (.txt will be
added): ','s');

%check to see if file exists
cfid=fopen(strcat(filename,'.txt'));
if cfid== -1, disp(pwd); error('file not found in current directory'); end
fclose(cfid);

%what type of data file is it?
fprintf(1,'\n %s\n', ' What type of surface profilometer is this data from?');
fprintf(1,'  %s\n  %s\n  %s\n  %s\n', '1 - Dektak IIA', '2 - Dektak 3ST', '3 -
AlphaStep 200', '4 - KLA-Tencor P10');
ptype=input('  Choose a profilometer [2]: ');
    if isempty(ptype)
        ptype = 2;
    end
fprintf(1,'\n');

%%1
%read in data from the data file

fprintf(1, '  \n %s\n','Reading data file:');
```

```
if ptype == 1 %Dektak IIA
    dek1=dk2rd(filename,1,1);
elseif ptype == 2 %Dektak 3ST
     dek1=dk3rd(filename,1,1);
elseif ptype == 3 %AlphaStep 200
    dek1=as2rd(filename,1,1);
elseif ptype == 4 %KLA-Tencor P-10
    dek1=p10rd(filename,1,1);
    close(2); %close the extra figure from P10
end

%the file read routine will plot the data


%%2
%select the portion of data that represents the cantilever, starting at the root
%  approximately is fine, err on the side of the beam, rather than the root

figure(1); %select the plot of the data
hold on; %so we can plot the position of the user selection on the existing plot

top=max(dek1(:,2));  %data range with 10% scaling for nice looking plot
bottom=min(dek1(:,2));
graphrange=top-bottom;
top=top+0.1*abs(graphrange);
bottom=bottom-0.1*abs(graphrange);


fprintf(1,'\n\n %s\n', 'Select the portion of the data to be analyzed (Figure No.
1):');


r=input(' Enter the cantilever start point (r) (um): ');
plot([r r], [top bottom], '-r', 'LineWidth', 2); %plot the r boundary on the data
plot

figure(1); %bring the figure to the front

m=input(' Enter the cantilever data endpoint (m) (um): ');
plot([m m], [top bottom], '-r', 'LineWidth', 2); %plot the m boundary on the data
plot

%slice out the specified section of the dektak data
% and reset position coordinates to start at 0
deks=dslice(r,m,dek1,1);

%plot the selected data
figure;
plot(deks(:,1),deks(:,2));
title('Selected Data');
xlabel('Scan Length (um)');
ylabel('Profile (um)');
grid on;


%%3
%plot the selected data
% work with dekc0
dekc0=deks;



%figure for the conditioned data and the curve fit
figure; hold on;

%plot the selected data
plot(dekc0(:,1),dekc0(:,2),'.b');
```

72

```
%%4
%fit a cubic polynomial to data. plot the fit.

%perform polynomial fit:

%scale position data by max position so polyval won't whine
scalex=dekc0(:,1)./dekc0(end,1);

%polynomial fit
%3rd order
pf3=polyfit(scalex,dekc0(:,2),3);
Y3=pf3(1)/(dekc0(end,1)^3); %Y is the third-order coefficient, unscaled

%generate the curve from the polynomial fit
pfc3=polyval(pf3,scalex);

%record the difference between the data and the fit
diff3=dekc0(:,2)-pfc3;

%plot the fit
plot(dekc0(:,1),pfc3,'g');

%plot the difference between data and fit
plot(dekc0(:,1),diff3,'.m');

%gussy up that plot
title('Deflection Data with Cubic Fit');
xlabel('Scan Length (um)');
ylabel('Deflection (um)');
legend('data','cubic fit','difference',3);
grid on;


%get cantilever parameters
width=input(' Enter the width of the cantilever (um): ');

thick=input(' Enter the thickness of the cantilever (um): ');

force=input(' Enter the force applied by the profilometer (mg): ');
force=force*-9.81; %convert to uN

Ic=width*(thick^3)/12;


%%8
%get answers
points=length(dekc0); %how many data points are there?

%extract youngs modulus from the x^3 coefficients
youngs3=(force/(3*Ic*Y3))*1e-3;

%calculate the multiple correlation coefficient r^2
%  notation from "Applied Regression Analysis", by Kleinbaum, Kupper, Miller,
CUED EP.243
SSE3=sum(diff3.^2);
SSY3=sum((dekc0(:,2)-mean(pfc3)).^2);
R2=(SSY3-SSE3)/SSY3;

%calculate the standard error (SE) for the coefficients
%  from "Analyzing Multivariate Data", by Green, CUED EP.196D; pages 66-72
%R=corrcoef([dekc0(:,1) dekc0(:,1).^2 dekc0(:,1).^3 dekc0(:,1).^4]); %correlation
matrix
R=corrcoef([dekc0(:,1) dekc0(:,1).^2 dekc0(:,1).^3]); %correlation matrix
invR=inv(R);
r1=corrcoef(dekc0(:,2),dekc0(:,1)); %simple correlations between y and x^n
r2=corrcoef(dekc0(:,2),dekc0(:,1).^2);
r3=corrcoef(dekc0(:,2),dekc0(:,1).^3);
```

73

```
ry=[r1(1,2); r2(1,2); r3(1,2)]; %column vector of simple correlations
sy=std(dekc0(:,2)); %standard deviation of y
% smatrix is std(y) / std(x^n)
%smatrix=[sy/std(dekc0(:,1).^4) sy/std(dekc0(:,1).^3) sy/std(dekc0(:,1).^2)
sy/std(dekc0(:,1))];
smatrix=[sy/std(dekc0(:,1).^3) sy/std(dekc0(:,1).^2) sy/std(dekc0(:,1))];
% ssroot is just some formula, given in Green, p72
%ssroot=[sqrt((invR(4,4)*(1-R2))/(points-4-1)) sqrt((invR(3,3)*(1-R2))/(points-3-
1)) sqrt((invR(2,2)*(1-R2))/(points-2-1)) sqrt((invR(1,1)*(1-R2))/(points-1-1))];
ssroot=[sqrt((invR(3,3)*(1-R2))/(points-3-1)) sqrt((invR(2,2)*(1-R2))/(points-2-
1)) sqrt((invR(1,1)*(1-R2))/(points-1-1))];
% multiply to get the standard error in all of the coefficients (except the
intercept)
SE=smatrix.*ssroot;
% get the coefficients from the correlation matrix, just to check to see if they
match
b=invR*ry;
b=b'; b=fliplr(b); %b is in reverse order from smatrix, polyfit, etc., so flip it
around
%pfr has calculated coefficients, not scaled
pfr=(b.*smatrix);


%print the answers
fprintf(1,'\n');

fprintf(1,'    %s\n    %0.3f %0.3f %0.3f %0.3f\n','The scaled fit coefficients
are:', pf3(1), pf3(2), pf3(3), pf3(4));
fprintf(1,'    %s %f\n', 'The coefficient of determination (r^2) for the cubic
fit is:', R2);
fprintf(1,'   %s %e\n', 'The Standard Error in Y (Yx^3) is:', SE(1));

fprintf(1,'\n\n');

fprintf(1,'   %s %e\n', 'The Y parameter is:', Y3);
fprintf(1,'   %s %0.1f %s\n','The Young''s Modulus value from the Y parameter
is:', youngs3, 'GPa');

fprintf(1,'\n');
```

References

1. Tai, Y.-C., Aerodynamic control of a delta-wing using MEMS sensors and actuators. Proceedings of the 1997 International Symposium on Micromechatronics and Human Science, 1997. Published September 1998. 6(5): p. 671-677.
2. Petersen, K., Silicon as a Mechanical Material. Proceedings of the IEEE, 1982. 70(5): p. 420-457.
3. Moore, D.F. and R.R.A. Syms, Recent developments in micromachined silicon. Electronics & Communication Engineering Journal, December. 11(6): p. 261-270.
4. Wu, M.C., Micromachining for optical and optoelectronic systems. Proceedings of the IEEE, November 1997. 85(11): p. 1833-1856.
5. Mounier, E., MEMS Mean Business, in OptoMEM. January 2002.
6. Bourne, M., It's Raining MEMS: Five-Year Forecast calls for Nice, Steady Showers. July 16, 2002, Reed Business Information: Scottsdale, AZ, USA.
7. Takeda Pacific, I., Nanotechnology and MEMS: Commercializing Ultrasmall Objects-Market Opportunities and Technologies. May 2002, Takeda Pacific, International Business Consulting: Fremont, CA USA. 129 pages.
8. Bostock, R.M., et al., Silicon nitride microclips for the kinematic location of optic fibres in silicon V-shaped grooves. Micromechanical Microengineering, Journal of. 8: p. 343-360.
9. Bostock, R.M., et al. Low cost integrated photonic systems. in Lasers and Electro-Optics Society Annual Meeting. 1997, IEEE 1996.
10. Moore, D.F. Thick layers of silicon nitride and other materials for micromechanical structures. in Extremely Hard Materials for Micromechanics, IEE Colloquium on. 1997.
11. Moore, D.F., R.M. Bostock, and J.E. Townsend. Silicon Nitride Microclips for Optic Fibre Connectors. in IEE Two-day Seminar (Ref. No. 1999/199). 1999.
12. Strandman, C. and Y. Backlund, Bulk silicon holding structures for mounting of optical fibers in v-grooves. Microelectromechanical Systems, Journal of, March 1997. 6(1): p. 35-40.
13. Strandman, C. and R. Gupta, Modelling of fibre holding elements in silicon. Microelectromechanical Systems, Journal of, September 1999. 9(3): p. 277-282.
14. SOTEC Microsystems SA; EPFL, SOTEC Microsystems WWW page: http://www.somisys.ch/microclips.html.
15. Boyle, P., Simulation of Microsystems. December 2001, CUED MEMS Research Group: Cambridge. 18 pages.
16. Boyle, P., D.F. Moore, and R.R.A. Syms. Micropackaging Using Thin Films as Components. in ECTC 2002: Electronic Components and Technology Conference. 2002. San Diego, CA USA, May 28-31, 2002: IEEE.
17. Boyle, P., R.R.A. Syms, and D.F. Moore. Packaging solutions for MEMS/MOEMS using thin films as mechanical components. in Design, Test, Integration, and Packaging of MEMS/MOEMS 2002. 2002. Cannes, France, SPIE.
18. New Wave Research, New Wave Research QuikLaze WWW product page: http://www.new-wave.com/products/quiklaze.html.
19. Schweitz, J.-A., Mechanical Characterization of Thin Films by Micromechanical Techniques. MRS Bulletin, July 1992. 17(7): p. 34-45.
20. Osterberg, P.M. and S.D. Senturia, M-TEST: A test chip for MEMS material property measurement using electrostatically actuated test structures. Microelectromechanical Systems, Journal of, June 1997. 6(2): p. 107-118.
21. Ashwell, D.G., The Anticlastic Curvature of Rectangular Beams and Plates. Royal Aeronautical Society, Journal of, 1950. 54: p. 708-715.
22. Yi, T. and C.-J. Kim. Tension Test with Single-Crystalline-Silicon Microspecimen. in ASME Int. Mechanical Engineering Congress and Exposition. 1999. Nashville, TN USA, November 1999.
23. Wortman, J.J. and R.A. Evans, Youngs' Modulus, Shear Modulus and Poisson's Ratio in Silicon and Germanium. Journal of Applied Physics, January. 36(1): p. 153-156.
24. Wilson, C.J., A. Ormeggi, and M. Narbutovskih, Fracture testing of silicon microcantilever beams. Journal of Applied Physics, March 1996. 79(5): p. 2386-2393.
25. CIT, Silicon Properties, California Institute of Technology, Engineering Design Research Laboratory.
26. Sato, K., et al. Micro tensile-test of silicon film having different crystallographic orientations. in TRANSDUCERS '97, Solid State Sensors and Actuators, International Conference on,. 1997. Chicago, IL USA, June 16-19, 1997.
27. Suo, Z., Fracture in Thin Films, in Encyclopedia of Materials: Science and Technology. 2001, Elsevier Science/PERGAMON.

28. Ashby, M.F. and D.R.H. Jones, Engineering Materials 2: An Introduction to Microstructures, Processing and Design. 2nd ed. Vol. 2. 1998: Butterworth-Heinemann.

29. Spearing, S.M., Personal communications on the topic: "Failure in silicon carbide microturbine components." August 2002.

30. Crandall, S.H. and N.C. Dahl, An Introduction to the Mechanics of Solids. Second ed. 1972: McGraw-Hill, Inc.

31. Senturia, S.D., Microsystem Design. 2001: Kluwer Academic Publishers.

32. Timoshenko, S. and J.N. Goodier, Theory of Elasticity. 3rd ed. 1970: McGraw-Hill Book Company, Inc.

33. Young, W.C., Roark's Formulas for Stress and Strain. 6th ed. 1989: McGraw-Hill, Inc.

34. Menčik, J. and E. Quandt, Determination of elastic modulus of thin films and small specimens using beam bending methods. Journal of Materials Research, May. 14(5): p. 2152-2162.

35. Weihs, T.P., et al., Mechanical Deflection of Cantilever Microbeams: A New Technique for Testing the Mechanical Properties of Thin Films. Journal of Materials Research, Sept/Oct 1988. 3(5): p. 931-942.

36. Baker, S.P. and W.D. Nix, Mechanical Properties of Compositionally-Modulated Au-Ni Thin Films: Nanoindentation and Micro-Cantilever Beam Deflection Experiments. Journal of Materials Research, December 1994. 9(12): p. 3131-3144.

37. Zhang, T.-Y., M.-H. Zhao, and C.-F. Qian, Effect of substrate deformation on the microcantilever beam-bending test. Journal of Materials Research, September 2000. 15(9): p. 1868-1871.

38. Ericson, F. and J.-A. Schweitz, Micromechanical fracture strength of silicon. Applied Physics, Journal of, December 1990. 68(11): p. 5840-5844.

39. Moore, D.F., et al., The fabrication of suspended microstructures for devices. Superconductor Science and Technology, September 1991. 4(9): p. 401-405.

40. COMSOL, Inc., FEMLAB WWW page: http://www.comsol.com/femlab/.

41. The Mathworks, Inc., MATLAB WWW page: http://www.mathworks.com/products/matlab/.

42. Peterson, R.E., Stress concentration factors; charts and relations useful in making strength calculations for machine parts and structural elements. 1974, New York: Wiley.

43. Florando, J., et al. Measurement of Thin Film Mechanical Properties by Microbeam Bending. in Materials Research Society Symposium Proceedings. 1999, 1999.

44. Timoshenko, S. and J. Gere, Theory of Elastic Stability. 2nd ed. 1961: McGraw-Hill Book Company, Inc.

45. Riley, W.F., L.D. Sturges, and D.H. Morris, Mechanics of Materials. 5th ed. 1999, New York: Chichester Wiley.

46. Veeco Instruments, Inc., Veeco Dektak Series WWW page: http://www.veeco.com/html/sub_products_productdisplay.asp_Q_GroupID_E_1.

47. KLA-Tencor, Inc., AlphaStep 500 WWW page: http://www.kla-tencor.com/products/metrology/alpha-step500/alpha-step500.html.

48. Petersen, K.E. and C.R. Guarnieri, Young's Modulus Measurements of Thin Films Using Micromechanics. Journal of Applied Physics, November 1979. 50(11): p. 6761-6766.

49. Mehregany, M., R.T. Howe, and S.D. Senturia, Novel microstructures for the in situ measurement of mechanical properties of thin films. Journal of Applied Physics. 62(9): p. 3579-3584.

50. Weihs, T.P., et al., Measuring the Strength and Stiffness of Thin Film Materials by Mechanically Deflecting Cantilever Microbeams, in Stresses and Mechanical Properties, M.R.S. Proceedings, Editor. 1989, MRS. p. 87-92.

51. Weihs, T.P., et al., The Determination of Mechanical Parameters and Residual Stresses for Thin Films using Micro-Cantilever Beams, in Stresses and Mechanical Properties, M.R.S. Proceedings, 1989, MRS. p. 93-98.

52. ASTM, ASTM E08 Subcommittee Activity WWW page: http://www.astm.org/COMMIT/CUSTOM1/E08.htm.

53. ASTM, STP 1413 Mechanical Properties of Structural Films. Special Technical Publication (STP), ed. C.L.M.S. Brown. 2001: ASTM. 341.

54. de Boer, M.P., et al., Integrated Platform for Testing MEMS Mechanical Properties at the Wafer Scale by the IMaP Methodology, in Mechanical Properties of Structural Films, ASTM STP 1413, C.L. Muhlstein and S.B. Brown, Editors. 2001, American Society for Testing and Materials: West Conshohocken, PA, USA.

55. Jensen, B.D., M.P. de Boer, and S.L. Miller. IMaP: Interferometry for Material Property Measurement in MEMS. in MSM '99: International Conference on Modeling and Simulation of Microsystems. 1999. San Juan, Puerto Rico, USA, April 19-21, 1999.

56. MTS Systems Corporation, Nanoindenter Product WWW page: http://www.mts.com/nano/.

57. Kraft, O., R. Schwaiger, and W.D. Nix, Measurement of mechanical properties in small dimensions by microbeam deflection. [not yet submitted].

58. Johansson, S., F. Ericson, and J.-A. Schweitz, Influence of surface coatings on elasticity, residual stresses, and fracture properties of silicon microelements. Applied Physics, Journal of, January 1989. 65(1): p. 122-128.

59. Greek, S., et al. In Situ Tensile Strength Measurement Of Thick-film And Thin Film Micromacrined Structures. in Solid-State Sensors and Actuators, 1995 and Eurosensors IX, Transducers '95. The 8th International Conference on. 1995, IEEE.

60. Wilson, C.J. and P.A. Beck, Fracture testing of bulk silicon microcantilever beams subjected to a side load. Microelectromechanical Systems, Journal of, September 1996. 5(3): p. 142-150.

61. Tai, Y.-C. and R.S. Muller. Measurement of Young's modulus on microfabricated structures using a surface profiler. in An Investigation of Micro Structures, Sensors, Actuators, Machines and Robots. 1990, IEEE.

62. Qin, M., et al. Measurement of Young's modulus of nickel silicide film by a surface profiler. in Electron Devices Meeting. 2000. Hong Kong, IEEE.

63. Hossain, N., et al., Characterization of the Young's Modulus of CMOS Thin Films, in Mechanical Properties of Structural Films, ASTM STP 1413, C.L. Muhlstein and S.B. Brown, Editors. 2001, American Society for Testing and Materials: West Conshohocken, PA, USA.

64. Ye, X.Y., et al. Measurement of Young's modulus and residual stress of micromembranes. in MHS'96: Proceedings of the Seventh International Symposium on Micro Machine and Human Science. 1996. New York, NY, USA, IEEE.

65. Herman, D., M. Gaitan, and D. DeVoe. MEMS Test Structures for Mechanical Characterization of VLSI Thin Films. in SEM Conference. 2001. Portland, Oregon, June 4-6, 2001.

66. Smee, S.A., et al., IC test structures for multilayer interconnect stress determination. IEEE Electron Device Letters, January 2000. 21(1): p. 12-14.

67. Fang, W., C.-H. Lee, and H.-H. Hu, On the buckling behavior of beams. Micromechanical Microengineering, Journal of, September 1999. 9(3): p. 236-244.

68. Fang, W. and J.A. Wickert, Comments on measuring thin-film stresses using bi-layer micromachined beams. Micromechanical Microengineering, Journal of. 5(4): p. 276-281.

69. Fang, W. and J.A. Wickert, Determining mean and gradient residual stresses in thin films using micromachined cantilevers. Micromechanical Microengineering, Journal of, September 1996. 6(3): p. 301-309.

70. Zou, Q., Z. Li, and L. Liu. Study of methods for measuring mechanical properties of thin films in microelectromechanical systems (MEMS). in Solid-State and Integrated Circuit Technology, 1995 4th International Conference on. 1995. Beijing, October 24-28, 1995.

71. Sharpe, W.N., Jr., Mechanical Properties of MEMS Materials. August 20, 2001, Johs Hopkins University: Baltimore, MD USA.

72. Sharpe, W.N., Jr., B. Yuan, and R.L. Edwards, A new technique for measuring the mechanical properties of thin films. Microelectromechanical Systems, Journal of, September 1997. 6(3): p. 193-199.

73. Sharpe, W.N., Jr., B. Yuan, and R. Vaidyanathan. Measurements of Young's modulus, Poisson's ratio, and Tensile Strength of Polysilicon. in Tenth IEEE International Workshop on Microelectromechanical Systems. 1997. Nagoya, Japan, IEEE.

74. Sharpe, W.N., Jr., et al., Effect of specimen size on Young's modulus and fracture strength of polysilicon. Microelectromechanical Systems, Journal of, September 2001. 10(3): p. 317-326.

75. Ogawa, H., et al. Measurements of mechanical properties of microfabricated thin films. in MEMS'97: Proceedings of the IEEE Tenth Annual International Workshop on Micro Electro Mechanical Systems. 1997. Nagoya, Japan, IEEE.

76. Jensen, B.D., et al., Interferometry of actuated microcantilevers to determine material properties and test structure nonidealities in MEMS. Microelectromechanical Systems, Journal of, Spetember 2001. 10(3): p. 336-346.

77. Zhang, T.-Y., et al., Microbridge Testing of Slicon Nitride Thin Films Deposited on Silicon Wafers. Acta Materialia. 48: p. 2843-2857.

78. Hopcroft, M.A., l Series version 1.1 User Guide. Oct 2002, CUED MEMS Research Group. 4 pages.

79. Madou, M.J., Fundamentals of Microfabrication. 2nd ed. 2001: CRC Press LLC.

80. Bado, P., W. Clark, and A. Said, Introduction to Laser Micromachining Handbook. 2001, Clark-MXR Ultrafast Laser Machining: Ann Arbor, MI USA. 19 pages.

81. Elwenspoek, M. and H.V. Jansen, Silicon Micromachining. 1998: Cambridge University Press.

82. University of Illinois, Anisotropic Crystal Etch Simulator: http://mass.micro.uiuc.edu/research/completed/aces/pages/home.html.

83. Pruitt, B., et al. Design of Piezoresistive Cantilevers for Low Force Electrical Contact Measurements. in *International Mechanical Engineering Congress and Exposition 2000*. 2000.

84. Pruitt, B., *Piezoresistive Cantilevers for Characterizing Thin-film Gold Electrical Contacts*, PhD Thesis in Mechanical Engineering, Stanford University, 2002. 227 pages.

85. Windischmann, H., Intrinsic stress and mechanical properties of hydrogenated silicon carbide produced by plasma-enhanced chemical vapor deposition. *Journal of Vacuum Science & Technology A: Vacuum, Surfaces, and Films*, July 1991. 9(4): p. 2459-2463.

86. Tabata, O., et al., Mechanical property measurements of thin films using load-deflection of composite rectangular membranes. *Sensors and Actuators*, 15 November 1989. 20(1-2): p. 135-141.

87. Ashby, M.F., *Materials Selection in Mechanical Design*. 2nd ed. 1999, Boston: Butterworth Heinemann.